KERNFORSCHUNGSZENTRUM

KARLSRUHE
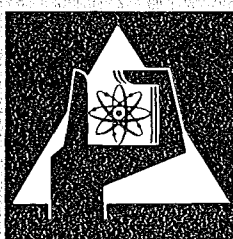
September 1974   KFK 2054

Institut für Angewandte Kernphysik

PROGRESS REPORT
of the Teilinstitut Nukleare Festkörperphysik

Editor: W. Schommers

GESELLSCHAFT
FÜR
KERNFORSCHUNG M.B.H.

KARLSRUHE

KERNFORSCHUNGSZENTRUM KARLSRUHE

KFK 2054

Institut für Angewandte Kernphysik

PROGRESS REPORT

of the

Teilinstitut Nukleare Festkörperphysik

(1.6.1973 - 31.5.1974)

Editor: W. Schommers

Gesellschaft für Kernforschung mbH., Karlsruhe

This progress report of the Teilinstitut Nukleare Festkörperphysik covers the period from 1st June 1973 - 31st May 1974. The arrangement has been chosen to emphasis the main areas of research in which the institute is presently involved.

These areas are Dynamics of Solids and Liquids, Electronic Structure and Magnetism of Solids and Development of Materials. Some of the technical developments relevant to these topics are also included.

Besides the Reactor FR2 and the Cyclotron the major research facilities at the Kernforschungszentrum Karlsruhe, neutron beam facilities at the High Flux Reactor in Grenoble have been used for part of the work described. The institute supports also external users of the neutron beam facilities at the Reactor FR2. Work done in cooperation with external groups is included in the report. The report contains only abstracts or references of those papers already published or in the process of publication. Premilinary results of work in progress are described more in detail. References to these results should be made only with the explicit permission of the authors.

Dieser Progress-Report des Teilinstituts Nukleare Festkörperphysik erfaßt den Zeitraum vom 1. Juni 1973 - 31. Mai 1974. Die Darstellung betont die Hauptforschungsgebiete, auf denen das Institut zur Zeit tätig ist. Diese sind: Dynamik von Festkörpern und Flüssigkeiten, Elektronenstruktur und Magnetismus von Festkörpern und die Entwicklung neuer Materialien. Einige technische Entwicklungen, die für die Forschungsarbeiten wichtig sind,,wurden ebenfalls in den Bericht aufgenommen.

Neben dem Reaktor FR2 und dem Zyklotron, den wesentlichen Forschungseinrichtungen des Kernforschungszentrums Karlsruhe, wurden die Neutronenstrahleinrichtungen am Hochflußreaktor in Grenoble für einen Teil der beschriebenen Arbeiten benutzt. Das Institut unterstützt auch externe Benutzer der Neutronenstrahleinrichtungen am Reaktor FR2. Arbeiten, die zusammen mit externen Gruppen durchgeführt wurden, wurden deshalb ebenfalls in den Bericht aufgenommen.

Von den Arbeiten, die bereits veröffentlicht bzw. zur Veröffentlichung vorbereitet sind, werden nur Kurzfassungen oder Literaturhinweise angegeben. Erste Ergebnisse von laufenden Arbeiten werden dagegen ausführlicher beschrieben. Diese Ergebnisse sollten nur mit Erlaubnis der Autoren zitiert werden.

C O N T E N T S

1. INVESTIGATIONS ON THE DYNAMICS OF SOLIDS AND LIQUIDS

1.1. INVESTIGATIONS ON THE PHONON DISPERSIONS

1.1.1 Phonon Dispersions in BiSb Alloys

B. Hofmann

The semimetals Bismuth and Antimony can be alloyed at any ratio to form solid solutions. In the concentration range $0.07 \leq x \leq 0.4$ $Bi_{1-x}Sb_x$ alloys are semiconductors. This behaviour can be explained by the descending of the T-point valence band relative to the L-point conduction band /1/, /2/.

Therefore phonon dispersion measurements on BiSb alloys are of special interest to study, how lattice dynamics is influenced by changes in the electronic band structure. The experiments described here are carried out by the inelastic neutron scattering technique, which requires single crystals. One sample with about 8 at % Sb could be purchased by Monocrystals Company. Another single crystal with 18 to 20 at % Sb was grown by B. Scheerer using Bridgman's method in the crystal growing apparatus of our institute.

By subsequent annealing close to the melting temperature of Bi stresses are reduced and homogenity is increased. In this way the mosaic spread of Scheerer's sample could be improved from 0.9° to 0.5°.

The Sb concentration of the alloys was determined by chemical analysis, elastic neutron and x-ray scattering. Diffraction techniques can be applied, because the lattice parameters vary linearly over a wide range of concentration $(0 \leq x \leq 0.3)$ /3/.
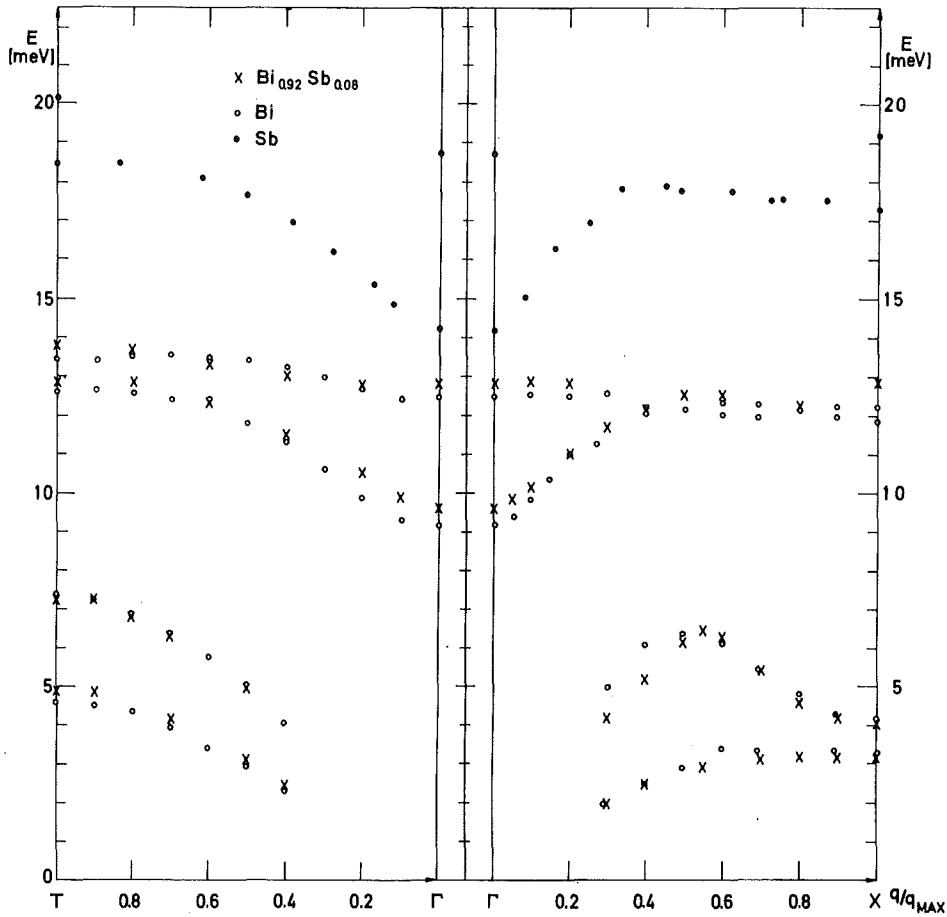
Fig. 1

The small size of the samples and the complicated trigonal-rhombohedral structure of BiSb with two atoms per unit cell require a good knowledge of the inelastic structure factors. These have been calculated with a computer program using the polarisation vectors $\varepsilon_K(\vec{q})$ for Bi /4/. There is qualitative agreement with the experimental results.

Using the phonon density of states for Bi /4/ the vibrational energy of localised modes of Sb in a Bi matrix has been calculated /5/. We get $E_{LM} = 14.4$ meV. So far the resolution was not sufficient to check this result experimentally.

Fig. 1 shows some experimental data on the phonon dispersion curves of a BiSb alloy containing 8 at % Sb. Measurements were performed in the symmetry directions ΓX and ΓT in the mirror plane. The optical phonons were scanned at T = 80 ^{O}K, while the acoustical branches were measured

at room temperature. For comparison the phonon dispersions of Bi /6/, /7/ and Sb /8/ are shown, too. It can be seen that the difference between the alloy data and Bi dispersions is q - dependent. At the X- point the deviation is 12 % of the energy difference between Bi and Sb dispersions. It is thus larger than the Sb - concentration of the BiSb alloy (8 %).

Measurements at T = 80 $^{\circ}$K of the acoustical branches and with other alloy samples are continued.

References

/1/ A. L. Jain, Phys. Rev. 114 (1959), 6

/2/ B. G. Martin, L. S. Lerner, Phys. Rev. B6, 8 (1972), 3032

/3/ P. Cucka, C. S. Barret, Acta Cryst. 15 (1962), 865

/4/ J. Salgado, Thesis, Universität Karlsruhe, 1974

/5/ Nicklow et al., IAEA Symposium (1968), 47

/6/ R. E. Macfarlane, Preprint of the Los Alamos Scient. Lab.

/7/ Yarnell et al., IBM J. Res. Rev. 8 (1964), 234

/8/ Sosnowski et al., IAEA/SM - 155 (1972)

1.1.2   Lattice Dynamics of NiO

W. Reichardt

The phonon dispersion relation of NiO at room temperature is currently being investigated on both TAS- and TOF-spectrometers at the FR2. The sample is a single crystal of approximately 5 cm^3 grown by the flame fusion technique (Koch Light Lab.). The black colour of the sample indicates, that the sample is nonstoichiometric with an excess of oxygen.

So far the investigations have been concentrated mainly on the acoustic branches (fig. 2). The slopes at the Γ-point are the results of an attempt to determine the elastic constants by extrapolating the measured dispersion
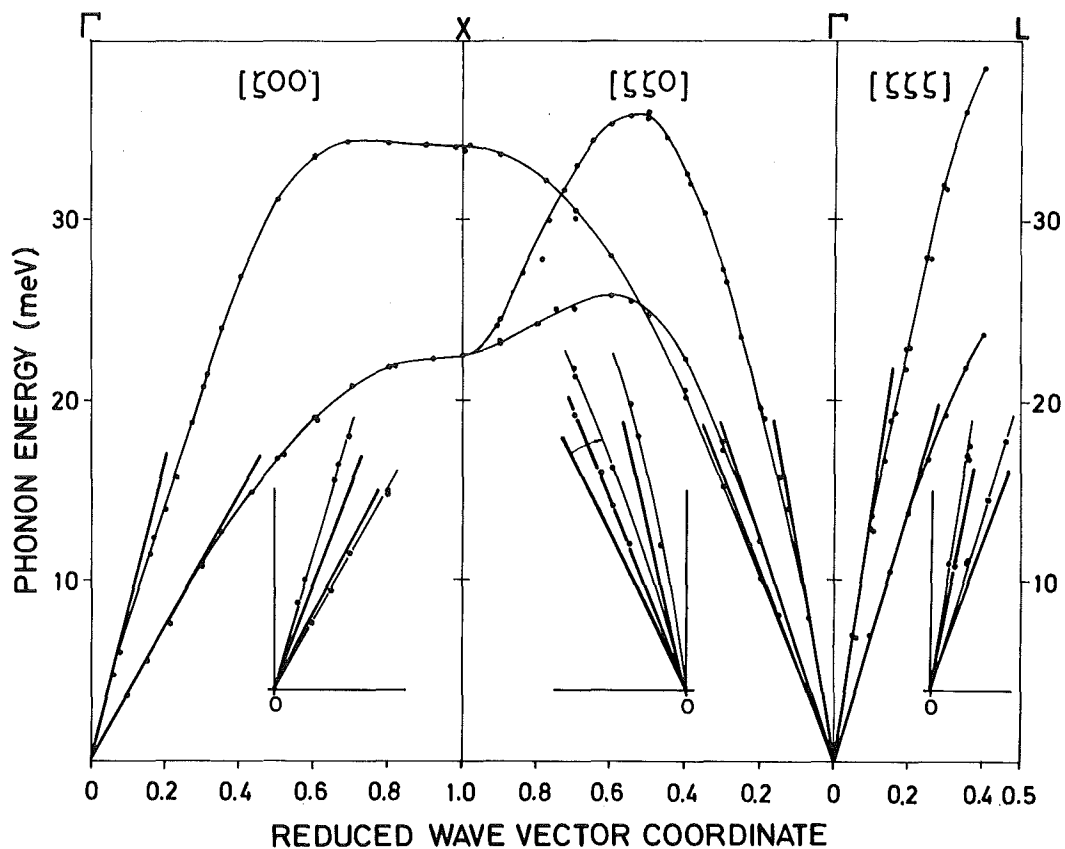
Fig. 2 Acoustic phonons of NiO

curves to q = O. The values of the eleastic constants are given in table 1. These values differ considerably from those obtained by ultrasonic measurements /1/ which are listed in the same table. So far we have no satisfactory explanation for this discrepancy.

Table 1 {units 10^{12} dyn cm^{-2}}

	c_{11}	c_{12}	c_{44}
this work	5.0	2.4	1.0
du Plessis	2.23	0.93	1.10

The slopes of the dispersion curves at Γ as determined from the ultrasonic data are shown in the inserts of fig. 2.

Some results have been obtained for the optic branches with $\hbar\omega_T(\Gamma) = 48.5$ meV compared to 44 meV /2/ and 49.2 - 50.2 meV /3/ determined by infrared measurements.

It is intended to complete the room temperature measurements (in colla-
boration with W. Kress, München and V. Wagner, Würzburg) and to study the
temperature dependence of the low frequency part of the dispersion relation
especially near the Néel-temperature.

References

/1/ P. de V. du Plessis et al., J. Phys. C4 (1971), 1983

/2/ R. Newman and R. M. Chrenko, Phys. Rev. 144 (1959), 1507

/3/ P. I. Gielisse et al., Journal of Applied Physics 36 (1965), 2446

1.1.3   Messung der Phononendispersion in α-Al_2O_3 (Saphir)
         durch inelastische Neutronenstreuung

H. Bialas und H. J. Stolz

Institut für Angewandte Physik der Universität Heidelberg

Al_2O_3 eignet sich wegen seiner geringen elastischen Anisotropie und wegen
seiner hohen Grenzfrequenzen sehr gut für das Studium der Ausbreitungs-
eigenschaften hochfrequenter Phononen durch Phononenstrahlexperimente /1/.
Zur quantitativen Beschreibung dieser Experimente ist die Kenntnis der
Phononendispersion des Ausbreitungsmediums unerläßliche Voraussetzung.

Die Neutronenstreueigenschaften von Al_2O_3 sind sehr günstig ($\sigma_{absorp.} \approx 0$,
$\sigma_{ink.} \approx 0$), dagegen ist die Kristallstruktur vergleichsweise kompliziert.
Seine Raumgruppe ist $R\bar{3}c$ (D_{3d}^6). Die rhomboedrische Elementarzelle hat die
Gitterkonstante a = 5.13 Å und den Basiswinkel α = 55.3 $^\circ$. Sie enthält
2 Al_2O_3 - Gruppen bei (OOO) und ($\frac{111}{222}$) in rhomboedrischer Indizierung. Es
treten deshalb 30 Dispersionszweige auf, die bis zu 27 THz reichen. Die
beiden Al_2O_3 - Gruppen in der Elementarzelle sind um 60 $^\circ$ gegeneinander
gedreht. Sieht man von dieser Drehung ab, so kann man die Struktur auch
durch eine quasikubische Elementarzelle mit nur einer Al_2O_3 - Gruppe be-
schreiben. Diese Elementarzelle ist nur halb so groß wie die rhomboedrische.
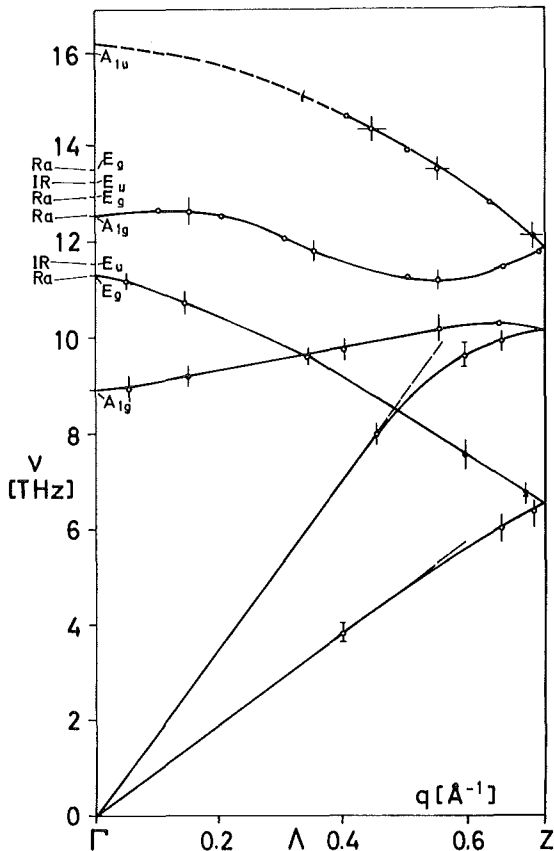
Fig. 3 Phononendispersion von

Al_2O_3 in c-Richtung.

Das Spektrum reicht bis

27 THz. Es sind 6 von

insgesamt 20 Zweigen

eingezeichnet.

Die Messungen wurden an den Drei-Achsen-Spektrometern des R6- und des C3-Kanals und am Flugzeitspektrometer des R7-Kanals durchgeführt. Die Einfallsenergien waren 69 meV mit (00.4)-Graphit, 85 meV mit (00.4)-Graphit und 72 meV mit (311)-Cu, respektive. Fig. 3 zeigt das Ergebnis der Messungen in c-Richtung, der (dreizähligen) Hauptsymmetrierichtung. Von den 30 Zweigen sind 10 zweifach entartet, so daß hier 20 Zweige zu erwarten sind. Von diesen sind 13 optisch aktiv (6 infrarot- und 7 Raman-aktiv). Die 6 niedrigsten optisch aktiven Moden sind mit eingezeichnet. Die zu den optisch inaktiven Moden A_{2g} und A_{1u} gehörenden Zweige wurden jenseits der Zonengrenze ($q_{max} \leq q \leq 2q_{max}$) gemessen, wodurch die kubische Überstruktur nachgewiesen wurde.

References

/1/ P. Herth, O. Weis "Experimente zur thermischen Phononenstrahlung in Saphir- und Quarz-Einkristallen", Acustica 21 (1969), 162

1.1.4 Zero Sound in RbJ

A. Loidl and J. Daubert

Institut für Kernphysik der Universität Frankfurt

The theory of anharmonic interactions of phonons predicts two modes of propagation of sound waves in ionic crystals. At low frequencies known as the first sound region, the applied frequency Ω is less than the inverse lifetime Γ of most of the thermal phonons in the crystal. Zero sound, with $\Omega > \Gamma$, is the opposite case. Theoretical investigations predict differences between zero and first sound elastic constants of alkali halides of about 10 % at 300 K /1/.

Experimentally first sound velocities are determined with ultrasonic techniques, while inelastic neutron scattering covers the zero sound region. Measurements of phonon dispersion in RbJ at 80 K (2) show discrepancies of approximately 10 % for c_{11} and 30 % for c_{12} and c_{44} in comparison with ultrasonic results /3, 4, 5/.

We performed inelastic neutron scattering measurements in the zero sound region to determine absolute differences at room temperature. The experiment was carried out at the research reactor FR2, using a time-of-flight spectrometer with a pseudostatistical chopper (6). The LA branch in $[00\zeta]$ direction and the LA and T_2A branches in $[0\zeta\zeta]$ direction were measured. In addition we investigated the dispersion in off-symmetry directions. Altogether about 100 phonons with reduced wave vectors less than 0.3 in units 2π/lattice constant have been determined. The observed neutron groups have been corrected for a) transformation from a time to an energy scale b) variation of the neutron-scattering cross section across the energy spread and c) vertical divergence.

The fig. 4 shows the experimental results for the phonon-dispersion in off-symmetry directions. Assuming linear dispersion, for representation, all off-symmetry phonons with wave vectors $0.1 \leq q \leq 0.2$ were normalized to $q = 0.1$ in units 2π/lattice constant. The measured phonon energies (ϕ) are compared with Haussühl's ultrasonic results (3) (——) and with our numerical
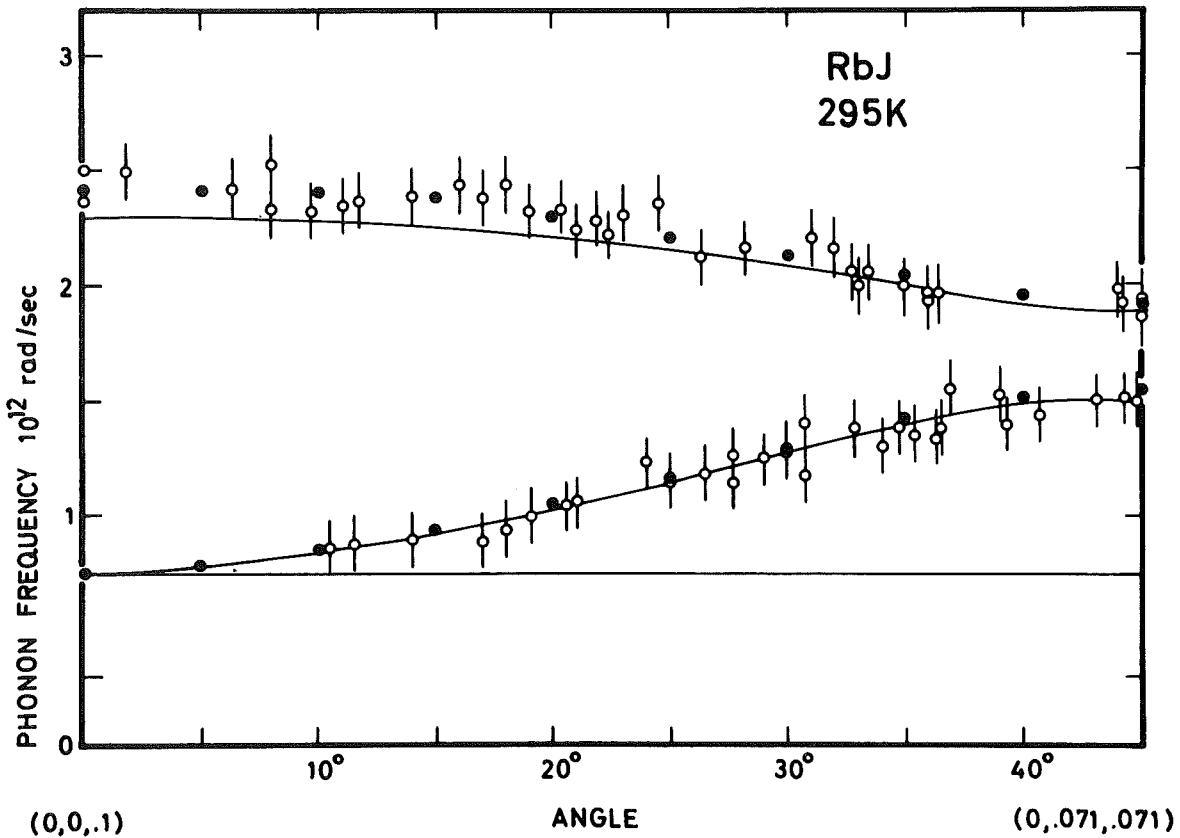
Fig. 4

calculation (o) based on the theory of Cowley /1/ and Niklasson /7/ including a breathing shell model for the lattice dynamics and realistic microscopic Grüneisen parameters for the third order coupling /8/. There are significant deviations near the $[00\zeta]$ direction in the LA branch, while zero and first sound are very close and within experimental error near $[0\zeta\zeta]$ LA. The deviations are within the error bars over the whole range of the T_2A branch.

References

/1/ R. A. Cowley, Proc. Phys. Soc., 90 (1967), 1127

/2/ G. Raunio and S. Rolandson, Phys. Stat. Sol. 40 (1970), 749

/3/ S. Haussühl, Z. Physik 159 (1960), 223

/4/ K. Reinitz, Phys. Rev. 123 (1961), 1615

/5/ J. T. Lewis, A. Lehoczky and C. V. Briscoe, Phys. Rev. 161 (1967), 877

/6/ F. Gompf, W. Reichardt, W. Gläser, and K.-H. Beckurts, Neutron Inel. Scatt. II (IAEA Vienna 1968) p. 417

/7/ G. Niklasson, Phys. kondens. Materie 14 (1972), 138

/8/ H. Jex, Phys. Stat. Sol. (b) 62 (1974), 393

1.1.5 Investigations of the Linear Conductor

$K_2Pt(CN)_4Br_{0.3} \cdot 3D_2O$ by Elastic and Inelastic Neutron Scattering

A main part of the experimental work deals with the giant Kohn anomaly, the Peierls distortion and the gradual development of a 3-d phase at lower temperatures. Most of the results have been published in two papers. Their abstracts are given below.

1. B. Renker, H. Rietschel, L. Pintschovius, W. Gläser, P. Brüesch, D. Kuse and M. J. Rice, Phys. Rev. Lett. 30 (1973), 1144

Abstract

Longitudinal acoustic phonons have been measured by coherent inelastic scattering in the direction of the platinum chains of a single crystal of the one-dimensional conductor $K_2Pt(CN)_4Br_{0.3} \cdot 3H_2O$ at room temperature. The phonon dispersion curve shows a pronounced anomaly at the phonon wave number $q_o = 0.32 \; \overset{o}{A}^{-1}$ and is interpreted as the logarithmic Kohn anomaly characteristic of a one-dimensional metal.

2. B. Renker, L. Pintschovius, W. Gläser, H. Rietschel, R. Comès, L. Liebert and W. Drexel, Phys. Rev. Lett. 32 (1974), 836

Abstract

A study of the temperature dependence of the $2k_F$ instability in the one-dimensional (1-d) conductor $K_2Pt(CN)_4Br_{0.3} \cdot 3D_2O$ using neutron scattering technique is reported. Whereas the extra scattering at room temperature has a 1-d character corresponding to a periodicity along the c axis of 6.66 c (where c is the Pt-Pt spacing), below 220 K it indicates the gradual development of a 3-d superlattice structure with a new unit cell 2a x 2a x 6.66 c. However, this transition seems to be incomplete, in the sense that the coupling between adjacent chains does not achieve long range order down to 6 K. Details of the temperature dependence of the $2k_F$ scattering are discussed.

Further investigations concerning temperature dependent inelastic neutron measurements are in progress. Measurements of the phonon dispersion at 90 K have almost been finished. Additional measurements of the temperature dependence of the $2k_F$- mode at $\hbar\omega \neq o$ as well as high resolution measurements at $\hbar\omega = o$ are carried on in cooperation with groups at Orsay and Grenoble.

Theoretical Investigations of Linear Conductors

1. H. Rietschel, Solid State Commun. 13 (1973), 1859

Abstract

It is shown that the "giant Kohn phonon anomaly" which is characteristic of a one-dimensional metal may also be found in a Peierls semiconductor. A simple model reflecting roughly the LA-phonon dispersion of $K_2Pt(CN)_4Br_{0.3} \cdot 3H_2O$ has been used to get numerical results.

2. H. Rietschel, Solid State Commun. 14 (1974), 699

Abstract

Using a diagrammatic expansion we investigate the cubic and quartic anharmonicities of a one-dimensional metal. They are shown to exhibit a pronounced resonance structure around the q-point where a Kohn anomaly occurs. A free electron model has been used to get numerical results.

1.1.6   Anharmonic Effects in Solids

W. Mehringer

The use of Bogolubov's hierarchy equations, containing a statistical description of classical many particle systems, may provide a new and convenient approach to anharmonic problems in condensed matter at high temperature, especially solids. This was demonstrated in a treatment of a model system, the classical hard core solid in thermal equilibrium. Neglecting anisotropic effects, a Gaussian approximation was used for the one particle probability density $f_1^{(j)}(\vec{x}_j - \vec{s}_j, \vec{p}_j)$ of particles (j) at lattice points $\vec{s}_j$. Approximate (isotropic) expressions for the equation of state in terms of f_1 and f_2 were derived. From a factorizing approximation of f_2 according to $f_2^{(j,1)}(\vec{x}_j,\vec{p}_j,\vec{x}_1,\vec{p}_1) \simeq f_1^{(j)}(\vec{x}_j,\vec{p}_j) f_1^{(1)}(\vec{x}_1,\vec{p}_1) \phi(|\vec{x}_j - \vec{x}_1|)$, with ϕ describing the hard core correlations, an accuracy of about 30 % was obtained in the description of the equation of state. An accuracy of about 10 % was obtained from a renormalization procedure.

1.2 INVESTIGATIONS ON THE SCATTERING LAW OF SOLIDS AND LIQUIDS

1.2.1 The Phonon Density of States of Vanadium

P. Schweiß

The aim of this experiment was to test the time-of-flight spectrometer TOF1 at the thermal beam tube R7 at the FR2 Karlsruhe after the installation of a straight slit Fermichopper.

The measurements have been made at room temperature and at liquid nitrogen temperature. The latter was performed to study background effects of the cryostat walls and to reduce multiphonon processes. To reduce the multiple scattering corrections, the transmission of the sample was 86 % and the sample was intersected by gadolinium foils. The incoming energy was 65.1 meV,
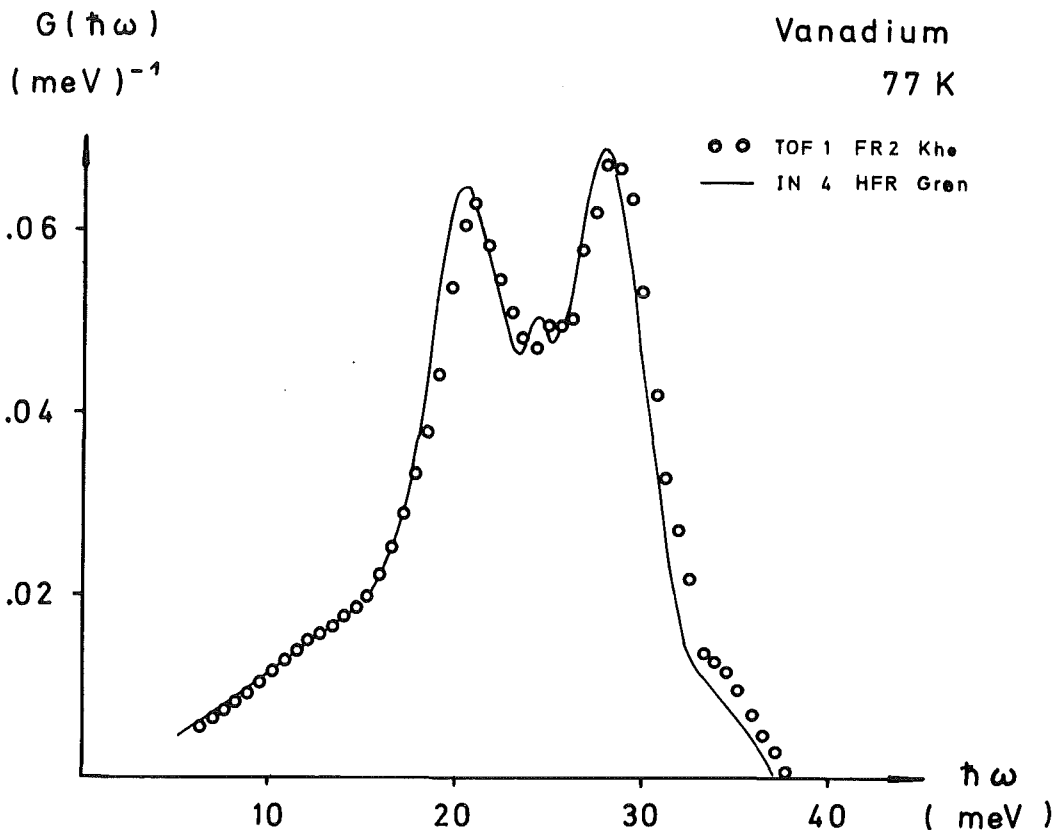
Fig. 5

the neutrons were scattered to lower energy. The momentum transfers were between 3 and 10 $\overset{o-1}{A}$. From the time-of-flight spectra the double differential scattering cross section and the scattering law were calculated. The density of states was determined by the extrapolation method of Egelstaff and Schofield. The results are corrected for multiple scattering but not for instrumental resolution. A comparison of this measurement (open circles in fig. 5) with a recent measurement (full line, Schweiß and Drexel, 1973, to be published) shows a good agreement in the shape of the spectra. The discrepancy of 2 % in the energy scale is not yet understood.

This evaluation suggests, that a) the high energy tail, found by several experimentalists and not to be expected for bcc metals, and b) the peak at 8 meV, shown in some experiments and interpreted as a Kohn anomaly, are due to an incomplete multiphonon correction.

1.2.2   The Phonon Density of States of V_3Si at Different Temperatures

P. Schweiß

The intermetallic A-15 compounds are of special interest because of their high T_c for superconductivity. It is well established that T_c depends sensitively on the form of the phonon density of states.

As V_3Si scatters predominantly incoherent one can determine a generalized density of states directly from the scattering law by an extrapolation method proposed by Egelstaff /1/. As the ratio $\frac{\sigma}{M}$ is almost identical for the two components this generalized density of states is very close to the true density of states. The measurements were made at several temperatures (296 K, 77 K, 4.2 K) in order to see how the well known anomalous temperature dependence of the elastic constants /2/, /3/, /4/ is reflected in the phonon density of states. The scattering law measurements were performed on the IN4 time-of-flight spectrometer at the HFR Grenoble. They are the
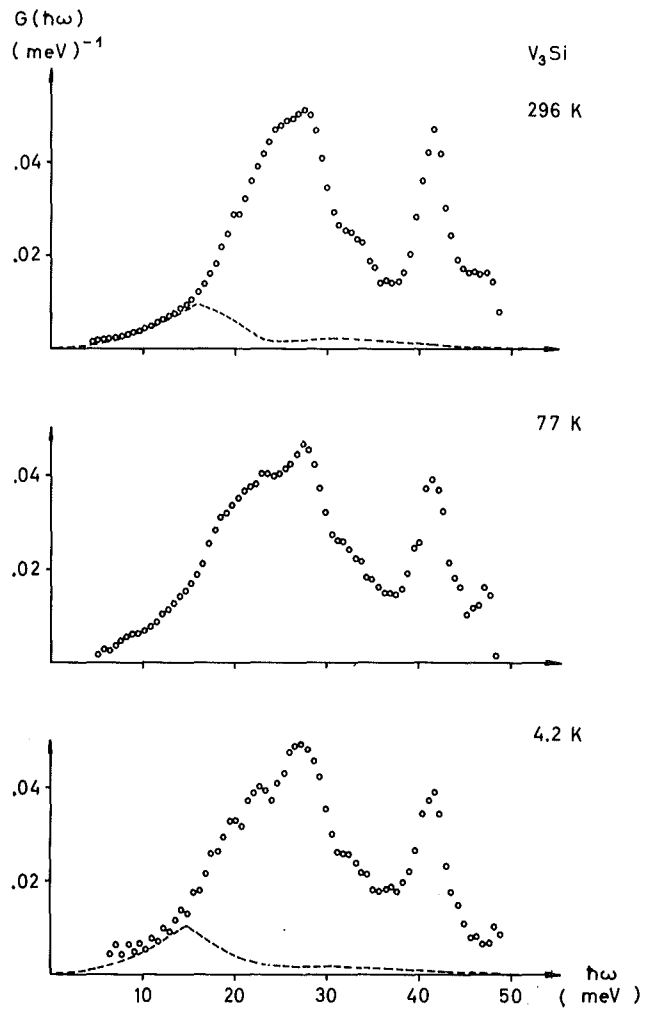
Fig. 6
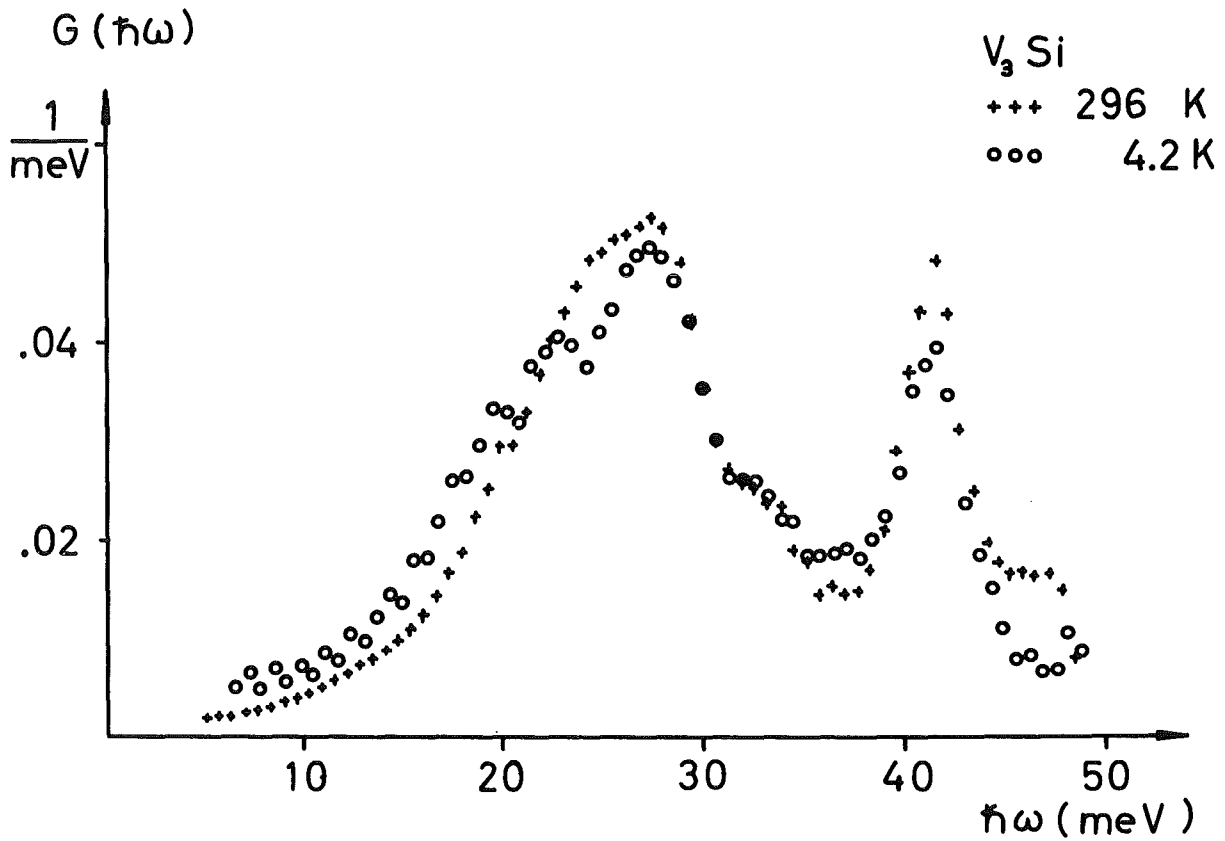
Fig. 7

continuation of investigations in Vanadium-based A-15 compounds at room temperature, which have been started on the TOF1 spectrometer at the FR2 Karlsruhe. The liquid He temperature experiment was carried out in collaboration with W. Drexel (ILL). Because of the thermal occupation factor and in order to improve the resolution we measured in the down scattering mode.

The incoming energy was 60 meV, the momentum transfers were between 2 and 10 $\overset{o}{A}^{-1}$. Choosing a special sample geometry multiple scattering was reduced. No corrections for instrumental resolution are applied to the data. In the spectra we distinguish two regions. It is suggestive to attribute the broad distribution around 25 meV to the vibrations of the Vanadium and the high frequency peak to the vibrations of the lighter silicon atoms. The pronounced differences which occur on cooling in the range below about 27 meV (fig. 7) are produced by softening of special phonon modes. From the elastic constants and the neutron scattering data of the low frequency part of a few acoustic branches /4/, Testardi has tried to estimate the densities of acoustic states for two temperatures. These are drawn in fig. 6 in broken lines. The rest, 21/24 of the area, contains the optical modes; up to now there are no data available of their dispersion curves. The acoustical shear mode in 110 direction which show the strongest softening among the acoustical modes extends up to about 20 meV. As in addition the contribution of the acoustic modes to the density of states becomes extremely small above 20 meV it is suggestive to assume that there is also a considerable softening of optical branches.

The mean square frequency is shifted from 27.6 meV at room temperatures to 25.7 meV at liquid He temperature. Assuming a constant $\alpha^2(\omega)$ this shift enhances the electron phonon coupling constant by 13 %.

References

/1/ Egelstaff, P. A. "Inelastic Scattering of Neutrons in Solids and Liquids". IAEA, Wien (1961) 25

/2/ Testardi et al., Phys. Rev. 154, 2, 399 (1966)

/3/ Testardi and Bateman, Phys. Rev. 154, 2, 402 (1966)

/4/ Shirane et al., Solid State Communications 9, 397 (1971)

1.2.3   The Phonon Density of States of Nb_3Sn

E. Schneider, V. Tripadus and W. Reichardt

We have performed scattering law measurements on polycrystalline Nb_3Sn with the aim to obtain information about the phonon density of states. By such an experiment only a generalized density of states $G(\omega)$ can be determined which is defined by $G(\omega) = (\frac{\sigma}{M})_{Nb} F_{Nb}(\omega) + (\frac{\sigma}{M})_{Sn} F_{Sn}(\omega)$ whereas the phonon density of states is given by $F(\omega) = F_{Nb}(\omega) + F_{Sn}(\omega)$. However, $G(\omega)$ exhibits the same characteristic features as $F(\omega)$. The cross-section to mass ratio σ/M is 0.071 and 0.041 for Nb and Sn respectively.

The sample was the same that had been used for the structural investigations (see 1.2.4). Measurements at room temperature have been performed on two multidetector time-of-flight spectrometers at the FR2 with incident energies E_o of 5.05 meV and 65.1 meV. So far we have tried to determine the generalized density of states by an experimental sampling method i.e. by averaging the one-phonon cross-section over a large range of scattering angles /1/. Fig. 8 gives a comparison of the two results for E_o = 5.05 meV and E_o = 65.1 meV. No corrections for resolution and multiple scattering contributions have been applied yet. The differences between the two distributions indicate that for E_o = 5.05 meV the sampling volume in q-space is not large enough for a satisfactory determination of $G(\omega)$. By a comparison with results from other A15 compounds we conclude that the high frequency peak at 25 meV is due to vibrations of the tin atoms. This is somewhat surprising as the Sn-atom is heavier that the Nb-atom.

In fig. 9 we compare our results with the tunnelling density of states $\alpha^2(\omega) F(\omega)$ which has been determined by Shen /2/. The overall structure and the peak positions agree very well although there is a stronger weighting of the high frequency part for the neutron data compared to the tunnelling results. If our assumption is correct that the high frequency peak is due to the Sn vibrations the difference between $\alpha^2(\omega) F(\omega)$ and $F(\omega)$ will be even more pronounced. A detailed comparison is not yet possible as the two results have been obtained at different temperatures.
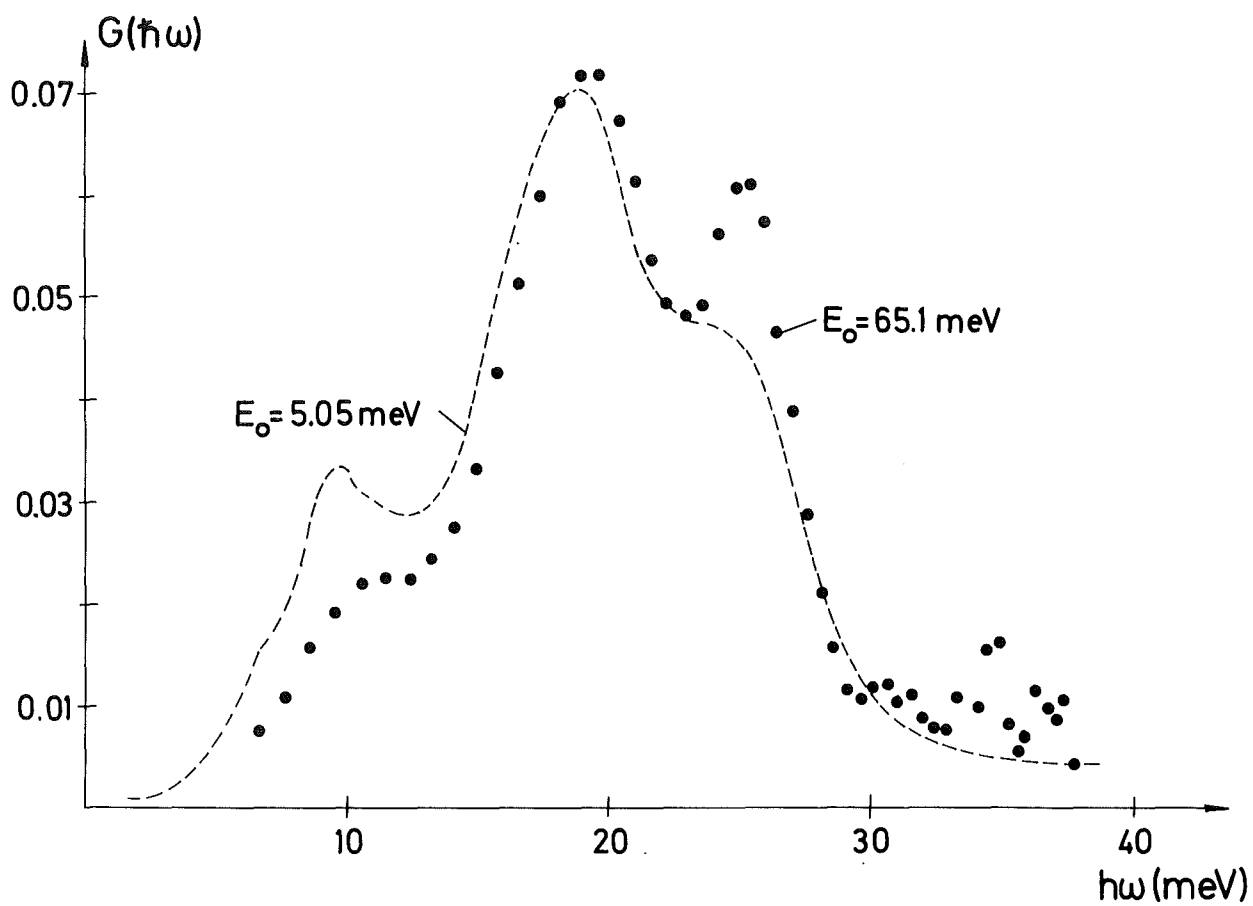
Fig. 8
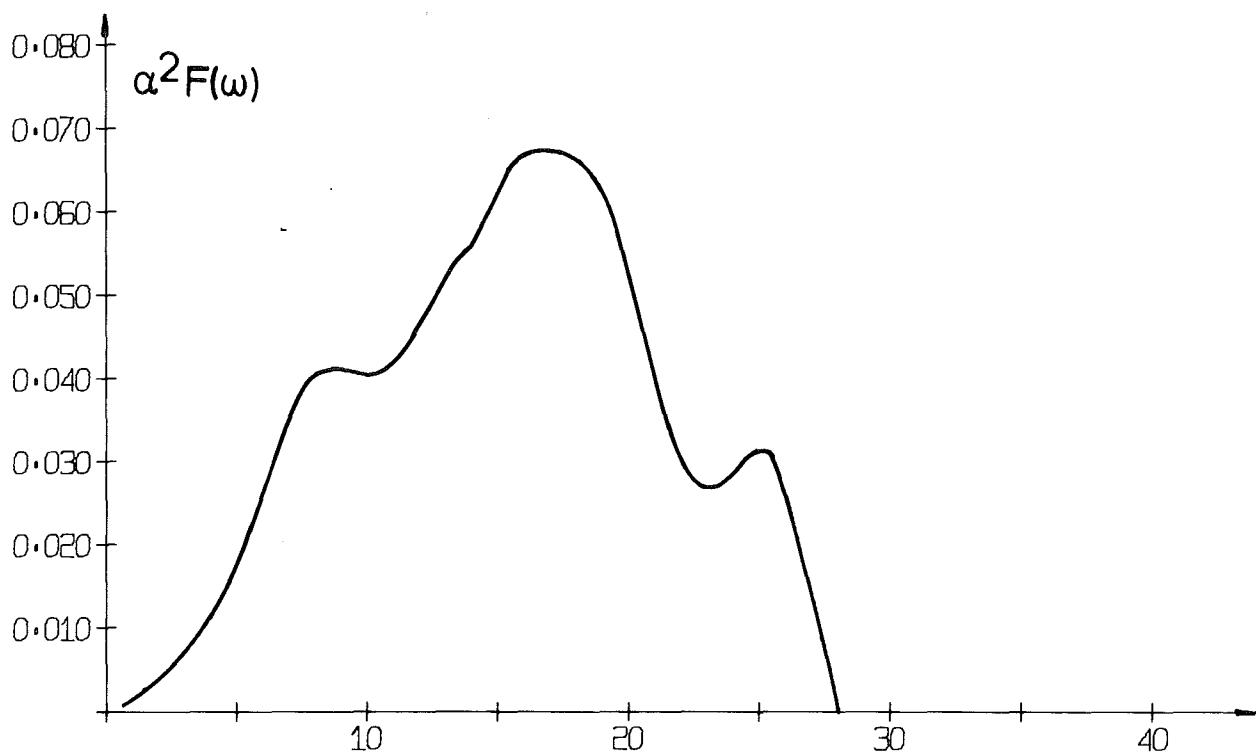
Fig. 9

Measurements at 77 K have just been finished. A preliminary analysis of the data shows a very similar increase of the frequency spectrum at small energy transfers as that observed for V_3Si (see 1.2.2). An experiment to determine the phonon density of states at Helium-temperature is in preparation at the HFR Grenoble.

References

/1/ M. M. Bredov et al., Soviet Physics - Solid State 9, 1 (1967), 214

/2/ L. Y. L. Shen, Phys. Rev. Lett. 29, 16 (1972), 1082.

1.2.4   Lattice Distortion and Superconducting Transition in Nb_3Sn

W. Reichardt, H. Rietschel and E. Schneider

By a heat treatment, we have prepared Nb_3Sn powder samples almost completely transforming from the cubic to the tetragonal phase. The Nb_3Sn powder (manufactured by CERAC) was pressed to pellets of about 2 cm^3 volume and annealed for 22 days at 1400 K under an argon pressure of about 2 atm.

Structure analysis has been performed using a high resolution two axis powder diffractometer with a neutron wavelength of 2.4 Å. We have investigated the | 4, 0, 0 | reflection at 300 K, 77 K and 4 K. At 4 K it is found to be split into 3 lines, a central line which is due to the undistorted cubic fraction of the sample and two outer lines caused by the tetragonality of the distorted Nb_3Sn. Fig. 10 shows the results for 77 K and 4 K. Evaluating
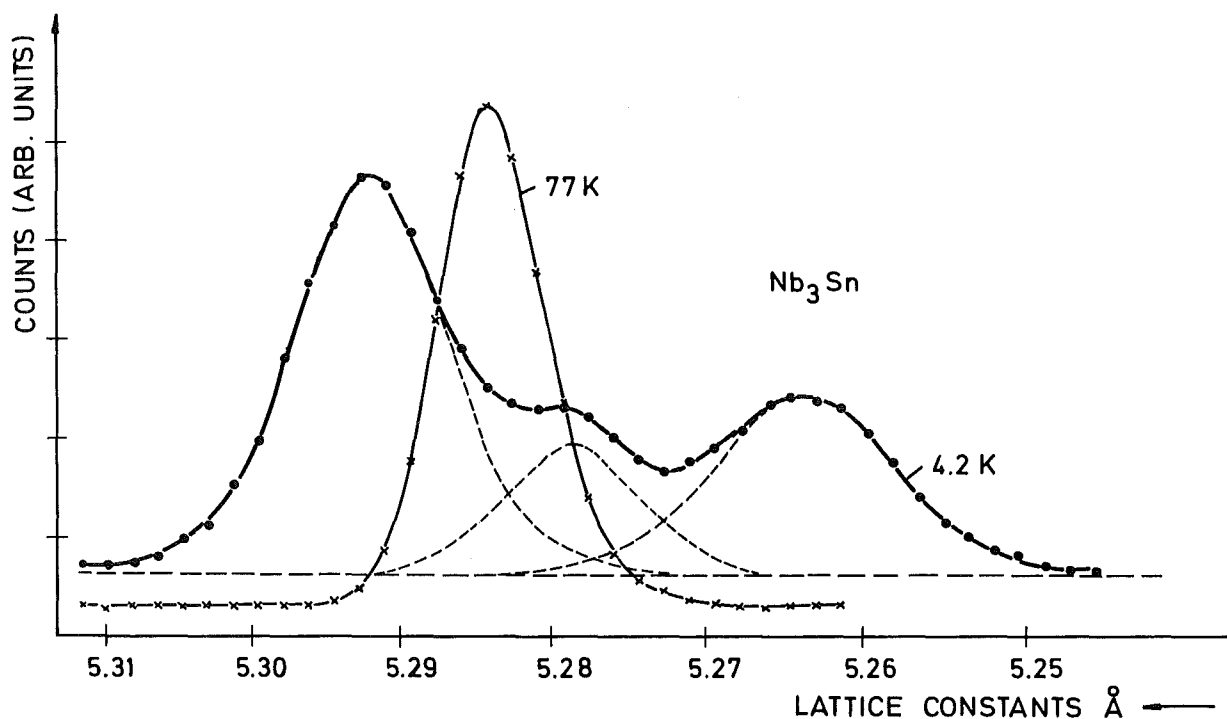
Fig. 10

the 4 K intensities we found the sample to be transformed by a fraction of 82 %. As expected the intensity ratio of the two tetragonal lines is nearly 2. The a/c-ratio was found to be 1.0054 which is slightly smaller than in earlier measurements /1/, /2/.

In addition to the neutron data the specific heat has been measured /3/ on a sample transforming to approximately 50 %. This sample was produced by annealing a Nb_3Sn pellet for only 20 hours. Thus, the superconducting transition temperature could be observed for both, the cubic and the tetragonal phase within the same measurement. The two transitions differ by 0.9 K. We intend to continue our measurements and to investigate the lattice distortion in powdered Nb_3Sn as a function of temperature.

References

/1/   B. W. Battermann and C. B. Barrett, Phys. Rev. 145 (1966), 296
/2/   L. J. Vieland, J. Phys. Chem. Solids 33 (1972), 581
/3/   H. Ch. Schopper, private communications

1.2.5   Direct Measurement of the Phonon Density of States
         of Niobium

F. Gompf and J. Salgado

The phonon density of states $G(\hbar\omega)$ for Nb has directly been determined
with the help of a new method using coherent inelastic neutron scattering
from polycrystalline samples /1/. The experiment was carried out at room
temperature with the double monochromator time-of-flight spectrometer
TOF III at the cold source of the FR2.

In fig. 11 our result is compared with $G(\hbar\omega)$ curves derived from measure-
ments of phonon frequencies with the help of lattice dynamical models.
These $G(\hbar\omega)$ are folded with the resolution of our spectrometer.
Nakagawa and Woods /2/ measured the dispersion relation in symmetry
directions and then used a Born-von Kármán force constant model including
eight neighbors to calculate $G(\hbar\omega)$. Sharp /3/ also measured phonons in
off-symmetry directions and analysed his results with the same model. Pal
and Gupta /4/ applied the Sharma and Joshi three-force constant model
which includes the effect of electrons on the lattice vibrations to
existing dispersion relations.
The Debye-temperature θ_D versus the temperature T curves derived from
these vibration spectra are shown in fig. 12 together with calorimetric
data /5/.

References

/1/ F. Gompf, H. Lau, W. Reichardt, J. Salgado, Neutron Inelastic Scattering
    137, IAEA, Vienna (1972)

/2/ Y. Nakagawa and A. D. B. Woods, Phys. Rev. Letters 11 (1963), 271

/3/ R. J. Sharp, J. Phys. C (Solid State Phys.), 2 (1969), 421

/4/ P. K. Sharma, B. S. Semwal and K. N. Mehrotra, Z. Naturforschung 26a
    (1971), 747

/5/ K. Clusius and P. Franzosini, Z. Naturforschung 17a (1962), 522
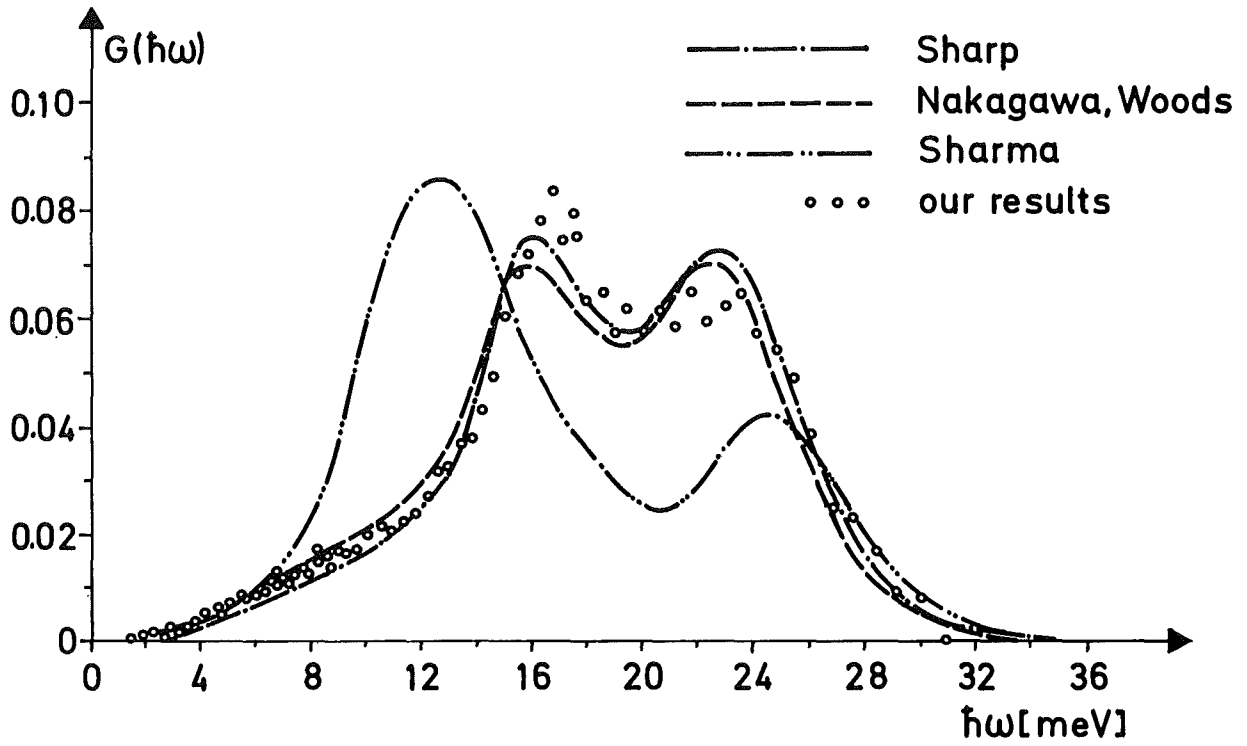
Fig. 11   The Phonon Density of States of Nb in Comparison with Model
          Calculations
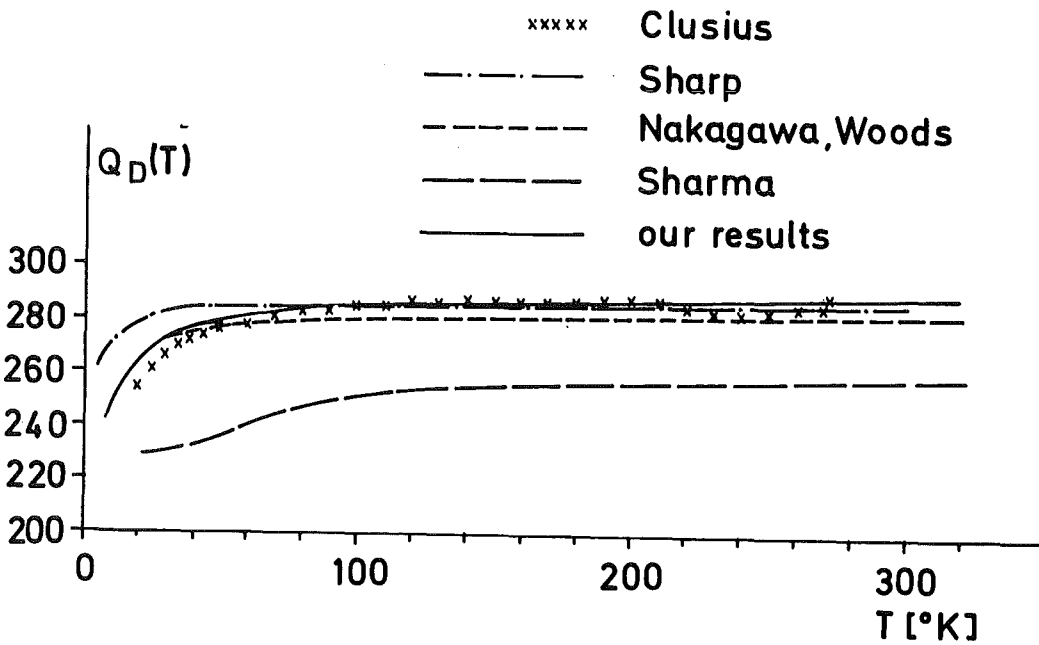
Fig. 12   The Debye Temperature for Nb as a Function of the Temperature

1.2.6 Investigation on the Phonon Density of States of some Transition Metal Carbides and Nitrides

F. Gompf, J. Salgado and W. Reichardt

The monocarbides and nitrides of the transition metals belonging to group IV to VI show a number of unusual features. They have extremely high melting points and are very hard. Their metallic conductivity is comparable to that of their metal component and some of them are high temperature superconductors. From experiments it is known that those compounds having 8 valence electrons (VE) are non-superconductors (T_c < 1.2 K) as for instance TiC, ZrC and HfC and that T_c rises rapidly with the increase of the number of VE as for instance NbC, ZrN, TiN with 9 VE and NbN with 10 VE /1/.

The phonon dispersion curves of some transition metal carbides have already been measured /2, 3/. Measurements of phonon dispersions of transition metal nitrides were not feasable up to now because no appropriate single crystals are available. Whereas the superconductors NbC and TaC exhibited anomalous dips in all the longitudinal acoustic branches and in some of the transvers acoustic branches the non-superconductors ZrC and HfC did not show such anomalies.

We are investigating how the anomalies affect the phonon density of states $G(\hbar\omega)$ for the monocarbides and nitrides with NaCl structure using coherent inelastic neutron scattering from polycrystalline samples (see 1.2.5.). All substances were chemically analysed, their lattice parameters and structure were determined with neutrons and their superconducting transition temperature T_c was measured.

The measurements were performed at the cold source time-of-flight spectrometers TOF II and TOF III and for TiC and TiN also at TOF I with a higher incident energy. The difficulties extracting $G(\hbar\omega)$ from the measured cross section arise mainly because two different atoms in the unit cell contribute with different weight to the scattering. The simplest correction for this can be achieved with the two-atomic linear chain approximation. Due to the large mass difference of the two components this correction works rather well.
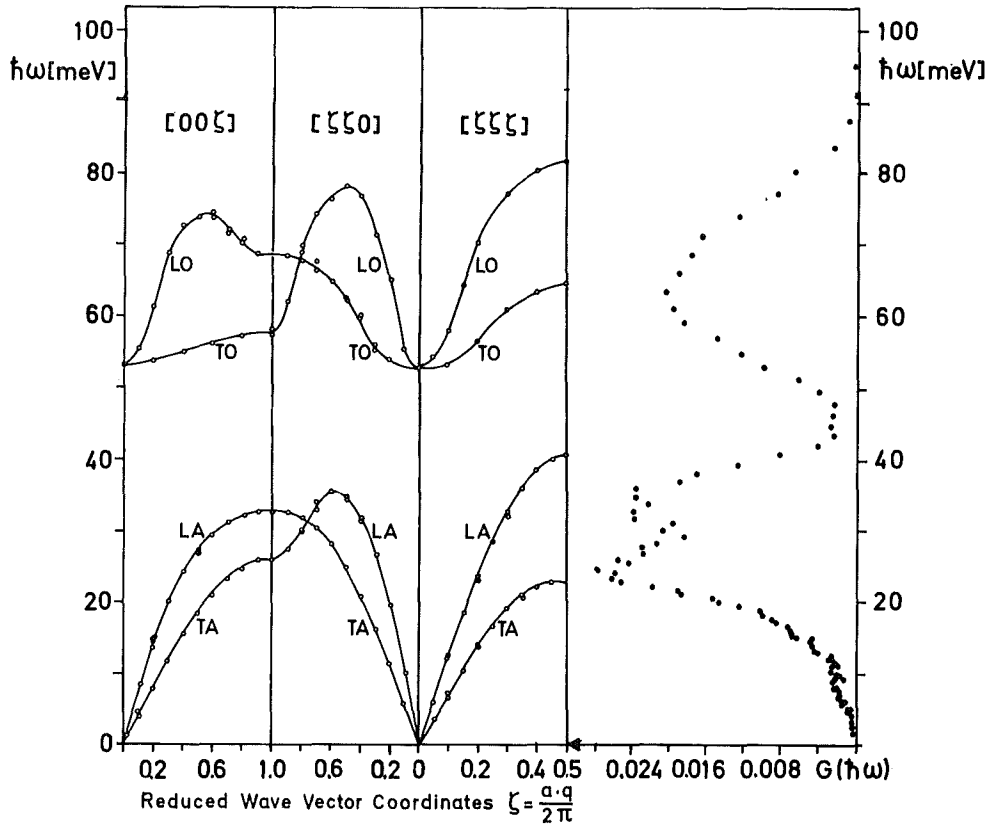
Fig. 13 Dispersion Relation /3/ and Phonon Density of States of ZrC
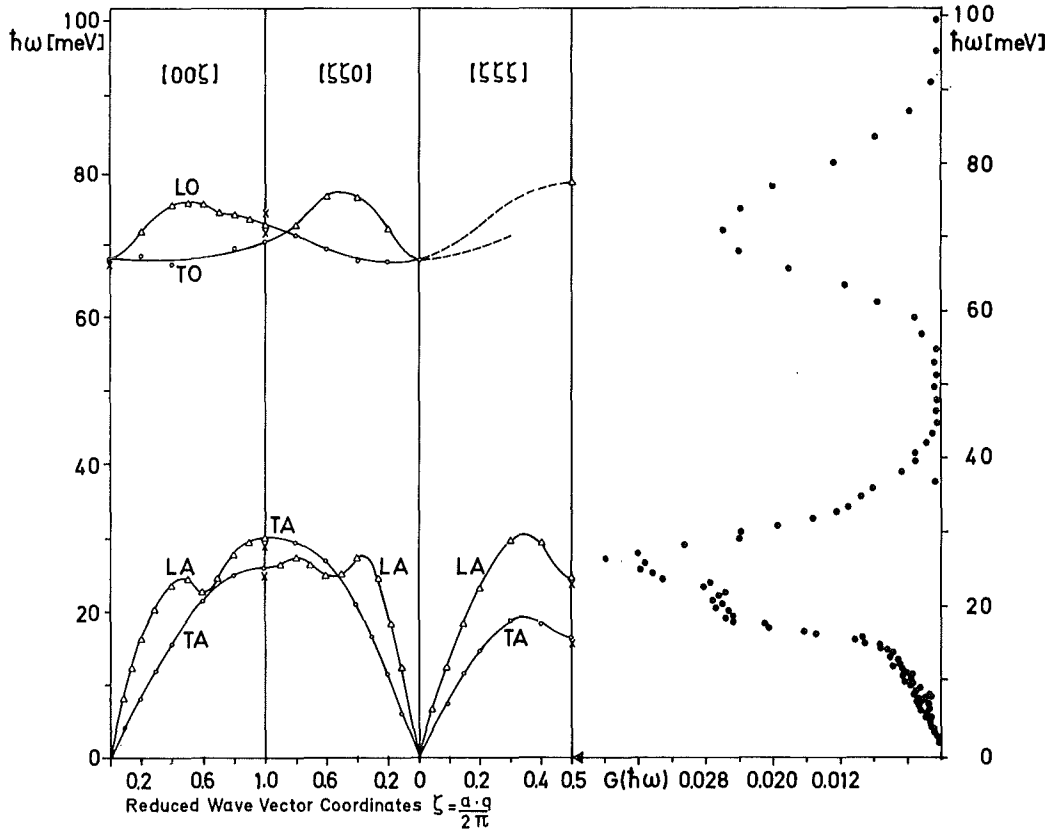
Fig. 14 Dispersion Relation /2/ and Phonon Density of States of NbC
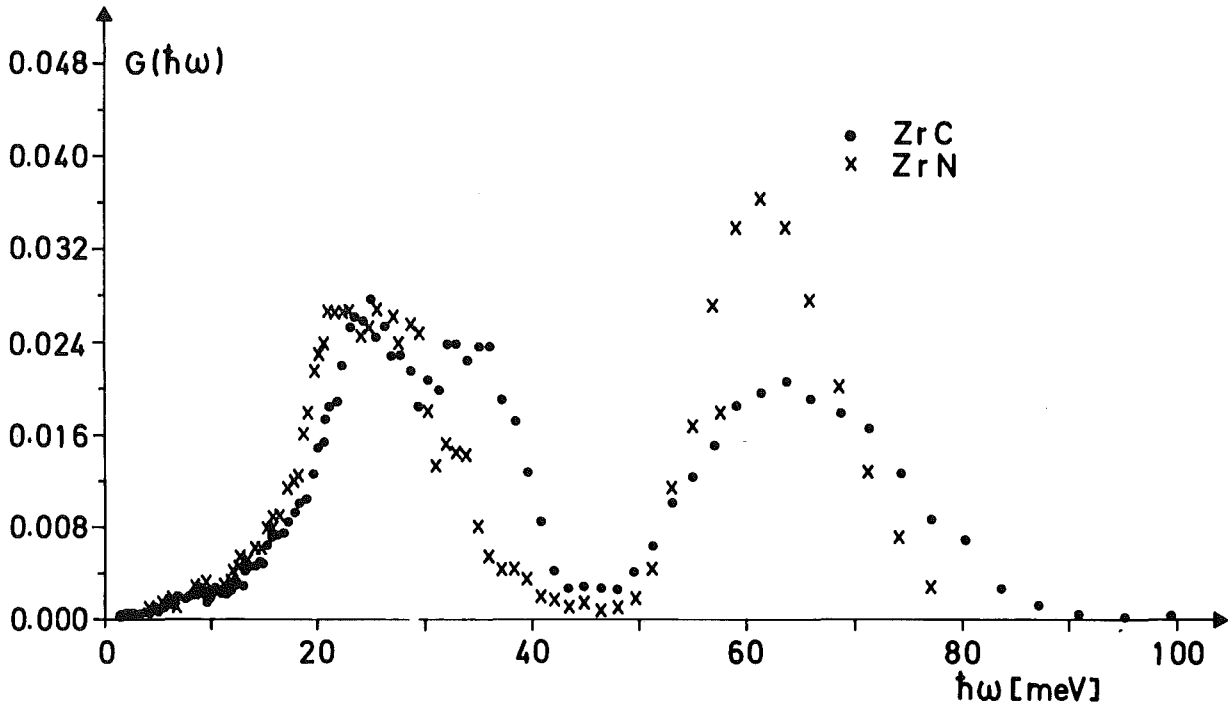
Fig. 15   Comparison of the Phonon Density of States of ZrC (8 VE) with ZrN (9 VE)
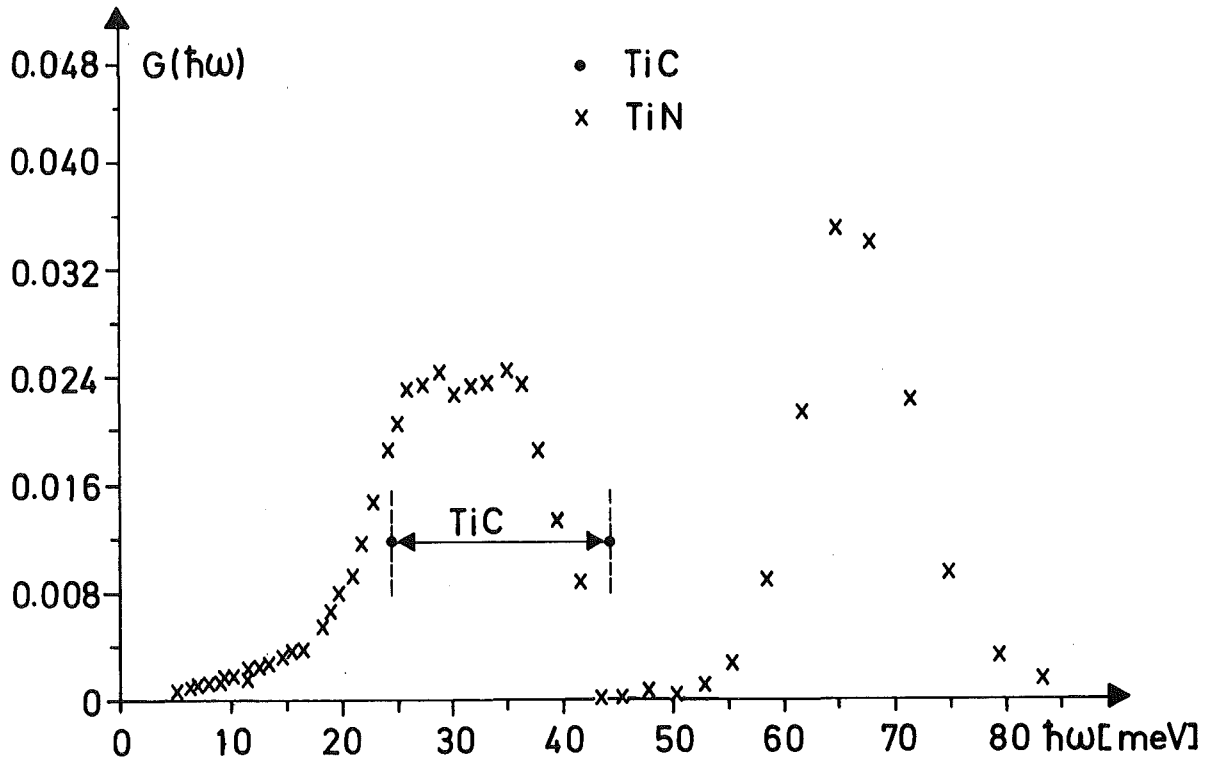
Fig. 16   Phonon Density of States of TiN (9 VE) with Indication of the
           Acoustic "Half width" of TiC (8 VE)

For all measurements the acoustic part of G($\hbar\omega$) is well separated from the optic part and the difference of the two areas is less than 3 to 4 percent. In fig. 13 and 14 we compare results for ZrC and NbC with the dispersion curves /2, 3/. For both materials the acoustic branches are rather similar except for the pronounced anomalies exhibited by the high temperature superconductor NbC. This is reflected in G($\hbar\omega$). The acoustic spectrum for NbC is strongly shifted to smaller frequencies mainly due to the lowering of the longitudinal branches. The less separated optic branches in NbC are probably caused by a smaller negative ionization of the nonmetal and lead to a narrower optical part than for ZrC and also widen the gap to the acoustic contributions.

In fig. 15 to 17 also G($\hbar\omega$) of substances whose dispersion relations have not been investigated are shown. The carbide is always compared with the nitride of the same metal. All of them have in common that with increase of the number of VE the acoustic part of the spectrum is shifted to smaller energies. For TiC the measurements have not been analysed completely but the shift is also clearly seen (indicated by arrows). This suggests that also the nitrides of these transition metals have strong anomalies especially NbN which has 10 VE and a T_c of about 17 K.
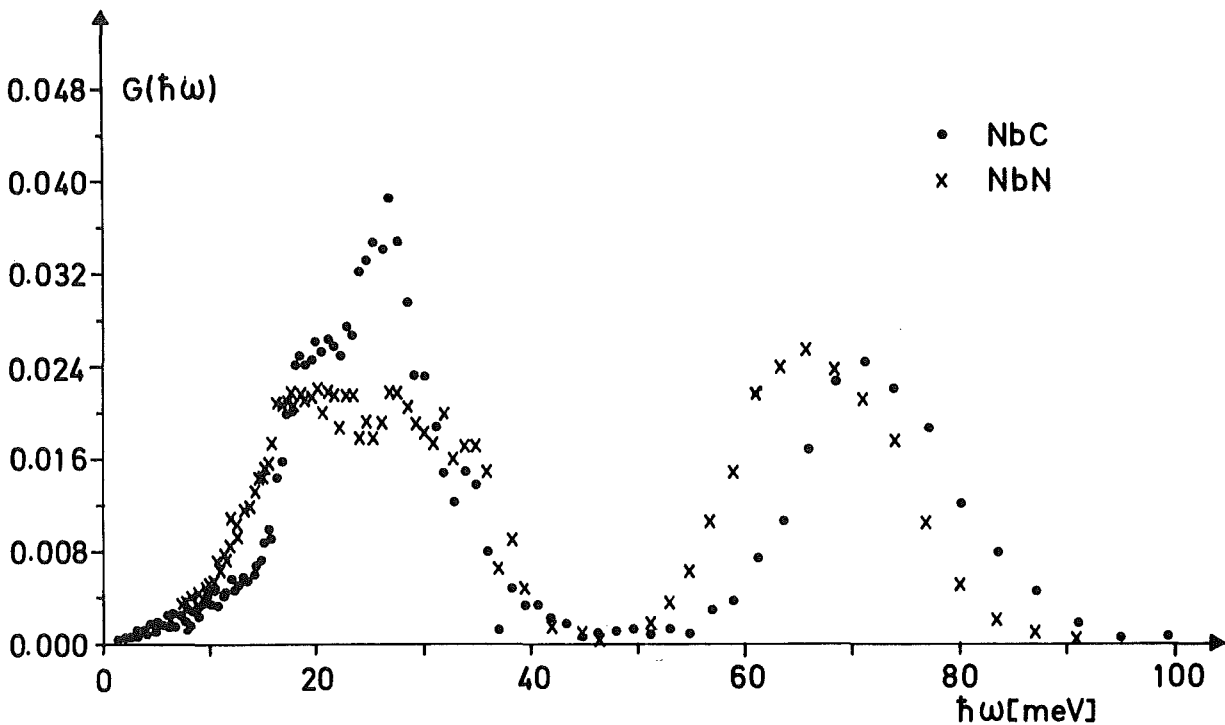
Fig. 17 Comparison of the Phonon Density of States of NbC (9 VE) with NbN (10 VE)

References

/1/ L. E. Toth, Transition Metal Carbides and Nitrides; Academic Press New York and London, 1971

/2/ H. G. Smith and W. Gläser, Phys. Rev. Letters 25 (1970), 1611

/3/ H. G. Smith and W. Gläser, in Phonons, Proc. Int. Conf. in Rennes (ed. M. A. Nusimavici), Flammarion, Paris (1970)

1.2.7   Direct Measurements of the Phonon Densities of States of Arsenic, Antimony and Bismuth

J. Salgado, F. Gompf and W. Reichardt

The semimetals As, Sb and Bi have a rhombohedral structure (A7) with two atoms in the unit cell. For Sb and Bi the dispersion relations have already been measured /1, 2/ but no satisfying lattice dynamical models have been determined. For As phonon frequencies have not been investigated because no appropriate single crystals were available.

The phonon densities of states $G(\hbar\omega)$ for As, Sb and Bi were directly measured with the help of a new method using coherent inelastic neutron scattering from polycrystalline samples /3/. This was done after a simulation of the
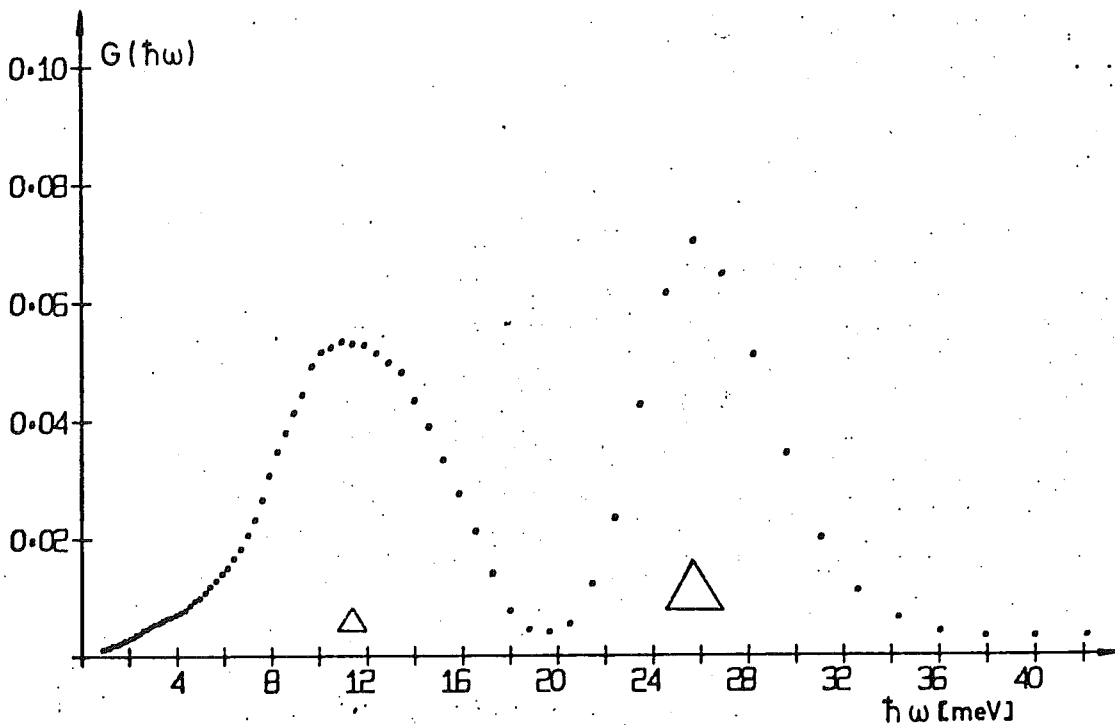
Fig. 18 Phonon Density of States of As
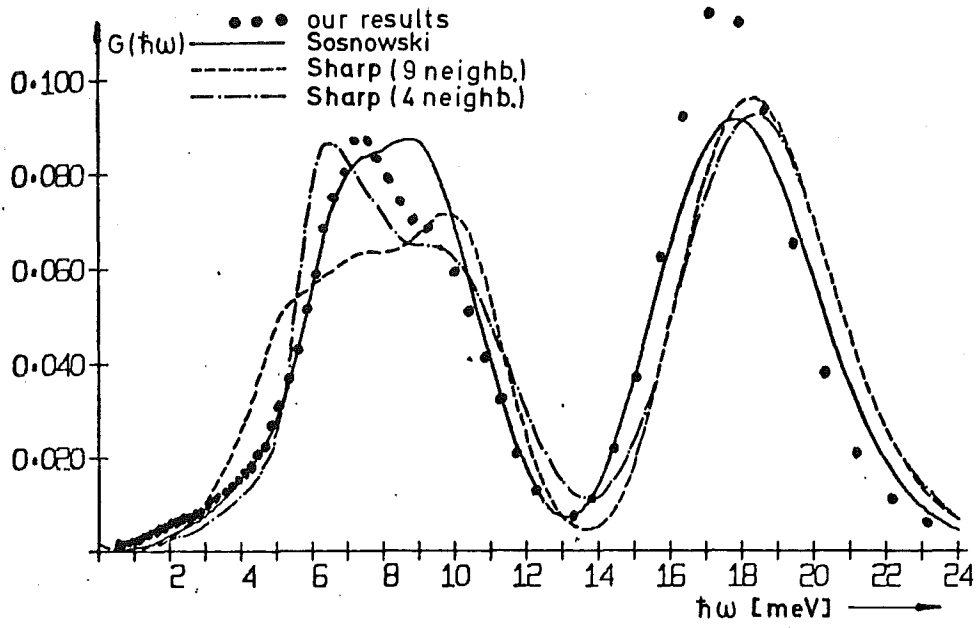
Fig. 19 Phonon Density of States of Sb in Comparison with Model Calculations
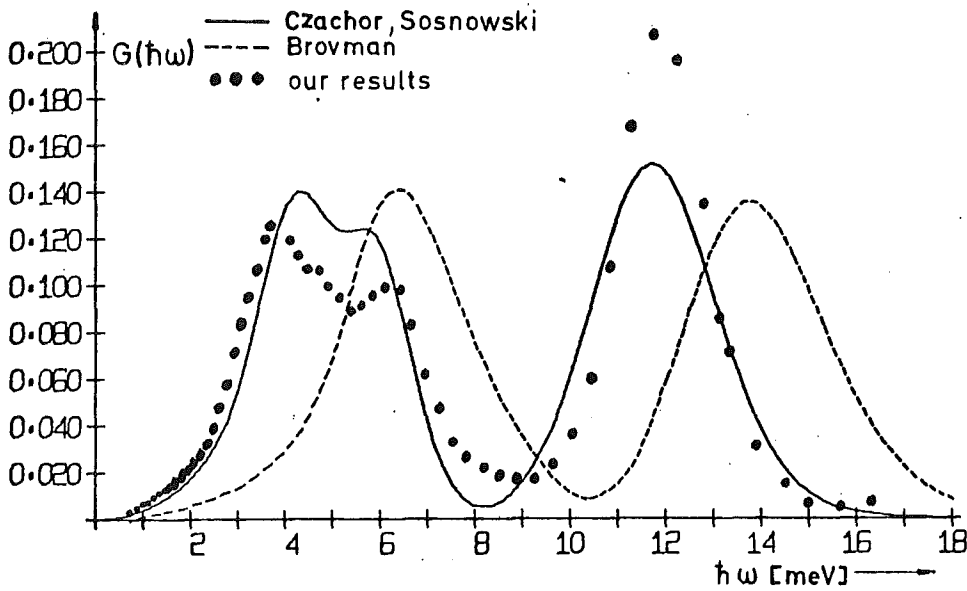
Fig. 20 Phonon Density of States of Bi in Comparison with Model Calculations

scattering experiment on a computer showed that $G(\hbar\omega)$ could be determined with sufficient accuracy /4/. The measurements were carried out at 296 K (Bi also at 80 K) using the cold source time-of-flight spectrometer TOF II.

The $G(\hbar\omega)$ for As, Sb and Bi are shown in fig. 18, 19 and 20 and are compared with lattice dynamical model calculations /5, 6, 7/ which are folded with the resolution of our spectrometer. For all substances the optic part of the spectrum is well separated from the acoustic contributions. Their areas differ by less than 2 %. The strong deviations of the lattice dynamical models proposed so far are not surprising, since they don't even give a good fit for the phonon branches which have been measured in symmetry directions only. It seems necessary to develop a shell model which takes the very long range of the interatomic forces better into account. From the vibration spectra the Debye-temperature as a function of the temperature was calculated /4/.

For 80 K the $G(\hbar\omega)$ for Bi is shifted 2 to 3 % to smaller energies relative to the room temperature data. From that shift we determined the Grüneisen constant to be about 2. In order to investigate the differences of the specific electronic structure the vibration spectra were normalized to the ionic mass and ionic volume of Bi (fig. 21). At first sight the normalized spectra are rather similar. The acoustic part for Bi however shows a strong
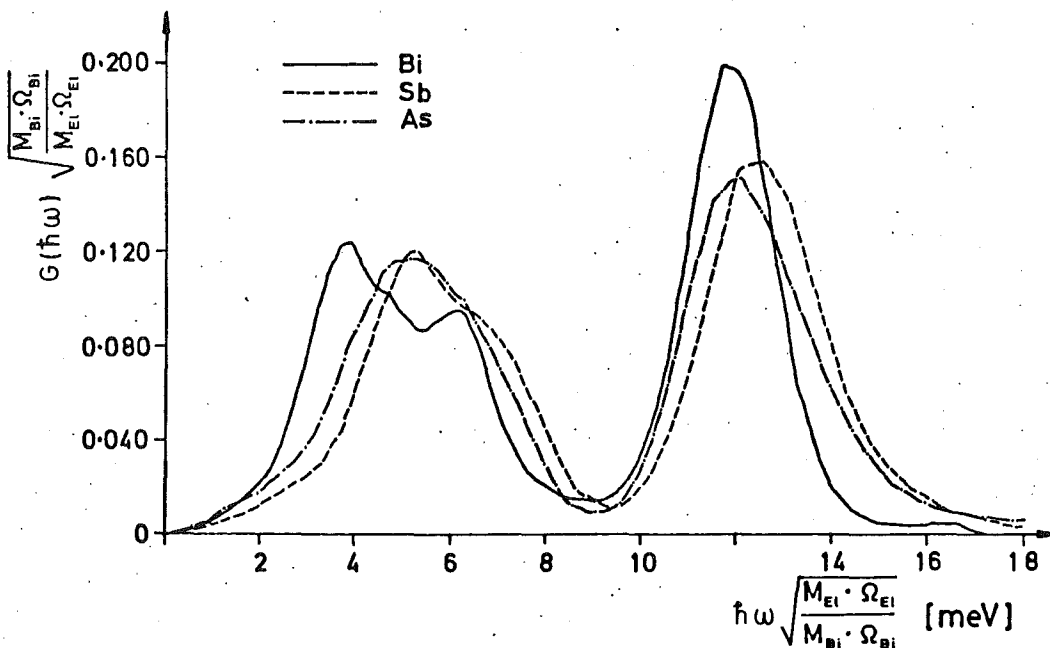
Fig. 21 Comparison of the normalized Phonon Density of States of As, Sb and Bi
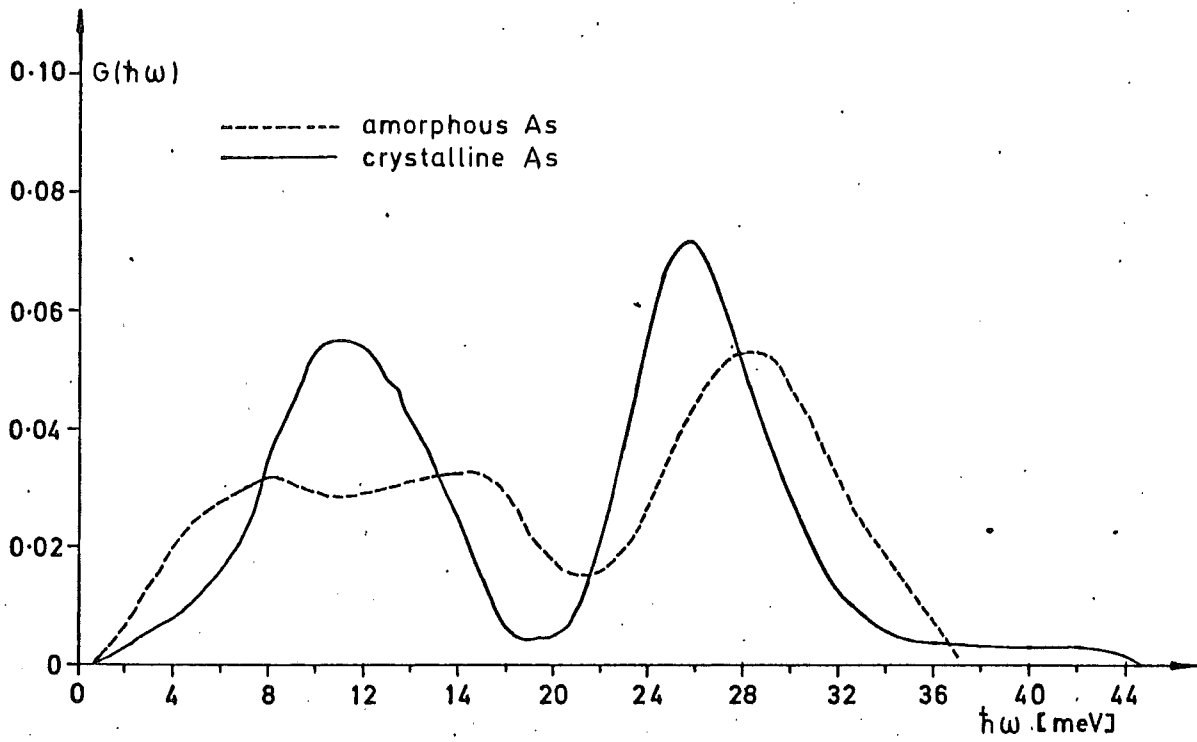
Fig. 22 Comparison of the Phonon Density of States of β-As with α-As
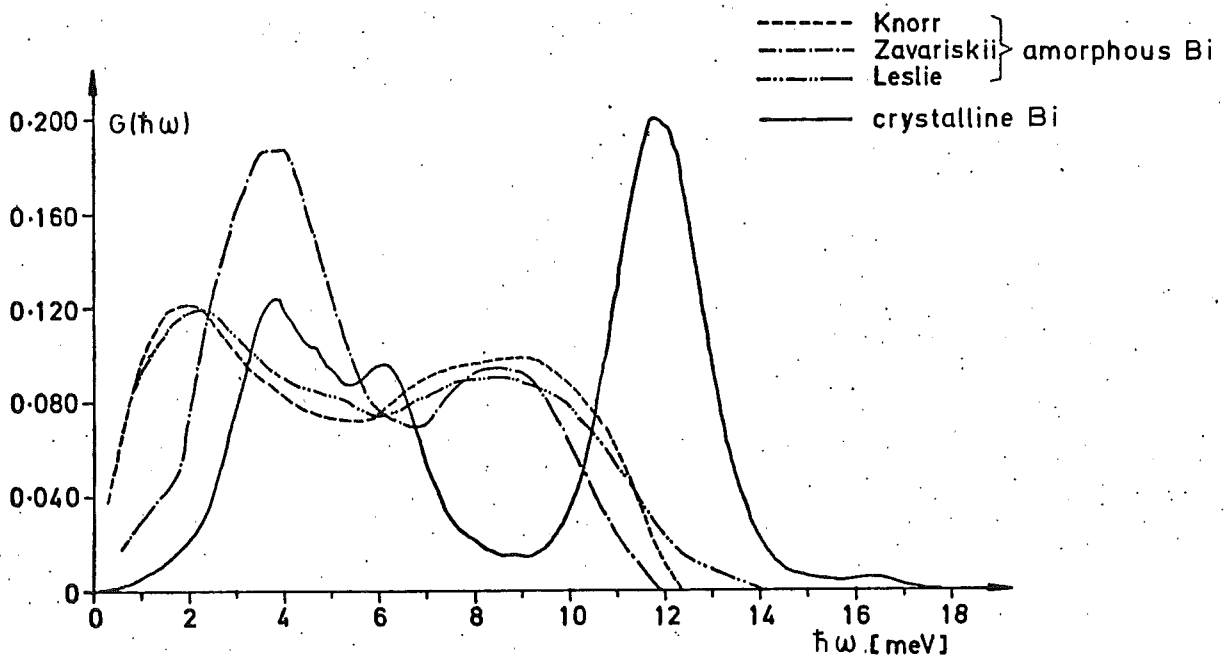
Fig. 23 Comparison of the Density of States of cristalline Bi with
Tunneling Spectra of Amorphous Bi

shift to smaller energies which seems to indicate the stronger metallic character in relation to As and Sb. G($\hbar\omega$) for amorphous As was also determined (fig. 22). The similarity with its crystalline modification suggests that β-As is a defect structure of α-As, i. e. a "crystalline-amorphous" structure.

In fig. 23 we compare G($\hbar\omega$) of crystalline Bi with the phonon spectrum of amorphous Bi derived from tunneling data /8, 9, 10/. The vanishing of the optic modes indicates that the short range order of the rhombohedral structure does not exist in amorphous Bi. Whether this substance has a truly "liquid-amorphous" structure is not certain however, since there are high pressure phases for Bi which could also be the cause of this behaviour.

This report is a short summary of the thesis of one of the authors (J. S.) /4/ finished in April 1974. Some of the experimental work has been done before 1. 6. 1973.

References

/1/ R. F. Sharp and E. Warming, J. Phys. F1 (1971), 570

/2/ R. E. MacFarlane, Reprint of the Los Alamos Scientific Lab. (1970)

/3/ F. Gompf, H. Lau, W. Reichardt, J. Salgado, Neutron Inelastic Scattering, 137, IAEA, Vienna (1972)

/4/ J. Salgado, Thesis (1974) KFK-Report 1954 (in print)

/5/ E. G. Brovmann, LA. TR. 68-33 (1967)

/6/ J. A. Czachor, A. Rajca, J. Sosnowski and A. Pindor, Acta Physica Polonica 1 (1973), 37

/7/ J. Sosnowski, A. Czachor and E. Mulizewski, IAEA/SM-155/A5 (1972)

/8/ N. K. Zararitskii, JETP Letters 5 (1967), 352

/9/ J. D. Leslie, J. T. Chen and T. T. Chen, Canadian Journal of Phys. 48 (1970), 2783

/10/ K. Knorr and N. Barth, Journal of Low Temperature Physics 4 (1971), 469

1.2.8 Frequency Moments of Liquid Rubidium up to the Fourth Moment and the Longitudinal High Frequency Dispersion

J.-B. Suck

We have corrected the measured scattering law of liquid Rubidium (318 K) /1/ for multiple scattering contributions /2/ using the models of Lovesey /3/ and alternatively the one of Pathak and Singwi /4/. The resulting data show a small influence of the model used in the correction. As the 0th and 2nd frequency moments calculated from these two alternative data sets do not show a significant difference, we took the one corrected with the model of Pathak and Singwi, which has a tendency of giving larger multiple scattering corrections for large energy transfers.

From hand-interpolated plots of the symmetrized scattering law for $\hbar\omega$ = const. $S(Q = const., \omega)$ was obtained /5/, the frequency moments

$$<\omega^n> = 2 \int_0^{\omega_{max}} \omega^n S(Q = const., \omega) \cosh(\beta/2) \, d\omega$$
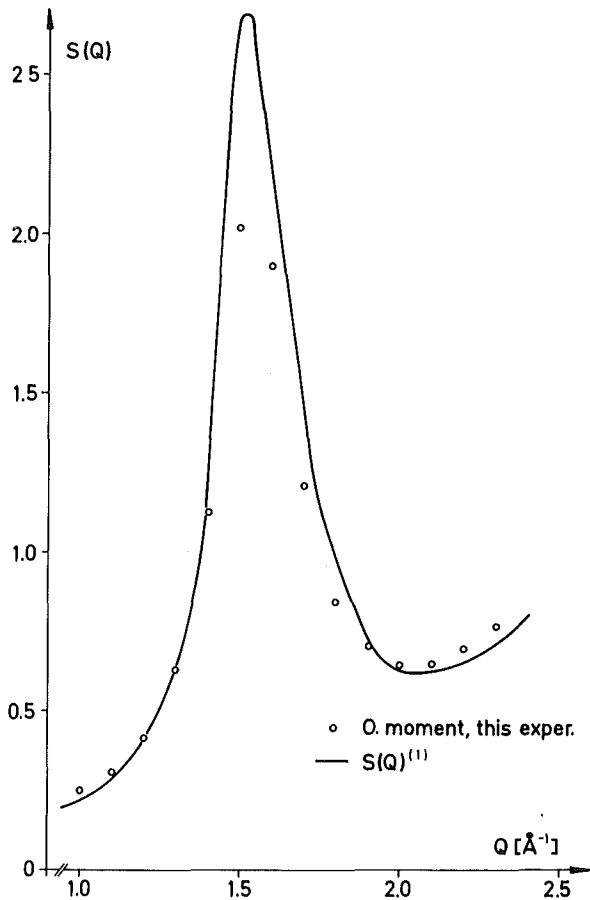
Fig. 24
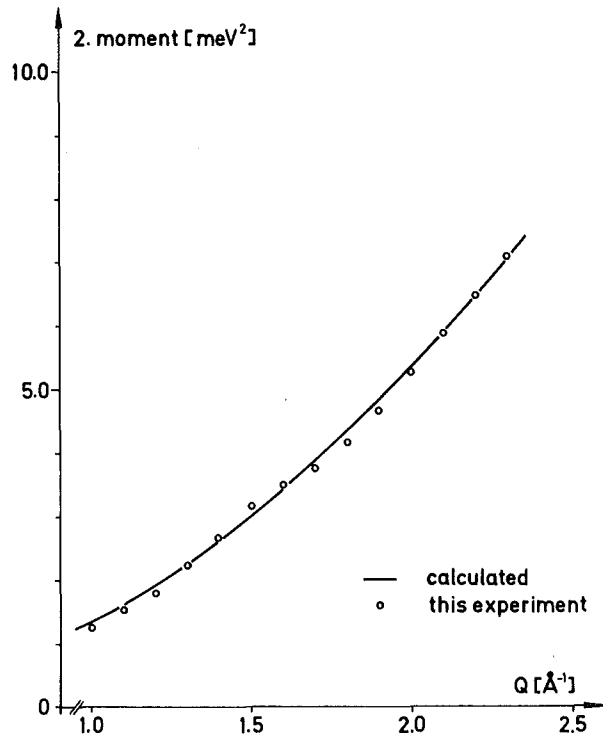
Fig. 25

$\beta = \hbar\omega/k_B T$, for n = O, 2, 4 and the longitudinal high frequency dispersion were calculated

$$\omega_1 = \left[\frac{\langle\omega^4\rangle}{\langle\omega^2\rangle} \right]^{\frac{1}{2}}$$

Due to monitor uncertainties the scattering law had to be scaled to the known second moment (see fig. 25). The scaling factor was 0.86.

The 0th moment does not fit very well the known S(Q) /6/, especially in the main peak of the structure factor (see fig. 24). This may be caused by the lack of resolution corrections which should contribute largest where the elastic scattering is large /7/ and by the fact that S(Q,O) could be obtained from the measurement only with a considerable uncertainty due to the large incoherent elastic scattering from the Vanadium container.

The integrands for the 2nd and 4th frequency moments of S(Q,ω) could be obtained to 99 % and 90 % resp. in the worst case (see fig. 26). The large errors of the experimental points are due to the large uncertainties of the multiple scattering corrections especially for large $\hbar\omega$- and low Q-values.
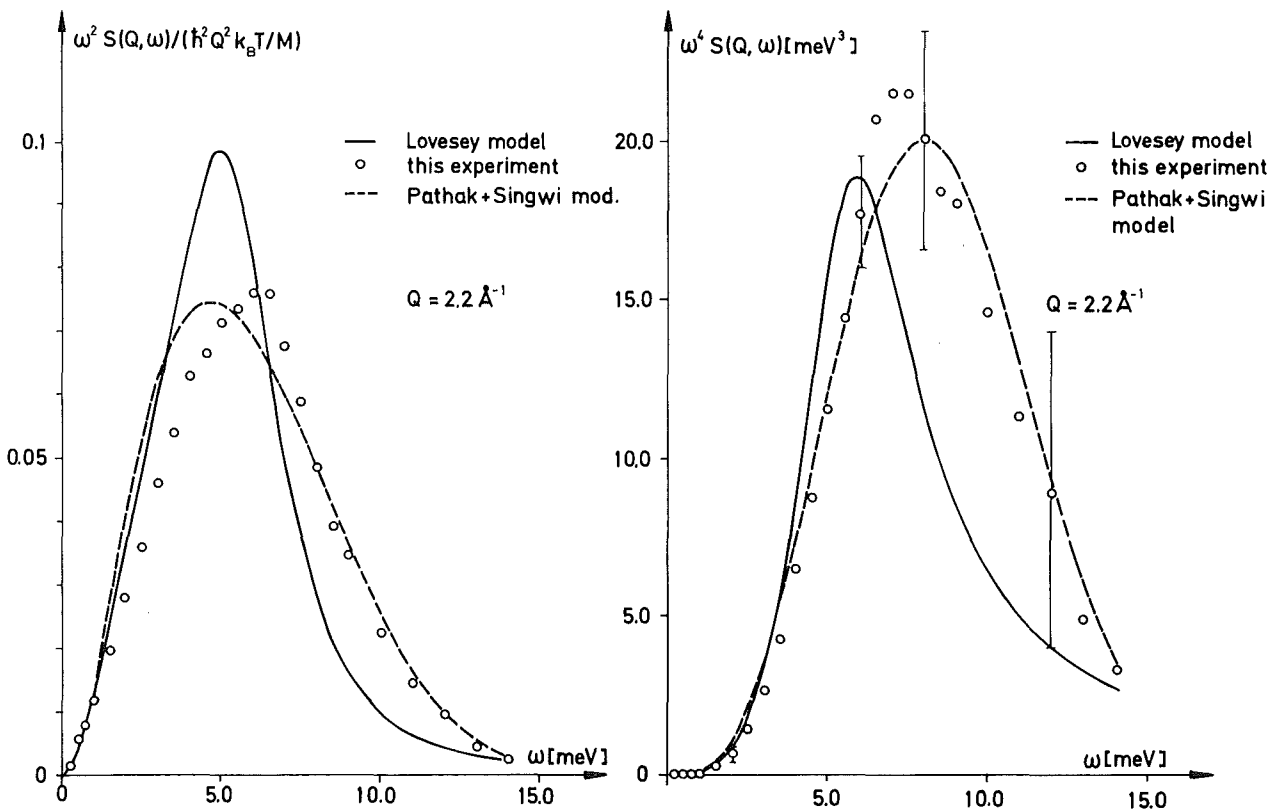
Fig. 26

The 4th moment is shown in fig. 27. It is compared to the one obtained by using the model scattering laws of Lovesey and Pathak and Singwi, integrating $\omega^4 S_{mod}$ in the same $\hbar\omega$-region as the experimental $\omega^4 S(Q,\omega)$ (O to 14 meV). Since the scattering law of Pathak and Singwi decreases more rapidly with increasing $\hbar\omega$ than Lovesey's does the cut of the integrand at 14 meV effects the 4th moment of the Lovesey model more than that of Pathak and Singwi.

As input for the model calculations the measured structure factor /6/ and a model for the high frequency dispersion /1/, /8/ were used. The model parameters r_o, ω_{E_1} and ω_{E_2} were determined by using the measured ω_1, which is independent of any scaling factor. $r_o = 4.8$ Å, $\omega_{E_1} = 4.3$ meV and $\omega_{E_2} = O$ meV were taken. r_o is near the first maximum of $g(r)$ and ω_{E_1} is about $(2/3)\omega_{max}$ of solid Rubidium. As both parameters are not independent from one another one should not take their values too serious. For the model for Lovesey $\zeta = 2/\sqrt{\pi}$ is used.

The model high frequency dispersion is shown in fig. 28, together with the experimental points and the isothermal dispersion. The maxima of $\omega^2 S(Q,\omega)$ lie between both dispersions. Their distribution in the Q-ω-plane corresponds to the dispersion $\omega_R(Q)$ used by Kugler /9/. The error bars are due to the uncertainty of the determination of the maxima of $\omega^2 S(Q,\omega)$.
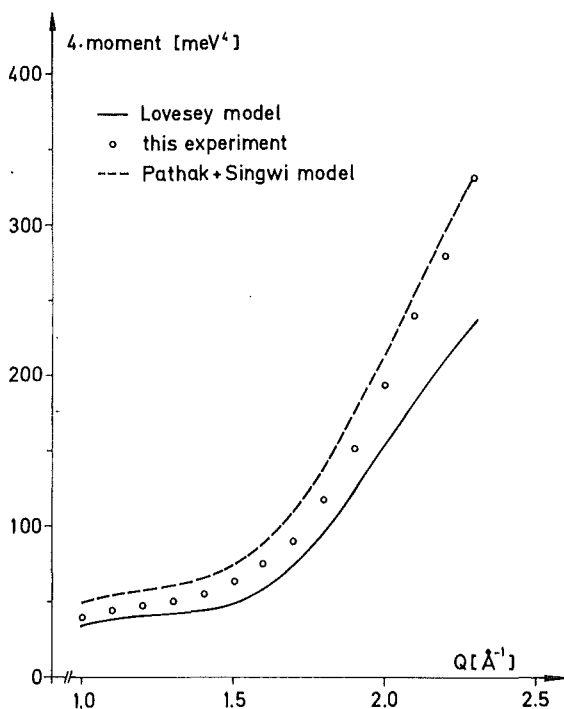
The large error bars at the experimental points of ω_1 are caused by the statistical errors of the scattering law, the uncertainties in the multiple scattering corrections and the incompleteness of the integrand of the moments. But we believe the experimental points to be more accurate than the given 20 % /10/.

Fig. 27

ω_1
ω_0 [meV]

7.0

6.0

5.0

4.0

3.0

2.0

1.0

0

ω_1

ω_0

Fig. 28

— ω_0, ω_1 calculated, ω_1 with $r_0 = 4.8\,\text{Å}$
$\omega_{E_1} = 4.3\,\text{Å}$
o ω_1 this experiment
x   max. of $\omega^2 S(Q,\omega)$ this experiment

Q[Å⁻¹]

0   0.5   1.0   1.5   2.0   2.5
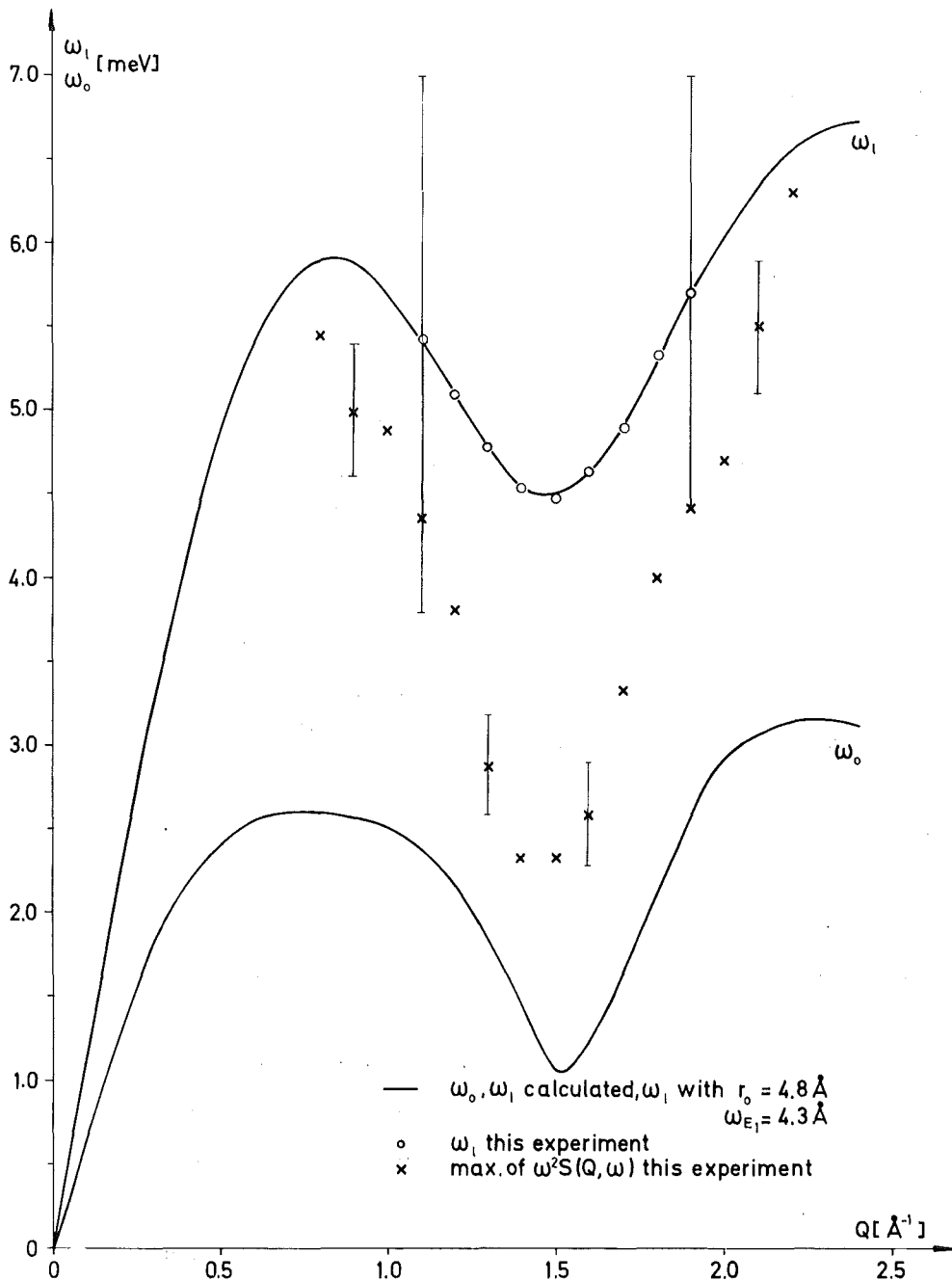
References

/1/ W. Gläser, S. Hagen, U. Löffler, J.-B. Suck, W. Schommers in The Properties of Liquid Metals, Taylor + Francis Ltd. (1973), 111

/2/ G. Ehret, F. Carvalho: VIPER, a program for multiple scattering corrections of thermal neutrons, unpubl.

/3/ S. W. Lovesey, J. Phys. C 4 (1971), 3057

/4/ K. N. Pathak, K. S. Singwi, Phys. Rev. A 2 (1970), 2427

/5/ W. Abel, INTERS a program for interpolating the measured scattering law with a light pen at the IBM 2250, unpubl.

/6/ obtained from: W. S. Howells, in The Properties of Liquid Metals, Taylor + Francis Ltd. (1973), 45

/7/ K. Sköld, J. M. Rowe, G. Ostrowski, P. D. Randolph, Phys. Rev. A6 (1972), 1107

/8/ J. Hubbard, J. L. Beeby, J. Phys. C2 (1969), 556

/9/ A. A. Kugler, J. Stat. Phys. 8 (1973), 107

/10/ J. R. D. Copley, S. W. Lovesey, preprint (to be publ. in Rev. Mod. Phys.)

1.2.9 Temperature Dependence of the Scattering Law of Liquid Rubidium

J.-B. Suck and N. Nücker

W. Drexel, Institut Max von Laue - Paul Langevin

The aim of this experiment is the determination of the scattering law of liquid Rubidium at 330 K and 430 K in an extended region of momentum transfers and with higher statistical accuracy compared to our results measured at the cold source at the FR2 in Karlsruhe.

The first part of this experiment (330 K) was done at the IN4 in July 1973. With an incident energy of 25.5 meV two sections of scattering angles were measured consecutively, (8 $^\circ$ to 68 $^\circ$) and (68 $^\circ$ to 158 $^\circ$). The half width of the elastic line in the V-experiment was about 0.7 meV. The region of momentum transfers Q was 1 to 7 (1/Å) with a Q-resolution of about 5 to 7 %.

Only a very preliminary evaluation of the data has been done so far. We plotted the time-of-flight spectra and, after interpolating over the Q-hω-plane, the symmetrized scattering law for constant hω. It turned out that the statistic of the result is not sufficient yet. Therefore we made no full evaluation of the data including corrections for multiple scattering and resolution effects as it is necessary to complete these results by adding up new data taken at 330 K. This will be done together with the 430 K experiment in 1975.

1.2.10 Investigation of Collective Atomic Motions in Liquid Gallium by Inelastic Neutron Scattering /1/

U. Löffler

Abstract

The inelastic coherent scattering of slow neutrons from liquid gallium has been measured at 305 K and 1253 K. The experiments were performed with the rotating crystal time-of-flight spectrometer at the cold source of

the reactor FR2. With an incident neutron energy of 5.2 meV for elastic scattering an energy resolution of 0.3 meV was achieved.

The scattering law $S(Q,\omega)$ determined from the experimental data is compared with several models. The collective excitations are discussed in terms of a dispersion relation $\omega_{\infty}(Q)$ and a Q-dependent relaxation time $\tau(Q)$. Both function were deduced by fitting model parameters to the quasielastic scattering (de Gennes narrowing). Attempts were also made to derive $\omega_{\infty}(Q)$ directly from the measured $S(Q,\omega)$ by determing the fourth moment. Special emphasis has been put on the study of the temperature dependence of the quasielastic scattering for Q-values around the first maximum of the static structure factor. The results are discussed in view of a model proposed by Schneider et al. relating the first minimum of $\Delta\omega(Q)$ with the liquid-solid phase transition.

References

/1/ U. Löffler, KFK 1875, November 1973

1.2.11   Study of the Triplet Correlation Function for Liquid Rubidium

R. Block

The triplet correlation function $g_3(\vec{r},\vec{s})$ is involved in many theories of liquids. Its knowledge is also of interest in systems which interact via a pair-potential $v(r)$, e. g. for determining $v(r)$ in a liquid if the pair-correlation is known. In order to investigate $g_3(\vec{r},\vec{s})$ it is useful to introduce the following function /1/:

(1) $H(\vec{r},\vec{s}) = H(r,s,t) = g(r)\ g(s)\ g(t) - g_3(r,s,t)$

where the condition for isotropy has been used and r,s,t are the relative distances of three particles. Experimental information on $H(\vec{r},\vec{s})$ which gives the deviation from the superposition approximation (S. A.), can be obtained by measuring the pressure dependence of the structure factor in liquids /1/. From these experiments it is only possible to determine the integral quantity $H(Q)$, which is the Fourier transform of:

(2) $H(\vec{r}) = \int H(\vec{r},\vec{s})\ d\vec{s}$
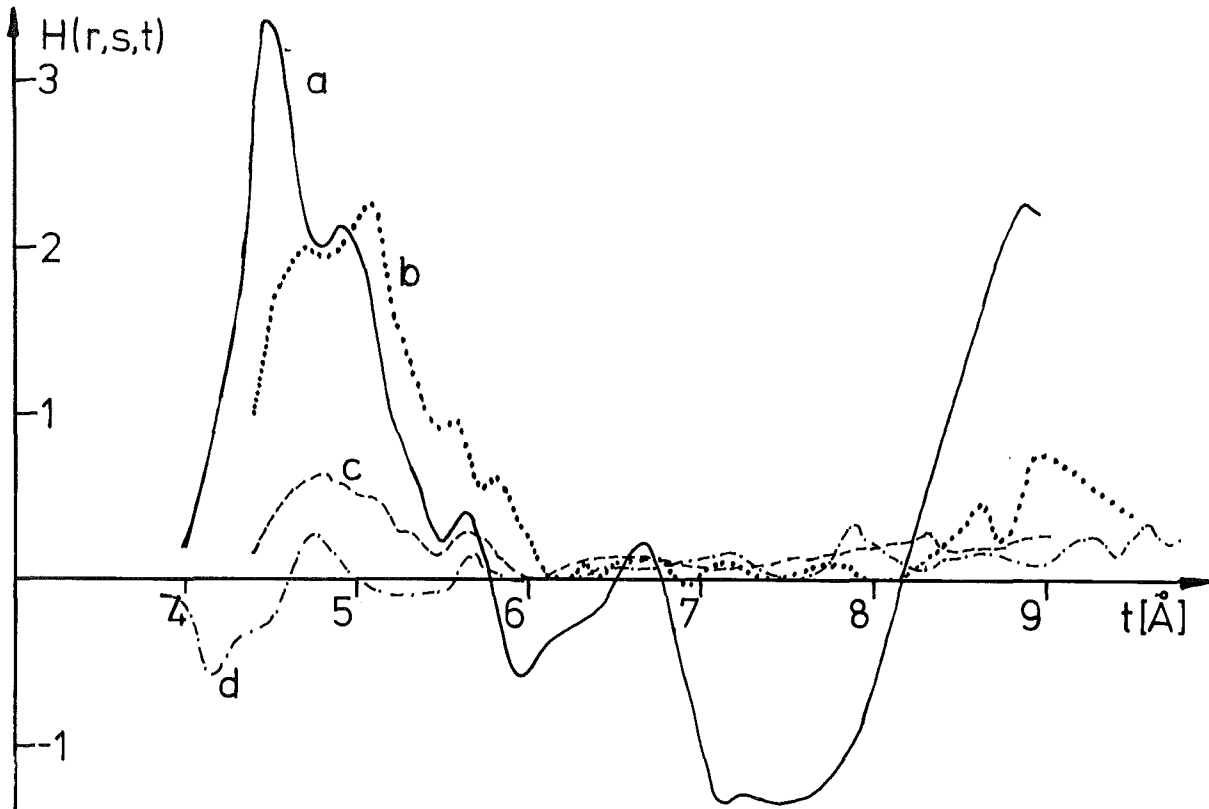
Fig. 29 $H(r,s,t) = g_3^{SA} - g_3(r,s,t)$ for a) $r = 4.7$, $s = 4.7$,

b) $r = 4.7$, $s = 9.1$, c) $r = 9.1$, $s = 9.1$, d) $r = 4.7$, $s = 6.6$

P. A. Egelstaff et al. /1/ have tested liquid theories with this function. A model for $H(r,s,t)$ which could be obtained from the experimental data is desirable. In the quoted paper a function is defined as:

(3)
$$H(r) = \gamma(\vec{r}) \int \gamma(\vec{r} - \vec{s}) \, \gamma(s) \, d\vec{s}$$

and

(4)
$$H(r,s,t) \approx \gamma(r) \, \gamma(s) \, \gamma(t)$$

is proposed as a convenient approximation. The question is whether a $H(r,s,t)$ obtained from (3) and (4) is an improvement over the S. A.. Per definition it describes exactly the experimental quantity $H(Q)$ but we do not know whether it would give better results for the pair-potential in an extended Born-Green equation. In the following we want to compare $H(r,s,t)$ for different configurations and the $\gamma_{rs}(t)$
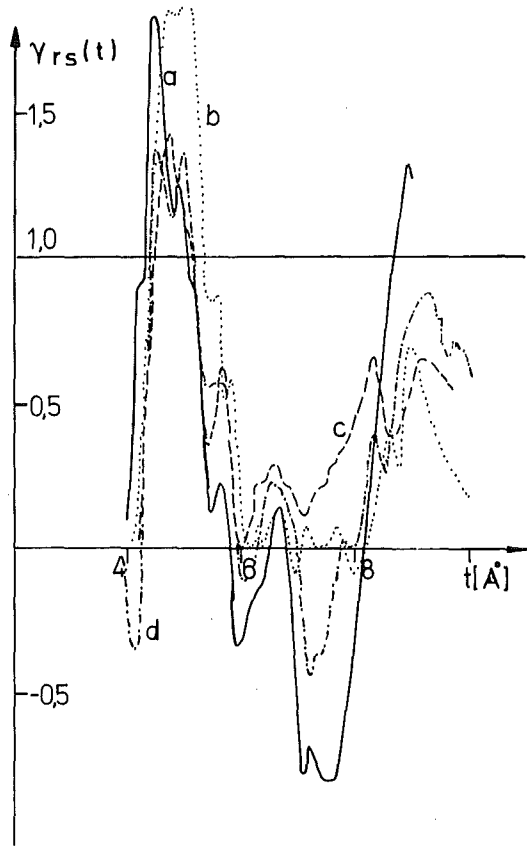
Fig. 30

The function $\gamma_{rs}(t)$ obtained from $H(r,s,t)$ for

    a) $r = 4.7$, $s = 4.7$
    b) $r = 4.7$, $s = 9.1$
    c) $r = 9.1$, $s = 9.1$
    d) $r = 6.6$, $s = 9.1$
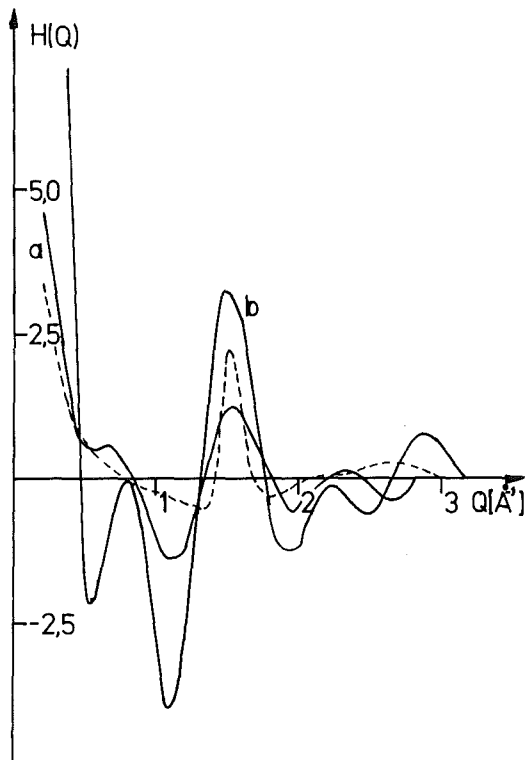
Fig. 31

$H(Q)$ the Fourier transform of $H(r)$ for

    a) $r = 4.7$, $s = 4.7$
    b) $r = 6.6$, $s = 9.1$

dotted line: expected from experiments

obtained from them by (4). The subcripts rs denote that $\gamma(t)$ is defined for a constant r,s configuration.

The data of $g_3(r,s,t)$ for liquid Rubidium near the triple point were taken from molecular dynamics calculations by W. Schommers /2/. In fig. 29 H(r,s,t) is plotted for four different configurations. r,s are held constant while t takes the values between $(r + s) \geq t \geq (r-s)$. Curve a) is a constant $r = s = 4.7$ Å plot. As g(r) has its maximum at this value the statistical errors in this curve are expected to be smaller than for other configurations. Characteristic are the negative values between 7 - 8 Å.

In fig. 30 the $\gamma_{rs}(t)$ as defined by (4) for each H(r,s,t) are plotted. They show some common features: a pronounced peak near 4.7 Å which is quantitatively almost equal for all curves and another peak near 9 Å. This two peaks give the $\gamma_{rs}(t)$ an oscillatory character. Two curves show a negative behaviour. This means that an effective $\gamma(t)$ would correct the S. A. near 5 and 9 Å, between 6 - 8 Å it would be an improvement for some configurations, but would give worse results than the S. A. for other configurations.

To test how close the $\gamma_{rs}(t)$ are to an effective $\gamma(t)$, as obtained from experiment, we have calculated H(Q) for two $\gamma_{rs}(t)$ and have compared them with experimental results in fig. 31 (the H(Q) was obtained from the structure factor S(Q) /3/ and a density model for its pressure dependence /1/).

References

/1/ P. A. Egelstaff, D. I. Page and C. R. T. Heard, J. Phys. C, Solid State Phys. 4 (1971), 1453

/2/ W. Schommers, Phys. Letters 43A (1973), 157 and private comm.

/3/ N. S. Gingrich and L. R. Heaton, J. of Chem. Phys. 34 (1961), 873

1.2.12   Single-particle Motion in Liquid Rubidium /1/

W. Schommers

Molecular dynamics calculations have been performed for liquid rubidium
at 319 ^{O}K, using model systems of 432 atoms. For the Rb-Rb-interaction
a realistic pair-potential was chosen /2/. The cut-off radius for the
potential was chosen alternatively at 4.5 $\overset{O}{A}$ and 9.8 $\overset{O}{A}$ to compare short-
and long-range effects. The molecular dynamics data were used to calculate
the velocity autocorrelation function $\psi(t)$ and the frequency spectrum $f(\omega)$.
The Gaussian behavior of the self-part of the intermediate scattering
function will be studied too.
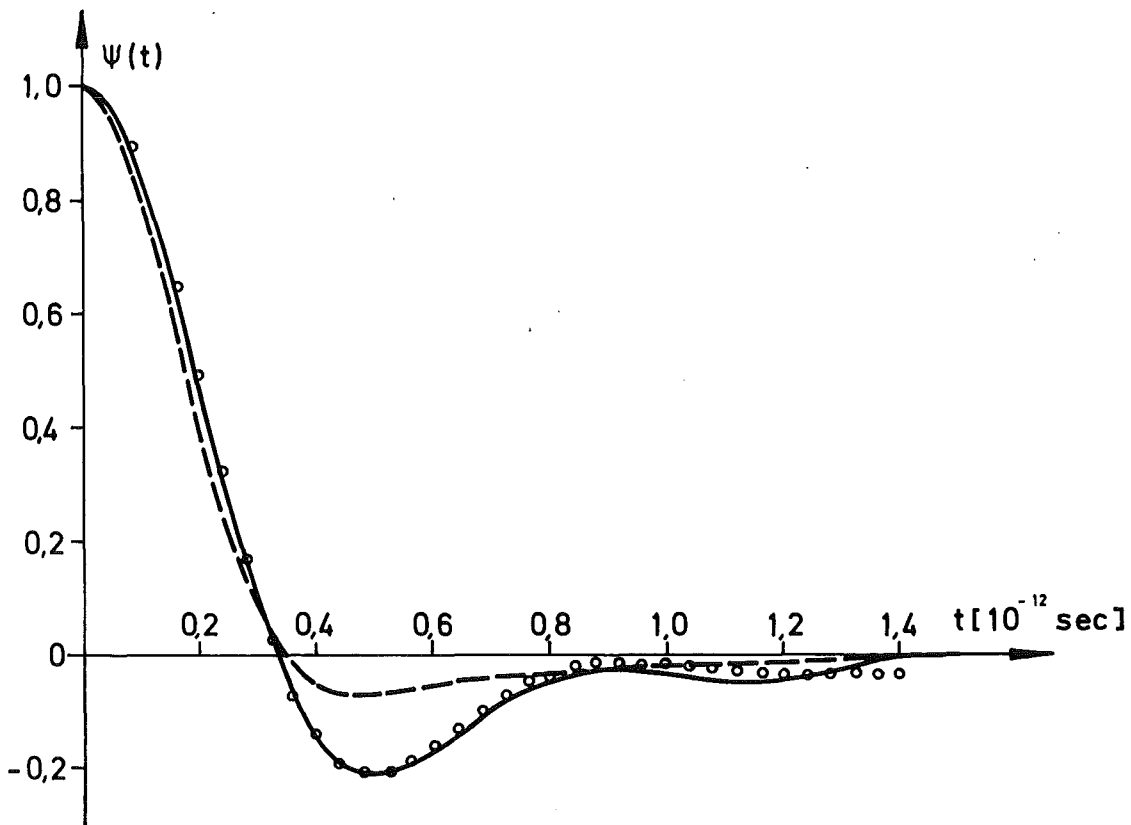
Fig. 32 Velocity autocorrelation function for Liquid Rb

        (oooo): model

        (———): molecular dynamics. Cut-off radius for the potential: 9.8 $\overset{O}{A}$

        (----): molecular dynamics. Cut-off radius for the potential: 4.5 $\overset{O}{A}$

A model for the memory function $\Gamma(t)$, which is defined by the integrodifferential equation /3/

$$\frac{d\ \psi(t)}{dt}\ +\ \int_{o}^{t}\ \Gamma(t-t')\ \psi(t') = 0$$

has been developed.

A satisfactory description of $\psi(t)$ is obtained, if the memory function is made up of two components with a different time-behavior (corresponding to two time-constants). One time-constant /3/, /4/ only is not sufficient. In fig. 32 the model-calculation is compared to the respective moleculardynamics data.

References

/1/ W. Schommers, to be published

/2/ W. Schommers, Phys. Letters A 43 (1973), 157

/3/ Berne, Boon, Rice, J. Chem. Phys. 45 (1966), 108

/4/ Singwi, Tosi, Phys. Rev. 157 (1967), 153

1.2.13   A Pair-Potential for Liquid Copper

W. Schommers

We have calculated a pair-potential for liquid Copper using a method described in detail in ref. /1/. This method uses molecular dynamics for an iterative computation of the pair-potential from the experimentally determined pair-correlation function g(r). The calculated potential is shown in fig. 33a. It corresponds to a particle-number density of n $= 0.0758\ \overset{o}{A}{}^{-3}$ and a temperature of T $= 1375\ {}^{o}K$. The molecular-dynamical computation based on this potential and on 500 atoms yields a g(r) given in fig. 33b. As can be seen the deviations of the calculated from the experimental g(r) /2/ are small.
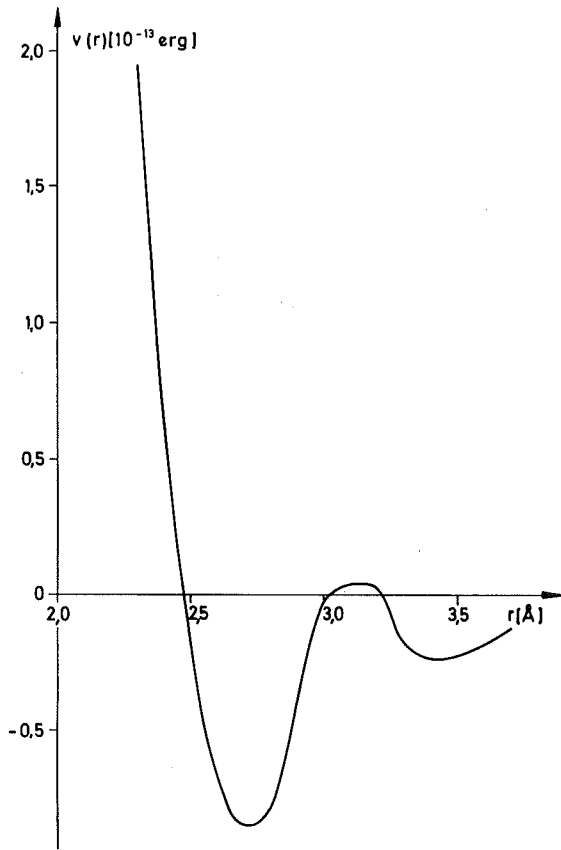
Fig. 33a   Pair-Potential for Liquid Cu
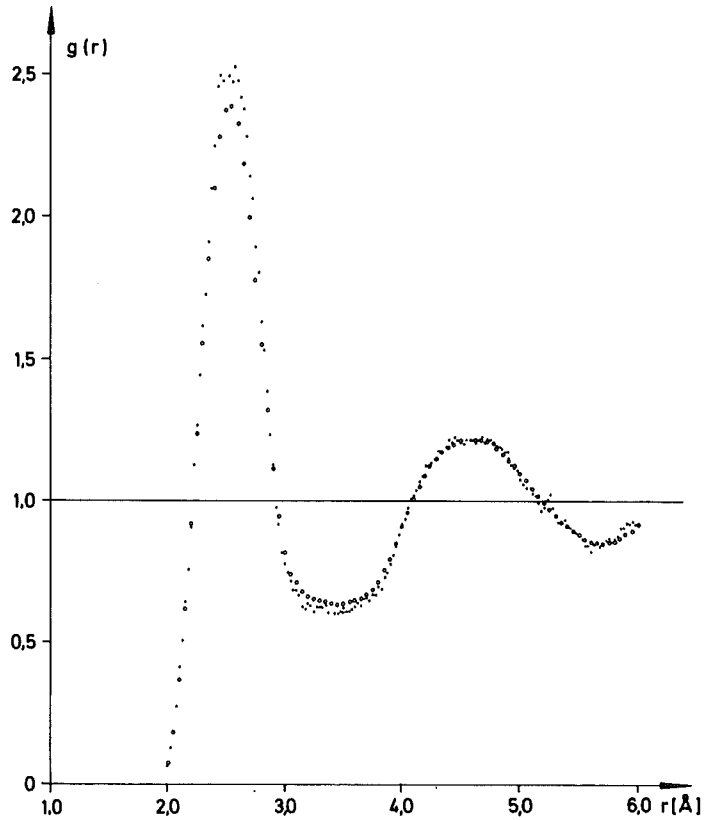
Fig. 33b Pair-Correlation Function for Liquid Cu, (····): molecular dynamics, (oooo): experimental data

The molecular-dynamical data were also used to determine the mean square displacement. From this we obtain for the diffusion constant D a value of $4.49 \cdot 10^{-5}$ cm^2/sec, which is in satisfactory agreement with the experimental value of $D = 4.25 \cdot 10^{-5}$ cm^2/sec /3/.

References

/1/ W. Schommers, Phys. Letters A 43 (1973), 157

/2/ M. Breuil and G. Tourand, J. Chem. Solids 31 (1970), 549

/3/ Henserson, Yang, Trans. Am. Inst. Min. Metall Engrs. 221 (1961), 72

1.2.14 Collective Excitations in Liquids

W. Mehringer

A new method developed for treating phonon-like excitations in systems
with short range order was used for a model calculation with one free
parameter of the dispersion in liquids. The dispersion ω(k) was obtained
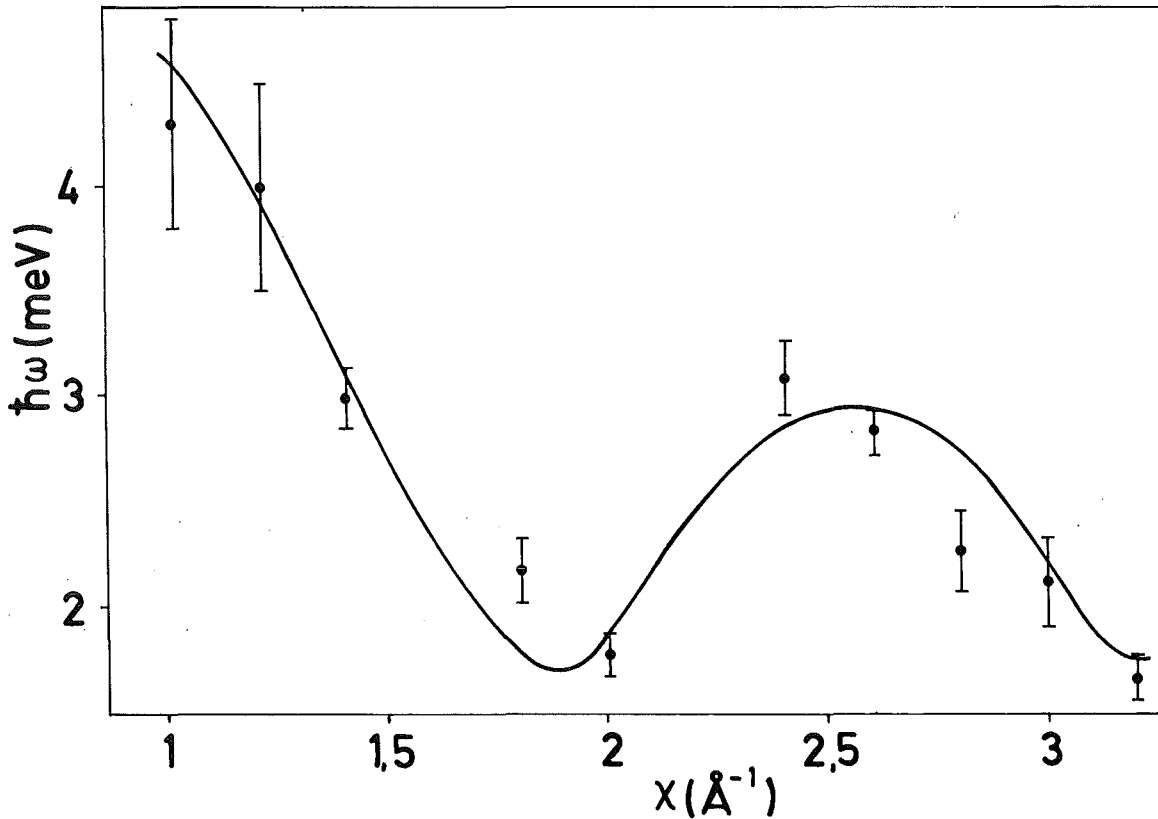
Fig. 34 Calculated dispersion ω(k) for liquid argon at T = 85.2 °K with
the use of a parameter value, which gives the best agreement
with the positions of peaks (uncertainty in determination indi-
cated by bars) in the experimental S(k,ω)

as the thermal average value of a "local" frequency. The parameter describes
a limitation in averaging to deviations from exact crystal configurations. In
an application to liquid argon good agreement was obtained with a dispersion
derived from a small peak structure in the coherent scattering function
S(k,ω) recently measured (Table IV of K. Sköld et al., Phys. Rev. A6 (1972),
1107). This is shown in fig. 34.

2. ELECTRONIC SCTRUCTURE AND MAGNETISM OF SOLIDS

2.1 Investigation of the Metal-to-Semimetal Transition in NiS by ^{61}Ni-Mössbauer Spectroscopy

J.Fink, G. Czjzek, K. Ruebenbauer and H. Schmidt

J. M. D. Coey and R. Brusetti, C. N. R. S., Grenoble

The compound NiS with the hexagonal NiAs-structure is metallic at room temperature and it undergoes a first-order transition to an antiferromagnetic, semimetallic state at a transition temperature T_t which depends strongly on the composition (Fig. 35). For stoichiometric NiS, T_t = 265 K.

The Mössbauer spectra of ^{61}Ni in compounds Ni_yS with $y \geq 0.971$ for $T < T_t$ consist of 12 lines, corresponding to a magnetic dipole and an electric quadrupole interaction. The concentration dependence of the magnetic hyperfine field and of the electric field gradient is shown in Fig. 35, together with the concentration dependence of the magnetic moment μ_{Ni} per Ni ion.

Spectra of Ni_yS in the metallic phase can be fitted with a single line. The presence of an electric quadrupole interaction of about the same strength as in the magnetic phase can not be excluded.

We find a strong decrease of the recoilless fraction f at the transition from the antiferromagnetic to the nonmagnetic state (Fig. 36). A fit of the temperature dependence of f and of the energy shift with a Debye-plus-Einstein-model gives for all samples in the antiferromagnetic state a Debye-temperature θ_D = 230 K. In the nonmagnetic state, θ_D = 193 K. Both results are in good agreement with specific-heat measurements /1/ and with the phonon dispersion curves determined by Briggs et al. /2/. The Einstein temperature, θ_E = 245 K, is within the experimental uncertainty the same in both states of the material, indicating the absence of a significant shift of the optical-mode frequencies at the transition.
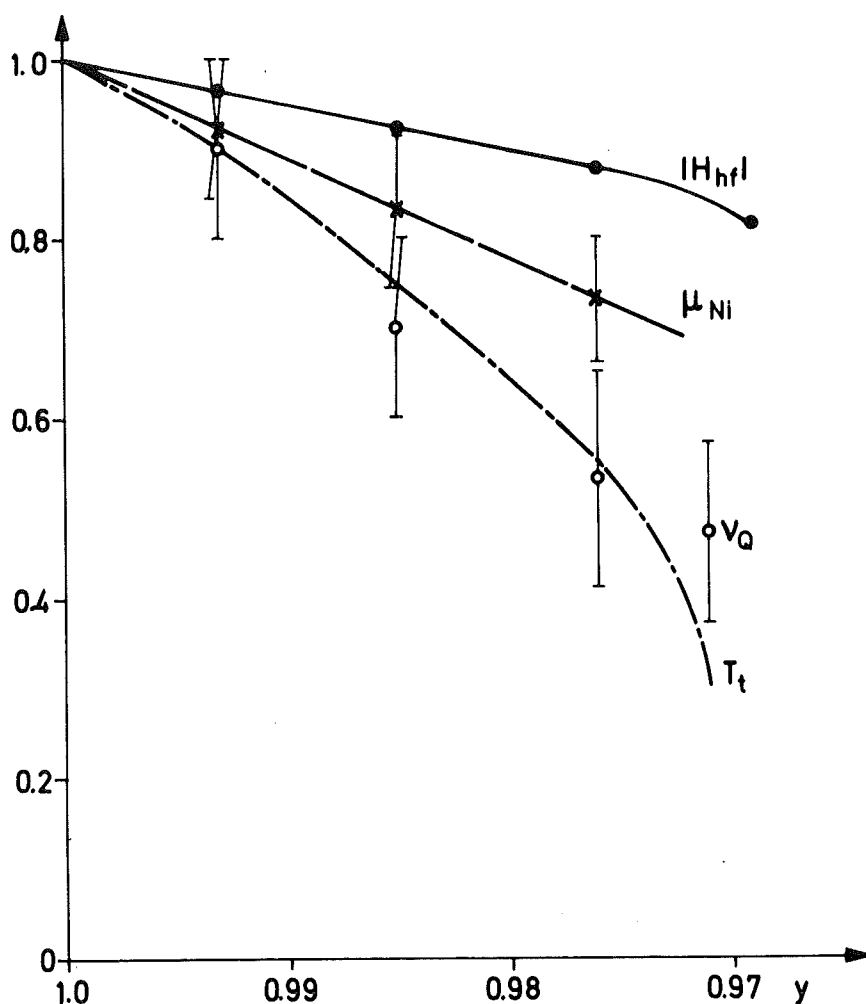
Fig. 35 Concentration dependence of the transition temperature T_t, the

magnetic moment per nickel ion μ_{Ni}, the magnetic hyperfine field

H_{hf}, and the quadrupole coupling constant ν_Q, in $Ni_y S$. The figure

displays relative values, normalized to 1 for $y = 1$. Absolute

values for $y = 1$ are $T_t = 265 \, K$, $\mu_{Ni} = 1.4 \, \mu_B$, $|H_{hf}| = 112 \, kG$, $\nu_Q = 1.6 \, MHz$,

The analysis of the energy shifts yields for the difference of the isomer

shifts between the magnetic and the nonmagnetic state the result:

$$\delta_{Is}^m - \delta_{Is}^{nm} = (2.5 \pm 1.2) \ \mu m/sec.$$

The magnetic hyperfine field changes quadratically with temperature,

$[H(0) - H(T)]/H(0) = \alpha \cdot T^2$, with $\alpha \approx 10^{-6} \, K^{-2}$ for $y = 0.993$,

$\alpha \approx 2 \cdot 10^{-6} \, K^{-2}$ for $y = 0.976$. As the neutron scattering experiments

by Briggs et al. (4) revealed the existence of a gap of about 12 meV and a stiffness constant of about 465 meV · $Å^2$ for the spin waves, this temperature dependence can not be explained by the spin wave model. It can be accounted for by single-particle excitations of an itinerant antiferromagnet.
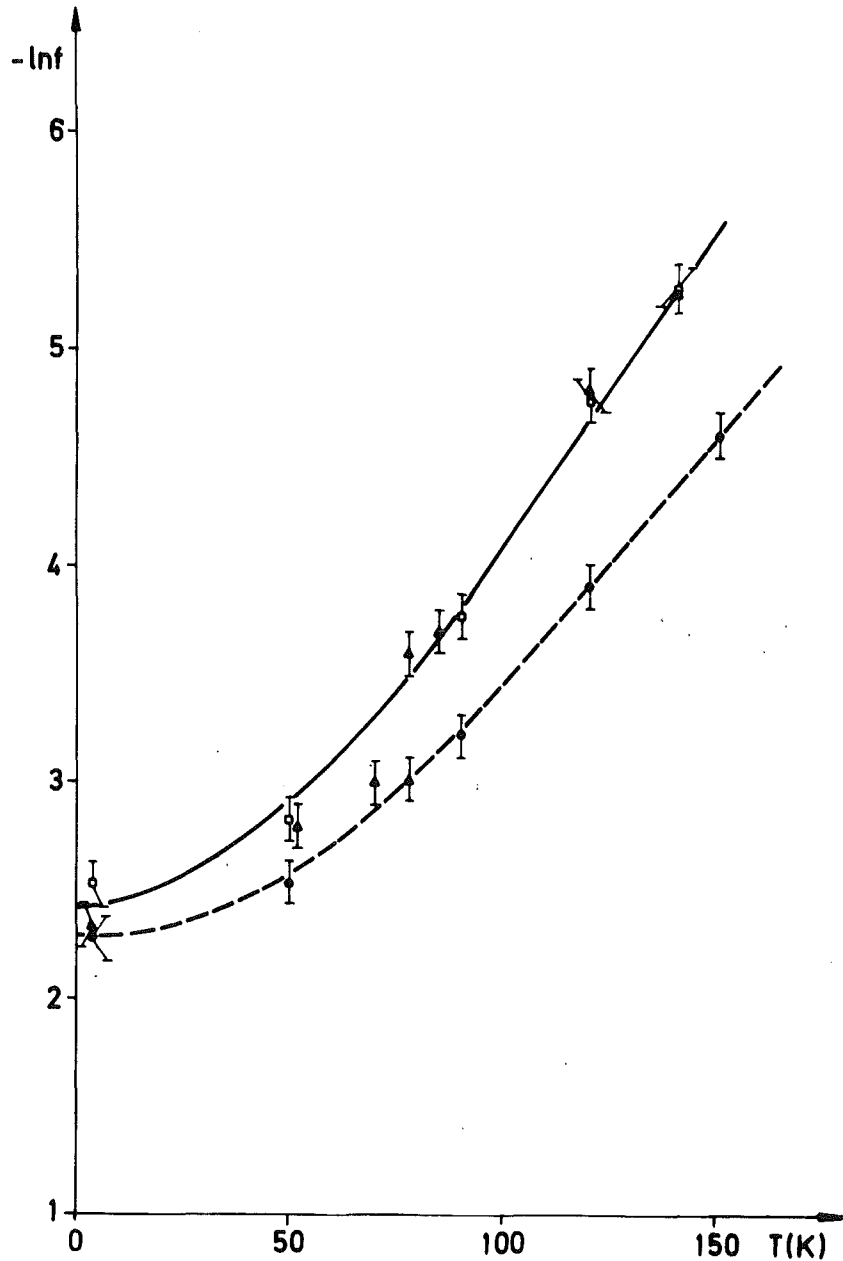
Fig. 36 Temperature dependence of ln f in Ni_yS: Antiferromagnetic state:
● $Ni_{0.993}S$, ▲ $Ni_{0.971}S$, ---- calculated with θ_D = 231 K, θ_E = 243 K. Nonmagnetic state: △ $Ni_{0.971}S$, □ $Ni_{0.965}S$, —— calculated with θ_D = 193 K, θ_E = 250 K.

A point-charge calculation of the lattice contribution to the electric field gradient gives a value which is about an order of magnitude larger than the measured value. The difference can be due to shielding of the ionic potentials by conduction electrons or to a compensating contribution by covalent admixture of sulfur 3p-electrons to the nickel valence states. Whichever of these mechanisms is dominant, it would also tend to reduce the intra-atomic exchange interaction at the nickel ions which is assumed to cause the magnetic ordering. The observed decrease of the quadrupole interaction with increasing deviation from stoichiometry indicates a strengthening of this mechanism, in agreement with the observed decrease of the transition temperature T_t. A similar decrease of the quadrupole interaction with increasing temperature supports this point of view.

References

/1/ J. M. D. Coey and R. Brusetti, to be published

/2/ G. A. Briggs et al., in Neutron Inelastic Scattering, IAEA, Vienna (1972), p. 669

2.2   Investigation of Magnetic Structures and Phase Transitions in NiS_2 by ^{61}Ni-Mössbauer Spectroscopy

G. Czjzek, J. Fink and H. Schmidt

G. Krill, F. Gautier and C. Robert, Laboratoire de la Structure Electronique des Solides, Université de Strasbourg

Recent studies of NiS_2 with cubic pyrite structure by neutron diffraction /1/ and by measurements of magnetic susceptibility and electrical resistivity /2/ have established the occurrence of two magnetic phase transitions in this material which becomes antiferromagnetic below $T_N \sim 40 - 50$ K, weakly ferromagnetic below $T_c \sim 30 - 31$ K.

We have taken a series of Mössbauer spectra of ^{61}Ni in the temperature range 4.2 K $\leq$ T $\leq$ 50 K of a sample with composition $NiS_{1.93}$. The results are summarized in Fig. 37.

For T > 45 K (paramagn. phase) we find an unresolved spectrum with some broadening, corresponding to a quadrupole coupling constant $\left|e^2qQ/h\right|$ = (8 ± 3) MHz.

For 31 K $\leq$ T $\leq$ 44 K (antiferromagn. phase) the ^{61}Ni-nuclei experience a magnetic hyperfine field H_{hf} whose temperature dependence is quite well described by the molecular-field-approximation for S = $\frac{1}{2}$ with T_N = 44.5 K and $\left|H_{hf}(T = 0)\right|$ = 47 kG. The effective quadrupole coupling constant ν_Q in this phase is given by $\nu_Q = \frac{1}{2}$ (3 $\cos^2\theta$ - 1) $\cdot$ e^2 $\cdot$ q $\cdot$ Q/h = (-5.8 ± 0.2) MHz, independent of temperature (θ is the angle between the principal axis of the field-gradient tensor and the direction of the magnetic hyperfine field).

From the fact that we find a unique hyperfine field and a unique value of ν_Q for all ^{61}Ni-nuclei in conjunction with the neutron-diffraction results /1/ we can conclude that the magnetic moment on any nickel ion in this phase is parallel to that (111)-direction which is the local trigonal symmetry axis. That is, θ = 0, and the experimental value of ν_Q is equal to e^2qQ/h.

At (30.9 ± 0.1) K a strong discontinuity of the slope of the H_{hf}-vs.-T-curve is observed for about 50 % of the ^{61}Ni-nuclei (β-sites), whereas the field on the other nuclei (α-sites) remains practically constant down to (30.2 ± 0.1) K. For T $\leq$ 30 K the field at all ^{61}Ni-nuclei deviates from the curve extrapolated from the antiferromagnetic phase, and for all lower temperatures we find two Ni-sites, differing in the values of H_{hf} (Fig. 37a) and of ν_Q (Fig. 37b). Between about 29 K and 25 K the fraction of ^{61}Ni-nuclei in β-sites decreases gradually from ~ 50 % to ~ 25 % (Fig. 37c).

In the temperature region between 31 K and 29 K we also observe a gradual change of the effective quadrupole coupling constant. Below 29 K we find: $\nu_Q^{(\alpha)}$ = (-2.8 ± 0.1) MHz, $\nu_Q^{(\beta)}$ = (2.4 ± 0.2) MHz, independent of temperature.
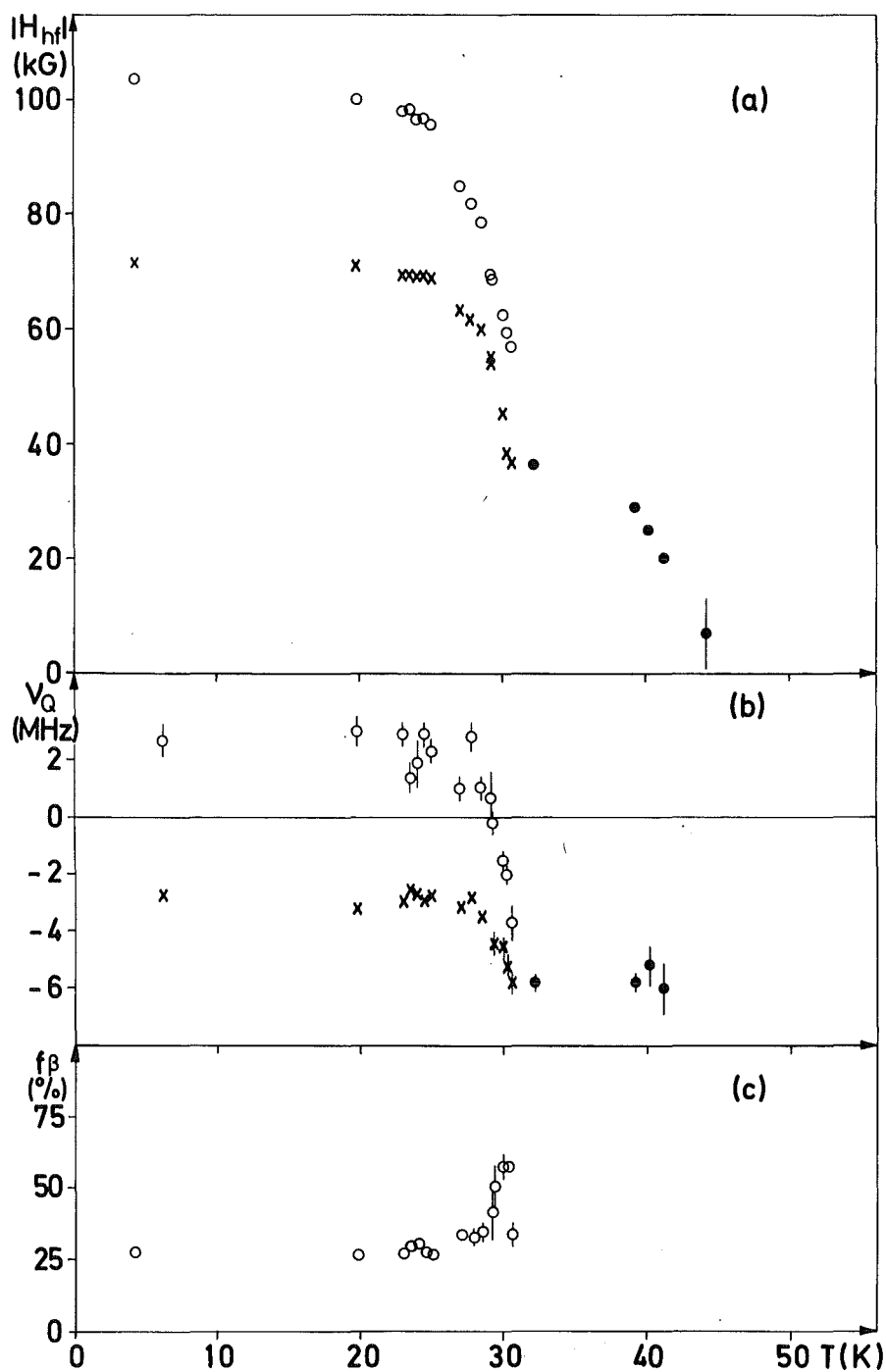
Fig. 37 Temperature Dependence of Hyperfine Interaction Parameters in
$NiS_{1.93}$

● antiferromagnetic phase, x α-sites, o β-sites

(a) Magnetic hyperfine field, (b) effective quadrupole coupling
constant, (c) fraction of ^{61}Ni-nuclei occupying β-sites.

The changes of H_{hf} near 30 K could be caused by similar changes of the magnetic moments of the Ni-ions. However, this would also lead to corresponding changes of the intensities of magnetic powder diffraction patterns which have not been observed (M. T. Hutchings, private communication). Therefore it seems more likely that the observed effects are caused by rotations of the magnetic moments in conjunction with anisotropic hyperfine interactions. As no significant structural changes have been observed in the critical temperature region, we analyse our results assuming changes only of the moment directions, not of the intrinsic hyperfine interaction parameters. From a comparison of the hyperfine fields at 4.2 K with the value extrapolated from the antiferromagnetic phase and using the ratio $\nu_Q^{(\alpha)}/\nu_Q^{(\beta)}$ we can then derive values for the angles $\theta^{(\alpha)}$ and $\theta^{(\beta)}$ between the directions of the magnetic moments and the local symmetry axis: $\theta^{(\alpha)} = 36°$, $\theta^{(\beta)} = 71°$. Using only the values of $\nu_Q^{(\alpha)}$, $\nu_Q^{(\beta)}$ and of ν_Q in the antiferromagnetic phase, we obtain: $\theta^{(\alpha)} = 39°$, $\theta^{(\beta)} = 77°$. The agreement between these results is quite satisfactory and lends support to the assumptions involved in the derivation.

References

/1/ J. M. Hastings and L. M. Corliss, IBM J. Res. Develop. 14, (1970) 227

/2/ F. Gautier et al., Solid State Commun. 11 (1972) 1201, and J. Phys. C6 (1973) L 320

2.3   Magnetic Hyperfine Interactions at ^{61}Ni in Face-Centered Cubic Ni-Mn Alloys

J. Fink, G. Czjzek and H. Schmidt

Mössbauer spectra of ^{61}Ni in disordered Ni-Mn alloys with concentrations ranging from 2.5 to 35 at % Mn, taken at 4.2 K, show a broad distribution of magnetic hyperfine fields. The spectra are not sufficiently resolved to give a detailed picture of the distribution. However, for all concen-
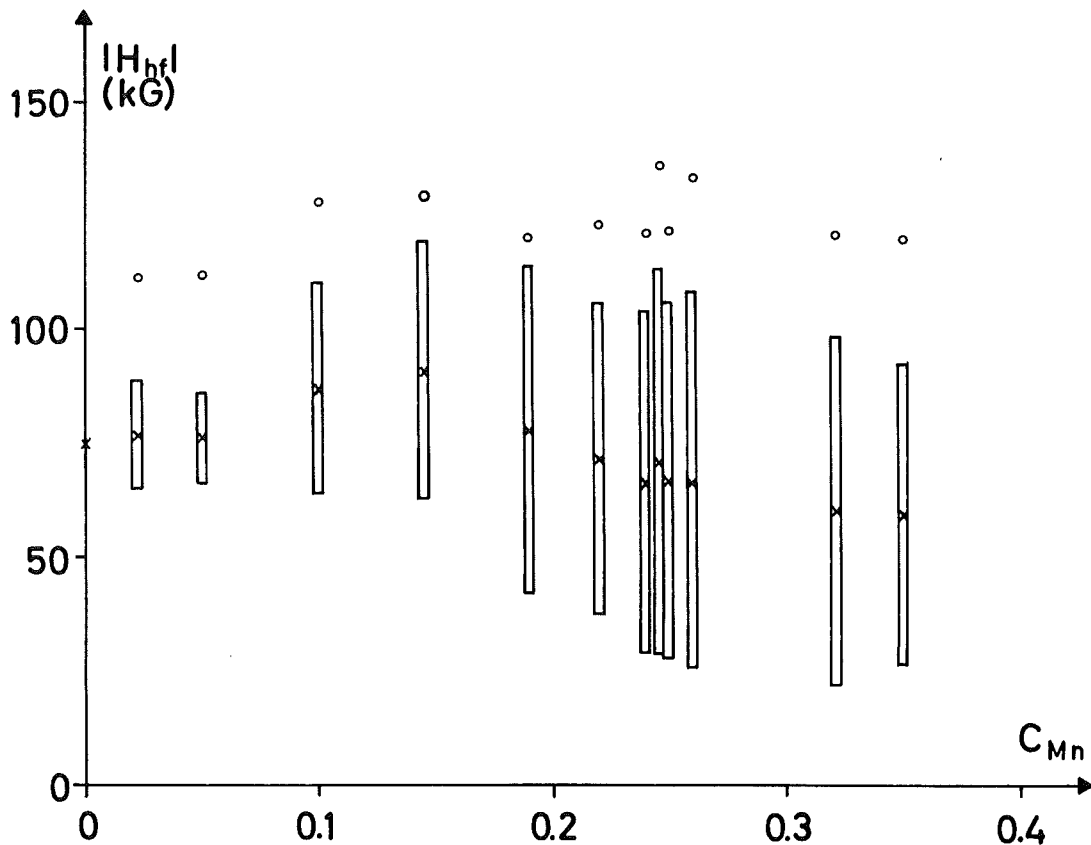
Fig. 38   Concentration dependence of magnetic hyperfine fields at ^{61}Ni-nuclei in disordered Ni-Mn alloys. All spectra show a broad distribution of hyperfine fields, indicated by the bars, and a pronounced component at some larger field-value, marked by a circle.

trations a rather pronounced component with a relatively large field (circles in Fig. 38) is found besides a wide distribution, apparently without prominent features (indicated by bars in Fig. 38). The crosses mark the average field for this part of the distribution. This result is similar to the distribution of hyperfine fields found at ^{55}Mn in Ni-Mn alloys /1/ and at ^{57}Fe in Fe-Ni alloys /2/.

The fraction of ^{61}Ni-nuclei experiencing the large field is near 20 % for $c_{Mn} \leq 15$ at %, near 10 % for higher Mn-concentrations.

This large-field component in the low-concentration alloys can possibly be ascribed to Ni atoms in the first coordination shell of a Mn atom, although

the concentration dependence of the relative intensity does not agree with that calculated for a random atomic distribution. The discrepancy may be due to a strong tendency toward short-range order.

In the higher-concentration alloys this component corresponds probably to small clusters with an atomic arrangement that favors locally a ferromagnetic polarization.

Whereas the bulk magnetization of Ni-Mn alloys at 4.2 K goes to zero near 30 at %.Mn, the Mössbauer spectra show no unsplit line corresponding to zero field up to 35 at % Mn, the highest concentration studied. The features of the hyperfine field distribution remain unchanged even in this concentration range.

Samples with a Mn-concentration near 25 at.% were annealed at 420 $^{\circ}$C, below the critical temperature for Ni_3Mn-type ordering. The result is an upward shifting of the magnetic hyperfine field values and an increase of the fraction found in the large-field component. After 30 days at 420 $^{\circ}$C, a time which leads to an ordering described by a long-range order parameter S near 0.9, we find for about 50 % of the ^{61}Ni-nuclei a hyperfine field of 207 kG, for the other ones again a broad distribution centered at 156 kG. The fraction of 50 % corresponds very well to the fraction of Ni atoms with the exact atomic arrangement corresponding to Ni_3Mn in the first coordination shell calculated for S = 0.9.

References

/1/ R. L. Streever, Phys. Rev. 173 (1968), 591
/2/ H. Rechenberg et al., J. Phys. Chem. Solids 34 (1973), 1251

2.4 Investigation of the Coexistence of Superconductivity and Magnetism in $Gd_xCe_{1-x}Ru_2$ by ^{155}Gd Mössbauer Spectroscopy

K. Ruebenbauer, G. Czjzek, J. Fink and H. Schmidt

Coexistence of superconductivity and ferromagnetism has been proposed to occur in certain rare-earth-substituted Laves-phase alloys of the type $R_xCe_{1-x}Ru_2$. With increasing x, T_c is rather slowly reduced. On the other hand, there is a linear depression of the magnetic ordering temperature θ_c with decreasing x. With R = Gd, $T_c(x)$ and $\theta_c(x)$ coincide for x = 0.135 at T = 4.8 K. It was our intention to investigate the magnetic structure of $Gd_xCe_{1-x}Ru_2$ in the range of concentrations where both superconductivity and magnetic ordering occur by measurements of magnetic hyperfine interactions of ^{155}Gd nuclei in $Gd_xCe_{1-x}Ru_2$ employing the Mössbauer effect of the 86.5 keV transition.

A source was produced by irradiating a ^{154}Sm in Al alloy in the Karlsruhe reactor FR2. The source was kept at 43 K. Below 40 K, the linewidth is considerably broadened by magnetic hyperfine interactions. Even at 43 K, there remains some quadrupole splitting. We prepared $Gd_xCe_{1-x}Ru_2$ absorbers with x = 0.05, 0.135, 0.24 and 0.5. For the samples with x $\leq$ 0.24 we used enriched to 92 % in ^{155}Gd. Susceptibility measurements on these samples were in agreement with previously reported data by Wilhelm and Hillenbrand /1/. Mössbauer spectra of these samples were taken at temperatures from 1.3 K up to 70 K. All spectra are poorly resolved and consist of two components, separated by a large isomer shift of more than 0.5 mm/sec. The intensity of the weaker component is increasing with increasing Gd concentration. The major component is split by magnetic hyperfine interaction below $\theta_c(x)$ for all x $\geq$ 0.135, irrespective of the transition to the superconducting state found for x = 0.135. The magnetic hyperfine field extrapolated to T = 0 K is about 350 kG, the temperature dependence follows a Brillouin function. Above the magnetic transition temperature, there remains some broadening of the absorption line not yet well understood. The measurements will be repeated with a single line source to get better resolution.

References

/1/ M. Wilhelm and B. Hillenbrand, Z. Naturforsch. 26a (1971), 141

2.5   Self-Diffusion in ^{7}Li-Metal and the Spin-Lattice
       Relaxation of the β Emitter ^{8}Li

H. Ackermann, D. Dubbers, H. Grupp, M. Grupp, P. Heitjans,

W. Hell and H.-J. Stöckmann, I. Physikalisches Institut der

Universität Heidelberg and Institut Laue Langevin, Grenoble

Spin-lattice relaxation processes in Li-metal have been studied several times
by classical NMR techniques /1/. In these experiments, however, the necessary
application of a resonant rf field implies some difficulties: restriction of
the accessible temperature and magnetic field ranges, skin effect, heating
of small particles etc.

In the case of Li the polarized neutron capture, β decay asymmetry method can be
well applied and avoids these difficulties: no rf field is required and one
works with bulk samples, T = 10 ... 1000 K and H_o = 0.1 ... 7 kOe are
accessible.

These experiments have been performed at the FR2 reactor (Karlsruhe) and at
the HFR reactor (Grenoble). The polarized ^{8}Li(τ_β = 1.2 s) nuclei have been
produced in ^{7}Li-metal, enclosed in a stainless steel box, by polarized
neutron activation. The β decay asymmetry was used to detect the nuclear
polarization. T_1 was measured in two ways: (i) by direct observation of
transients of the decay asymmetry a = a_o exp(-t/T_1) and (ii) by observation
of the steady state asymmetry a = a_o(1 + τ_β/T_1)$^{-1}$ for continuous activation
(an example is shown in Fig. 39).
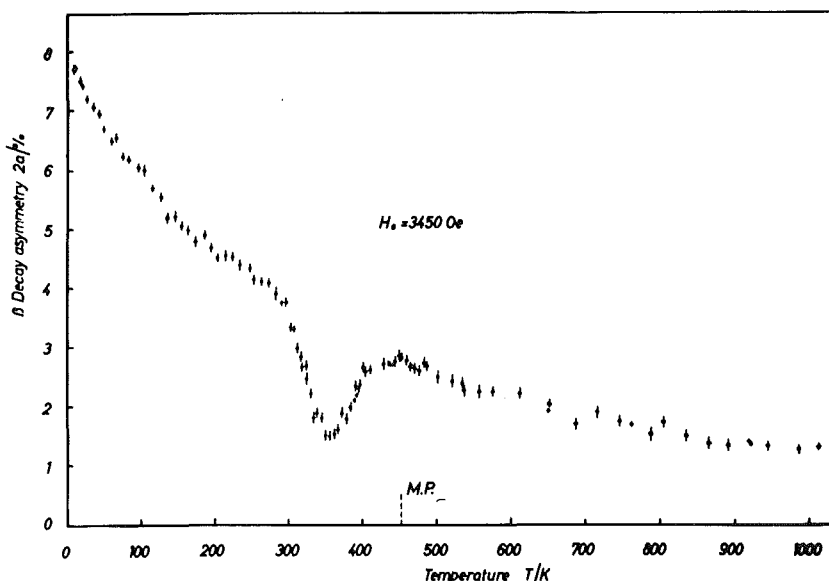
Fig. 39

β decay asymetry 2a
of ^{8}Li in ^{7}Li-metal
as a function of tem-
perature at H_o = 3450, Oe
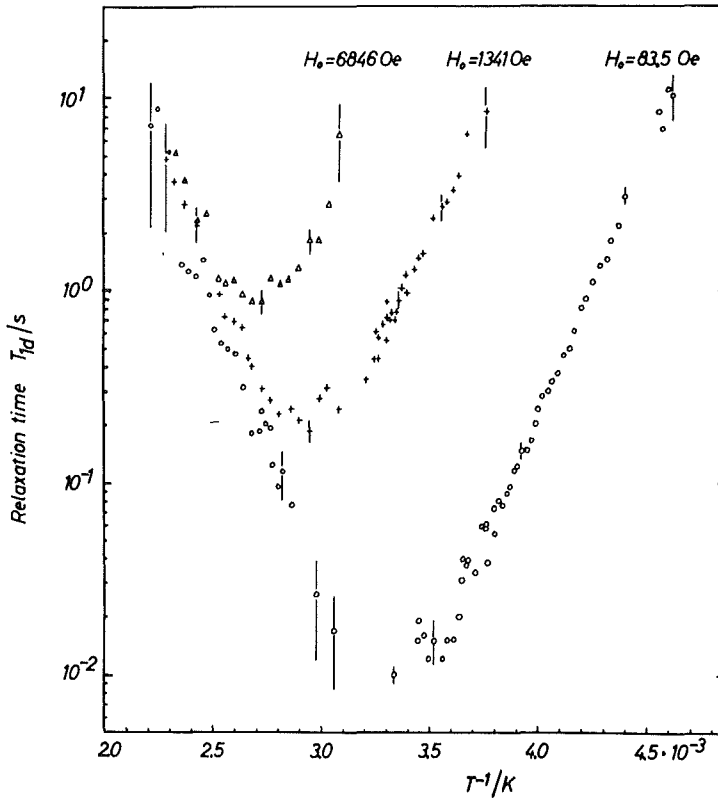
Fig. 40

Dipolar spin-lattice relaxation time T_{1d} of ^8Li in ^7Li-metal versus the reciprocal temperature for three values of H_o.

In pure solid metals the essential contributions to the measured relaxation rate are due to the hyperfine interactions of the nuclei with the conduction s-electrons and the fluctuating nuclear dipole-dipole interaction caused by the diffusional motion of the atoms: $1/T_1 = 1/T_{1e} + 1/T_{1d}$. According to the Korringa relation T_{1e} is proportional to $1/T$ (apart from effects of thermal expansion) and contributes over the whole temperature range. On the contrary, T_{1d} is finite only if the Larmor frequency ω_o is comparable with the mean jump frequency $1/\tau$ of the diffusing atoms. So T_{1d} and by that T_1 pass through a minimum when $\omega_o \tau \approx 1$. The mean time between jumps of a nucleus is generally assumed to obey the Arrhenius relation $\tau \propto \exp (E_A/kT)$, where E_A is the activation energy of the self-diffusion. Minima of T_1, i. e. of the β decay asymmetry, have been observed in the temperature range $T = 300 \ldots 370$ K, corresponding to $H_o = 100 \ldots 7000$ Oe.

From the measurements of T_1 we obtained T_{1d} by separating the electronic contribution. In fig. 40 minima of T_{1d} are shown for three different values of the magnetic field. The shape and precise $\omega_o \tau$ - value of these minima depend on the underlying diffusion mechanism. The analysis of these minima in terms of a monovacancy model /2/ is in progress and treats questions concerning the correlation of subsequent jumps, diffusion parameters, etc.

References

/1/ A. Seeger, H. Mehrer, in: Vacancies and Interstitials in Metals, p. 1; North-Holland, Amsterdam 1969; and References given there

/2/ D. Wolf, Z. Naturforschung 26a (1971), 1816

2.6 Analysis of the Temperature Dependence of Diffuse Neutron Scattering in Disordered Ni-Mn Alloys

P. v. Blanckenhagen and Chr. v. Platen

In connection with Mössbauer-experiments on Ni-Mn alloys we investigate the concentration and temperature dependence of the magnetic short range order in these alloys. The magnetic neutron scattering cross section is measured as the difference effect of scattered intensity without magnetic field and with magnetic field parallel ($\Delta_{||}$) resp. vertical ($\Delta_{\perp}$) to the scattering plane. To analyse the magnetic diffuse cross section, the nuclear diffuse cross section and the short range order must be known; both experimental cross sections have to be corrected for multiple and inelastic scattering, and contributions from critical magnetic scattering have to be separated.

Measurements have been done from 9 K up to the magnetic critical points on alloys containing 5 - 25 at % Mn. For the 15 % alloy inelastic scattering was determined by time of flight-experiments to check calculations of the inelastic cross section. Calculated multiple scattering could be related to the difference of measurements with 1.48 $\overset{o}{A}$ and 4.44 $\overset{o}{A}$ neutrons. A significant contribution at small momentum transfers was due to critical magnetic scattering already far below the transition point ($T/T_c \gtrsim 0.7$). The observed change of the sign of $\Delta_{\perp}$ below T_c and the apparence of a maximum of $\Delta_{||}$ below T_c may be attributed to simultaneous contributions of elastic diffuse, spin wave and critical scattering.

The results show the influence of the magnetic phase transition over a large temperature range; they demonstrate also the necessity of careful analysis of the concentration dependence of magnetic diffuse scattering data because of the simultaneous variation of T_c with concentration.

2.7 Untersuchungen der magnetischen Eigenschaften von Verbindungen $Na_2Ni^{II}Me^{III}F_7$ vom Typ des Weberit

G. Czjzek and J. Fink

G. Heger, FB Geowissenschaften der Universität Marburg

D. Babel, FB Chemie der Universität Marburg

R. Geller, Institut für Kristallographie der Universität

Tübingen

Die quaternären Fluoride $Na_2Ni^{II}Me^{III}F_7$ (Me^{III} = Fe, Al, Cr, ...) kristallisieren in der Weberit-Struktur (Na_2MgAlF_7) mit der orthorhombischen Raumgruppe Imm2 (C_{2v}^{20}) /1, 2/. Dabei besetzen die zwei- und dreiwertigen Übergangsmetallionen verschiedene spezielle Punktlagen, die durch verkantete Fluorbrücken miteinander verbunden sind. In dieser Anordnung können magnetische Superaustauschwechselwirkungen zwischen verschiedenen paramagnetischen Ionen untersucht werden.

Pulvermessungen der magnetischen Suszeptibilität und der Neutronenbeugung haben gezeigt, daß Na_2NiFeF_7 unterhalb von 88 K eine ferrimagnetische Ordnung aufweist /3/. Mit Mößbauer-Untersuchungen an ^{57}Fe wird versucht, aus der Temperaturabhängigkeit des Hyperfeinfeldes und aus der fluktuationsbedingten Linienverbreiterung am Phasenübergang kritische Exponenten zu bestimmen.

Ersetzt man die Fe-Ionen durch diamagnetische Al-Ionen, so beobachtet man das Verhalten eines eindimensionalen Antiferromagneten und unterhalb von 11 K eine verkantete antiferromagnetische Ordnung /4/. Zur näheren Untersuchung des kritischen Verhaltens in der Umgebung des Phasenübergangs wurden Mößbauer-Messungen an ^{61}Ni begonnen.

Pulversuszeptibilitätsmessungen an Na_2NiCrF_7, die für Temperaturen oberhalb von 4.2 K durchgeführt wurden, lassen für sehr tiefe Temperaturen eine ferrimagnetische Ordnung erwarten /2/. Mit Hilfe der Neutronenbeugung konnte eine magnetische Ordnung unterhalb von 4.1 K nachgewiesen werden. Wie die Temperaturabhängigkeit des magnetischen Beitrages zu dem
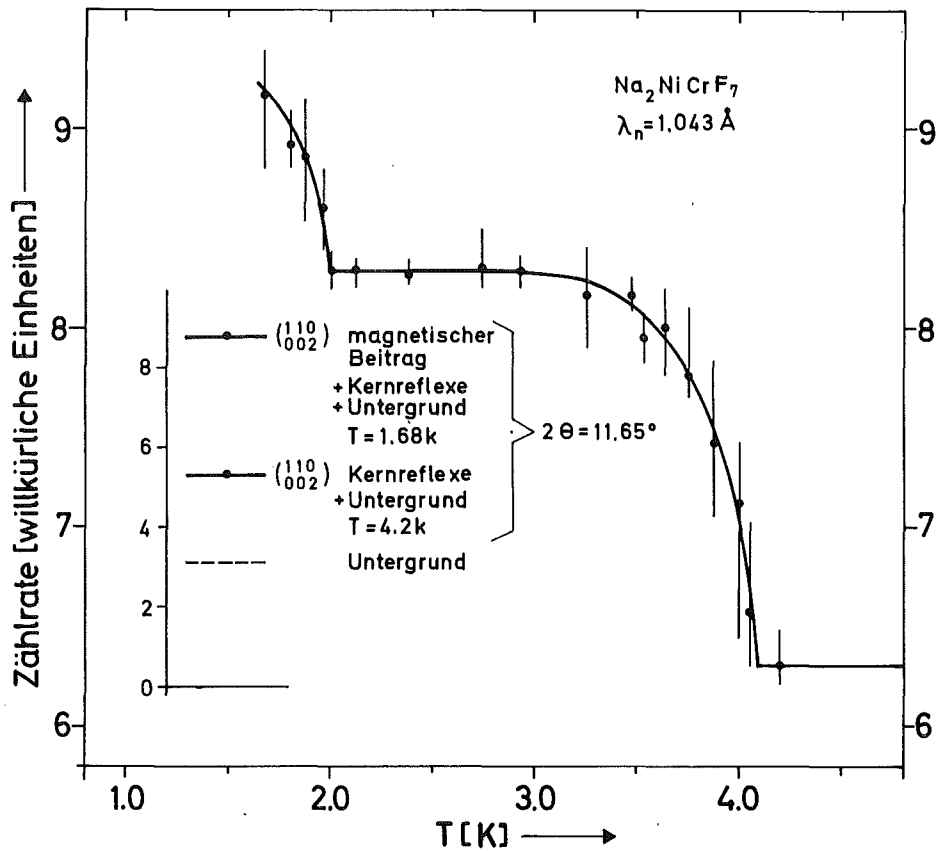
Fig. 41 Temperaturabhängigkeit des magnetischen Beitrags zum
(110, 002)- Reflex

(110, 002)- Reflex in Fig. 41 zeigt, gibt es darüberhinaus bei 2.0 K

einen weiteren magnetischen Phasenübergang. Unterhalb von 2.0 K läßt sich

die magnetische Struktur von Na_2NiCrF_7 nicht durch eine einfache kollineare

ferrimagnetische Anordnung, analog zu Na_2NiFeF_7, beschreiben. Eine Rechnung,

die mögliche Verkantungen berücksichtigt, wird durchgeführt.

References

/1/ Viebahn-Hänsler, R., Dissertation, Universität Tübingen (1971)

/2/ Dance, J.-M., Thèse, Universität Bordeaux (1974)

/3/ Heger, G., Viebahn-Hänsler, R., Solid State Commun. 11, 1119 (1972)

/4/ Heger, G., International Journal of Magnetism 5, 119 (1973)

2.8 Strukturelle Untersuchungen der intermetallischen Phasen vom Typ $(Cr_{1-x}Fe_x)_{1+\delta}Sb$ $(0 \leq x \leq 1; \delta \approx 0.13)$

G. Heger, E. Hellner, D. Mullen, J. Nösselt and W. Treutmann, FB Geowissenschaften der Universität Marburg

Nach Pulveruntersuchungen der magnetischen Suszeptibilität und der Röntgen-beugung bildet die Legierungsreihe $(Cr_{1-x}Fe_x)_{1+\delta}Sb$ im Bereich $0 \leq x \leq 1$ für $\delta \approx 0.13$ eine lückenlose Mischkristallreihe mit der hexagonalen NiAs-Struktur /1/. Die überschüssigen Übergangsmetallatome besetzen dabei statistisch den Sb-Punktlagen äquivalente Zwischenräume. Die magnetischen Untersuchungen, ergänzt durch Mößbauer-Messungen am ^{57}Fe, zeigten, daß die beiden binären Legierungen dieser Reihe, $Cr_{1+\delta}Sb$ $(x = 0)$ und $Fe_{1+\delta}Sb$ $(x = 1)$, antiferromagnetisch ordnen. Im Legierungsbereich $0.6 \leq x \leq 0.85$ wird ein ferromagnetisches Verhalten angenommen /1, 2, 3, 4/.

Um diese magnetischen Verhaltensweisen erklären zu können, werden Ein-kristalle gezüchtet und untersucht. Dabei soll zuerst die Frage der Ver-teilung der Übergangsmetallatome mit Hilfe von ergänzenden Röntgen- und Neutronenbeugungsmessungen bei Zimmertemperatur geklärt werden. Die Rönt-genuntersuchungen liefern für Einkristalle aus verschiedenen Züchtungen (Bridgman- und Fluxmethode) die exakten Werte der überschüssigen Atome. Damit erhält man aus den Neutronendaten die Verteilungen der Übergangs-metallatome für die einzelnen Punktlagen.

Für $x = 0.7$, wo bei tiefen Temperaturen eine ferromagnetische Ordnung an-genommen wird, ergab der Bridgman-Kristall die folgenden Ergebnisse:

Röntgenbeugung $> \delta = 0.22$, d.h. $(Cr_{0.3}Fe_{0.7})_{1.22}Sb$ $(R_r = 0.07)$
Neutronenbeugung $\Rightarrow$ statistische Verteilung der Fe/Cr für beide Punktlagen
$(0, 0, 0) + (0, 0, 1/2)$ und $(2/3, 1/3, 1/4) + (1/3, 2/3, 3/4)$ mit einem Verhältnis Cr : Fe = 30 : 70 $(R_n = 0.04)$.

Für $x = 0.5$ wird ein antiferromagnetisches Verhalten angenommen. Der Bridgman-Kristall ergab:

Röntgenbeugung   > $\delta = 0.20$, d. h. $(Cr_{0.5}Fe_{0.5})_{1.20}Sb$ $(R_r = 0.07)$

Neutronenbeugung > statistische Verteilung der Fe/Cr für (O, O, O) +

(O, O, 1/2) mit Cr : Fe = 55 : 45 und für den Überschuß

auf den Plätzen (2/3, 1/3, 1/4) + (1/3, 2/3, 3/4):

Cr : Fe = 37 : 63 $(R_n = 0.045)$. Damit ergibt sich als

Zusammensetzung: $(Cr_{0.52}Fe_{0.48})_{1.20}Sb$.

Untersuchungen eines Flux-Kristalls mit x = O.7 zeigten eine deutlich aus-
geprägte Überstruktur: die hexagonale c-Achse wird verdreifacht und die a
bzw. b-Achsen verdoppelt. Dies würde eine Ordnung der überschüssigen Über-
gangsmetallatome bedeuten. Die Auslöschungen der kompletten Überstruktur-
daten (OO1, mit 1 = 2n + 1) führen von der Raumgruppe $P6_{3/mmc}$ (NiAs-
Struktur) zu $P6_3$ oder $P6_{3/m}$. Die Auswertungen sind noch nicht abgeschlossen.

References

/1/ J. Nösselt, U. Sondermann, Verh. DPG (VI) 8, 548 (1973)
    International Journal of Magnetism 5, 277 (1973)

/2/ J. Takei, D. E. Cox, G. Shirane, Phys. Rev. 129, 2008 (1963)

/3/ T. Yashiro, Y. Yamaguchi, S. Tomiyoshi, N. Kazama, H. Watanabe
    J. Phys. Soc. Japan, 34, 58 (1973)

/4/ F. W. Richter, K. Schmidt, International Journal of Magnetism 5,
    283 (1973)

2.9   Strukturelle Modifikationen und Phasenübergänge von
      $(CH_3NH_3)_2MnCl_4$

G. Heger, FB Geowissenschaften der Universität Marburg

I. R. Jahn und K. Knorr, Institut für Kristallographie
der Universität Tübingen

Schichtstrukturen vom Typ $(C_nH_{2n+1}NH_3)_2MnCl_4$ zeigen viele interessante
Eigenschaften. Sie sind Beispiele für quasi-zweidimensionale Heisenberg
Antiferromagneten mit variabler magnetischer Zwischenschichtwechselwirkung.
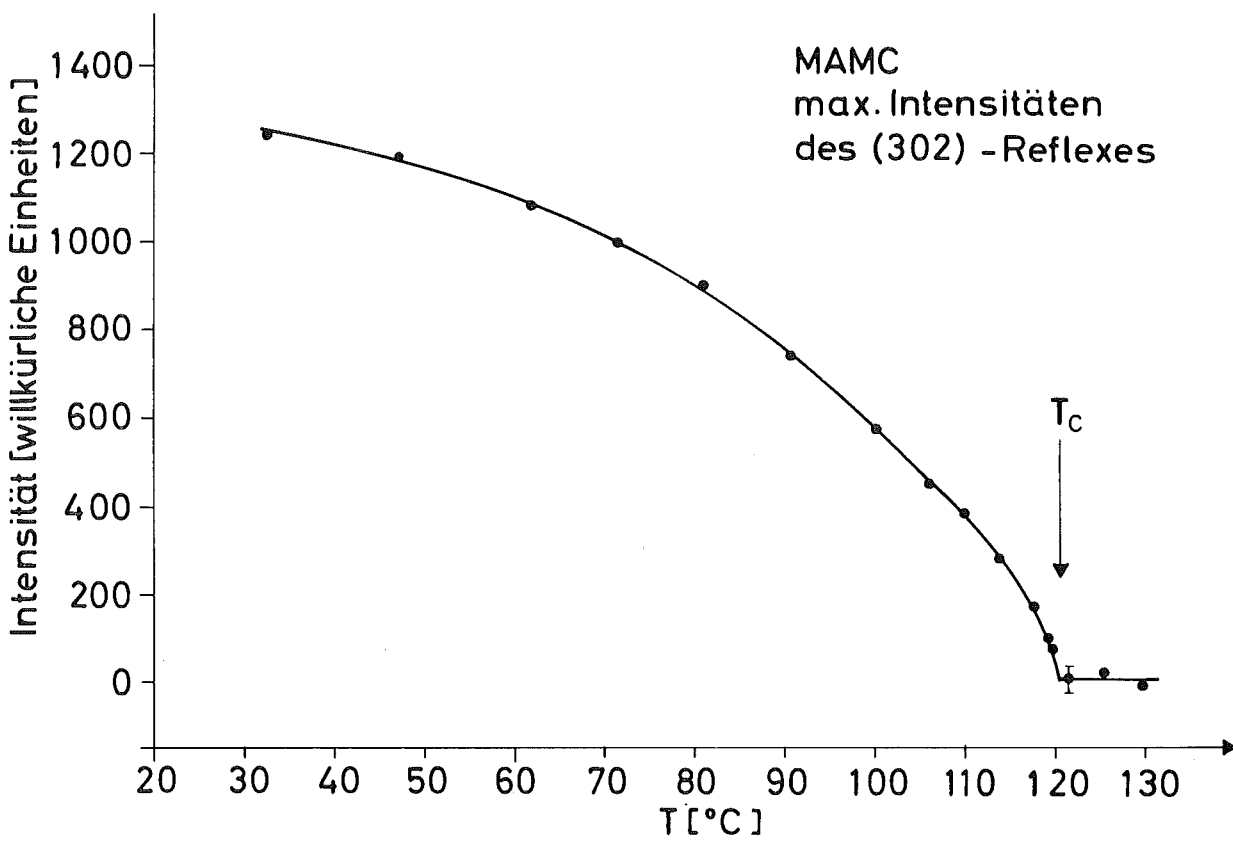
Fig. 42 Temperaturabhängigkeit der maximalen Intensität des orthorhombischen
(302)- Überstrukturreflexes (Neutronenbeugung)

Messungen der magnetischen Suszeptibilität und der Neutronenbeugung an
nichtdeuteriertem und deuteriertem $(CH_3NH_3)_2MnCl_4$, abgekürzt als MAMC, be-
stätigten das planare magnetische Verhalten mit einem Phasenübergang zu
einer dreidimensionalen antiferromagnetischen Ordnung bei 45 K /1, 2/. Neben
diesen magnetischen Eigenschaften wurden für MAMC verschiedene strukturelle
Phasenübergänge gefunden /2, 3, 4/:

$$T_{c1} = \frac{93.7}{95.1} \ K \qquad T_{c2} = \frac{256.5}{256.9} \ K \qquad T_{c3} = 393.8 \ K$$

monoklin $\rightleftharpoons$ tetragonal $\rightleftharpoons$ orthorhombisch $\rightleftharpoons$ tetragonal
diskontin.   diskontin.   Abma   kontinuierlich   T4/mmm
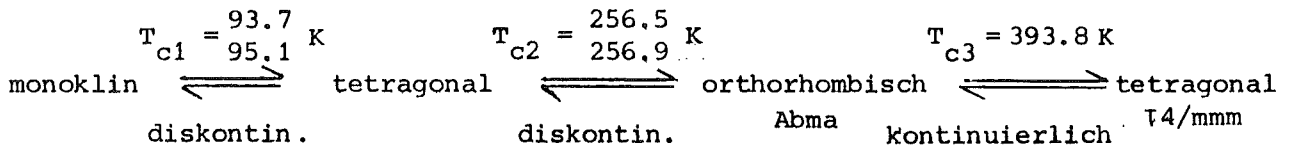
Der kontinuierliche Phasenübergang bei T_{c3} = 393.8 K zwischen der tetragonalen
Hochtemperatur- und einer orthorhombischen Kristallstruktur wurde mit Hilfe
der optischen Doppelberechnungsänderung, der Röntgen- und Neutronenbeugung
an Einkristallen untersucht. Zur Beschreibung von kontinuierlichen Phasen-
übergängen werden sogenannte kritische Exponenten verwendet, die den
Verlauf von bestimmten kennzeichnenden Größen in der Umgebung der Phasen-

umwandlung angeben. Z. B. wird der Verlauf des Ordnungsparameters (OP) durch einen kritischen Exponenten, üblicherweise mit ß bezeichnet, beschrieben:

$$OP \sim (1 - \frac{T}{T_c})^\beta$$

Als Quadrat des Ordnungsparameters wurde am Phasenübergang bei T_{c3} die temperaturabhängige Änderung der optischen Doppelbrechung Δn, der Differenz der Gitterkonstanten a - b (Röntgenbeugung) und der Intensität eines Überstrukturreflexes (Neutronenbeugung, siehe Fig. 42) gemessen. Die Auswertung der Intensitätsmessungen aus Fig. 42 ist in Fig. 43 dargestellt. Die verschiedenen Meßmethoden liefern mit hervorragender Übereinstimmung die folgenden ß-Werte:

$$\Delta n : \quad 0.31\underline{6} \pm 4$$
$$a - b : \quad 0.3\underline{1} \pm 1 \qquad > \qquad \beta_{T_{c3}(MAMC)} = 0.317$$
$$I_{(302)} : \quad 0.3\underline{25} \pm 10$$
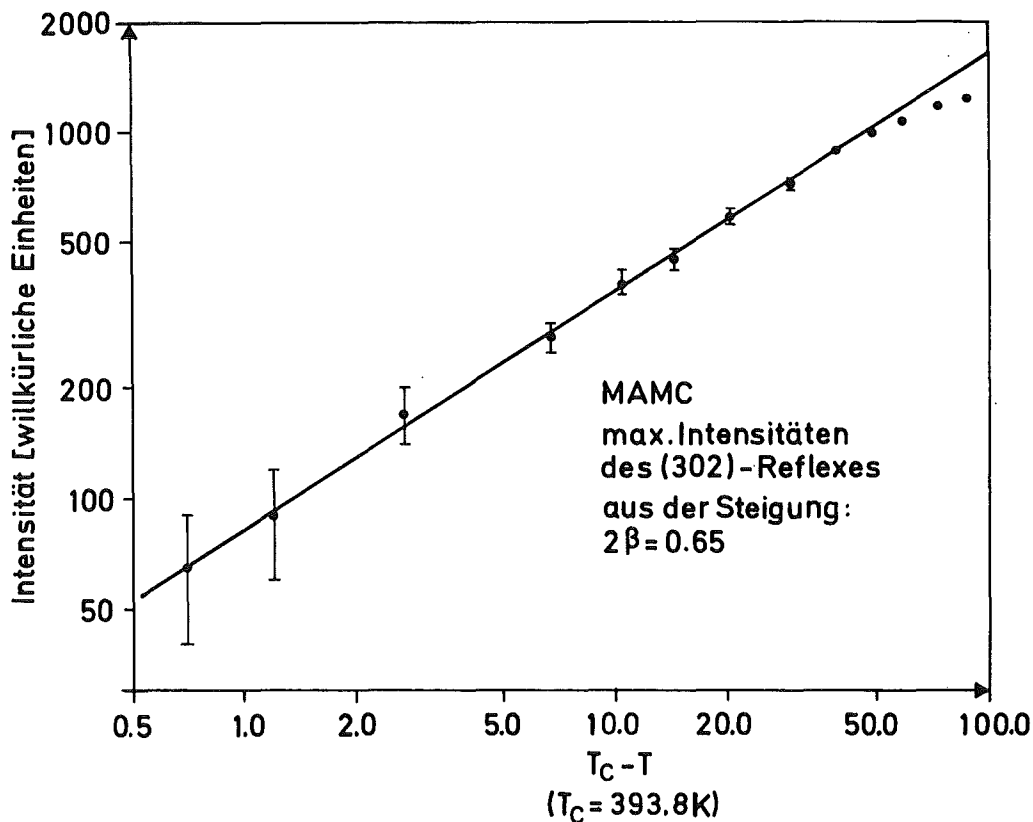
Fig. 43 Im doppeltlogarithmischen Maßstab erhält man aus der Steigung der Geraden: 2ß = 0.65

Um die exakten Punktlagen der CH_3- und NH_3-Gruppen in den verschiedenen
Modifikationen zu bestimmen, und damit die Mechanismen der Phasenüber-
gänge, werden Neutronenbeugungsmessungen an Einkristallen durchgeführt.
Die Messungen der tetragonalen Hochtemperatur- und der orthorhombischen
Zimmertemperaturmodifikationen sind abgeschlossen und werden ausgewertet.

References

/1/ van Amstel, W. D., de Jongh, L. J., Solid State Commun. 11, 1423 (1972)

/2/ Heger, G., Henrich, E., Kanellakopulos, B., Solid State Commun. 12,
     1157 (1973)

/3/ Arend, H., Hofmann, R., Waldner, F., Solid State Commun. 13, 1629 (1973)

/4/ Knorr, K., Jahn, I. R., Heger, G., Solid State Commun., erscheint demnächst.

3. MATERIALS RESEARCH

3.1 Preparation and Analysis of Superconducting Thin Films

B. Hofmann-Kraeft, O. Meyer, F. Ratzel, R. Smithey and M. Gettings

Thin superconducting films with thicknesses between 10^{-2} µm and 10 µm of several compounds with A-15 and NaCl-structure have been produced by sputtering and by electron beam evaporation. Analysis of these thin films have been performed by x-ray diffraction and by high energy ion backscattering together with careful thickness measurements. T_c-measurements have been performed by the usual resistance technique.

Equipment: The vacuum system of the sputtering modul is a bakable stainless steel chamber connected to ion getter and titanium evaporation pumps. For the preevacuation and during the sputtering process a turbomolecular pump is used. The anode consists of a separate vacuum chamber, where the substrate heating is performed by an electron cannon.

The evaporation system consists of a two boat electron cannon, where the power ratio of the electron beam in the two boats can be varied between 0 and 100 percent. Therefore the evaporation rates from two components can be adjusted in order to obtain the correct composition. A second electron cannon serves as a heatable substrate holder.

Results: The following compounds have been produced by codeposition (the highest T_c-values obtained up to now are given in brackets): $Nb_3Sn(18.3\ K)$; $Nb_3Si(9\ K)$; $Nb_3Ge(21.8\ K)$ and $V_3Ga(16\ K)$. $V_3Si(14\ K)$ has been produced by selective diffusion of Si from SiO_2 into an evaporated V-layer.

By sputtering and by reactive sputtering in a nitrogen-argon plasma the following carbides and nitrides have been prepared: $NbN(17.3\ K)$; $NbC(11.3\ K)$; $VN(10\ K)$; $VC(<\ 1.2\ K)$ and $MoN\ (4\ K)$.

In addition to results on NbN and on NbC, published in a previous paper
/1/, T_c of NbN could be increased to 17.3 K by increasing the substrate
temperature from 450 $^\circ$C to 750 $^\circ$C. Results obtained with ESCA technique
show, that the oxygen content in the surface of NbN is inversely proportional
to T_c and also to the layer composition Y (Y is defined as the ratio of the
number of nonmetal to metal atoms). The oxygen content at the surface was
found to increase with the number of nitrogen vacancies. In NbN the nitrogen
is mainly bound to the niobium whereas in sputtered NbC_xN_y films 50 % of the
nitrogen does not show a chemical shift.

Backscattering analysis together with thickness measurements on reactively
sputtered VN-layers showed, that the vanadium content and therefore the
layer density increased with increasing substrate temperature. This increase
in the vanadium content is correlated with an increase in T_c, as it is shown
in Fig. 44, indicating that T_c has a maximum at Y = 1. Even for Y = 1 the
layers seem to have a total vacancy concentration of 5 to 10 at %. X-ray
diffraction results showed that in NbN besides the cubic high T_c δ-phase,
two hexagonal phases exist: the metastable δ'-phase and the stable ε-phase.
For high T_c material the cubic phase component increased but a weak hexagonal
component was still visible. In VN-layers however only the cubic phase could
be detected.

Nb_3Ge (20 K) has been prepared /2/ by sputtering; the niobium cathode was
partly covered with a germanium plate. The geometrical arrangement has been
optimized by T_c and backscattering measurements. In principle the results of
Gavaler /3/ could be confirmed stating that a high substrate temperature
(700 - 800 $^\circ$C) as well as a high Ar-partial pressure (0.1 - 0.3 Torr) during
sputtering are necessary conditions in order to produce the high T_c Nb_3Ge-
phase. Difficulties in our system arose due to spurious discharges between
cathode and the guard ring at high Ar-partial pressure. This discharges were
found to increase the impurity content in the layer which results in a T_c
decrease. Test experiments are underway in order to overcome this problem.

Nb_3Ge (21.8 K) has also been sucessfully prepared by codeposition on a hot
substrate in our evaporation system /2/. The correct ratio of the niobium to
germanium deposition rates and the substrate temperature were found to be the
critical production parameters and have been optimized with regard to high
T_c-values in extensive calibration procedures.
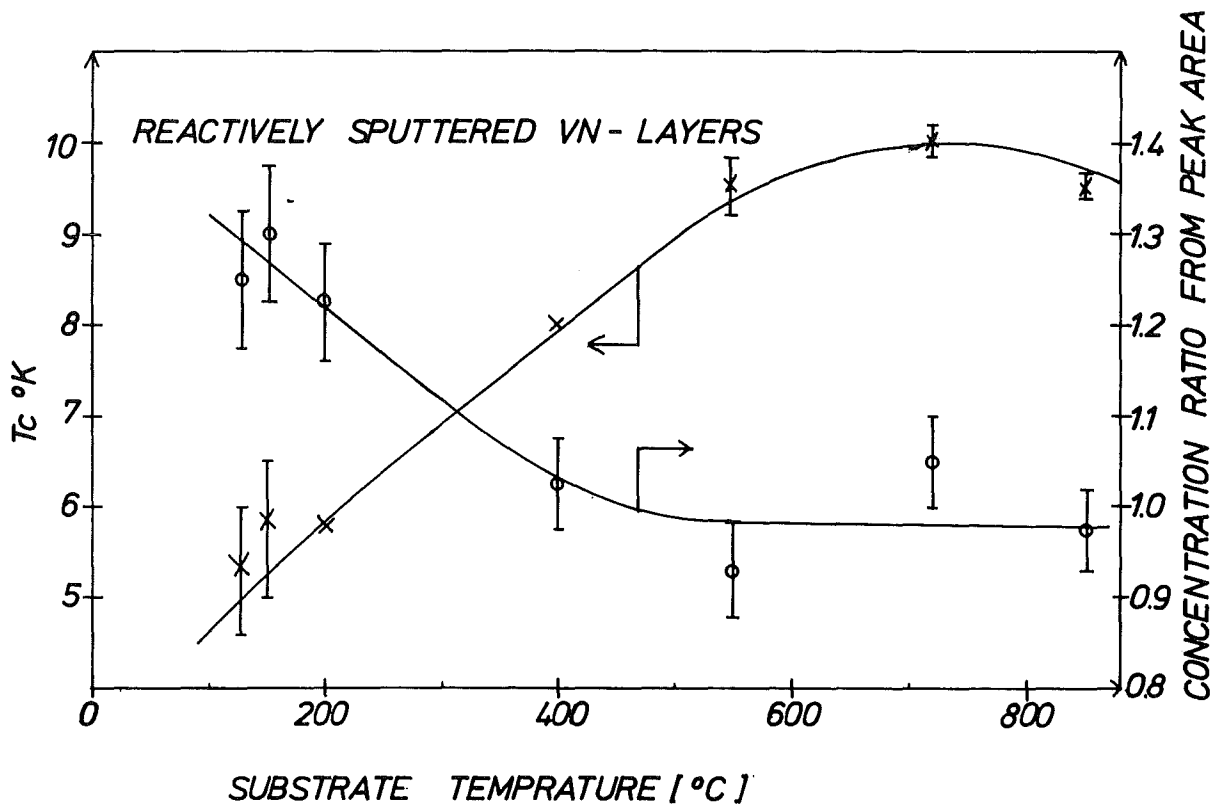
Fig. 44

X-ray studies revealed that the main component was the A-15 structure however some weak lines from the Nb metal bcc structure were also visible.

References

/1/ O. Meyer, G. Linker and B. Kraeft, Thin Solid Films 19 (1973), 217 - 226
/2/ M. Gettings and O. Meyer, Verhandl. DPG VI, 9 (1974), 847
/3/ J. R. Gavaler, Appl. Phys. Lett. 23 (1973), 480

3.2   The Influence of Heavy Ion Bombardment on the Transition Temperature of Thin Superconducting Layers

M. Kraatz, G. Linker and O. Meyer

Although the influence of radiation damage on the critical parameters (I_c, H_c) of superconductors has been extensively studied, little information is available on the influence of disorder produced by heavy ion bombardment on the superconducting transition temperature (T_c). We have investigated the influence of radiation damage on T_c of transition metal layers vanadium, niobium and tantalum and also preliminary measurements have been performed for compound superconductors having sodium chloride or A-15 structures (NbN, Nb_3Sn, Nb_3Ge). The results of such measurements are important when ion implantation is used as a doping technique for superconductors, when superconducting devices are applied in a radiation environment, and may be of interest when the mechanism of superconductivity is studied in disordered layers.

Layers of the transition metals have been prepared by electron gun evaporation in ultra high vacuum onto quartz substrates to thicknesses of about 1000 $\overset{o}{A}$. These layers usually had transition temperatures of bulk material. Compound superconductors have been made by simultaneous evaporation (Nb_3Ge, 21.8 K; Nb_3Sn, 18 K) or with the sputtering technique (NbN, 17 K; Nb_3Ge, 20 K). Layer composition, homogeneity, possible contamination and layer thickness have been controlled by backscattering of 2 MeV He^+ ions /1/.

Disorder in the layers has been produced by Ne^+ or He^+ ion bombardment at room temperature, the energy of the ions being chosen such that ions penetrated to the substrate and thus effected layer properties only by their energy lost in nuclear collisions with the target atoms on their path's through the layer. Sputtering effects have been found to be negligible in these experiments. The energy lost by the bombarding particles on their way through the target layer, i. e. the primary energy deposition profile has been calculated from universal $(d\varepsilon/d\rho)_n$ data tabulated by Schiott /2/ by converting his data from an energy to a depth scale for

the particular ion - target systems under consideration of energy lost by electronic stopping. In the actual computations an analytical expression for $(d\epsilon/d\rho)_n$ from Sigmund /3/ which is a good fit to Schiott's data and electronic stopping values from the theory of Lindhard et al. (LSS) /4/ were used and statistical fluctuations in the energy loss in the slowing down process have been neglected. The penetration depth of the particles has been estimated from LSS projected range statistics computed by Johnson and Gibbons /5/.

Rather homogeneous profiles were obtained in the energy range of 150 - 350 keV and similar densities for energies deposited in nuclear collisions in different materials were obtained by choosing appropriate fluences for the Ne or He ions. It should be emphasized however that primary energy deposition profiles are only a first step in an attempt to characterize the actual damage distribution as especially in metals a high defect recombination rate occurs during ion bombardment.

A decrease in T_c after ion bombardment has been observed for all super-conductors under investigation. This decrease ΔT_c has been found to be a function of the density of energy deposited in nuclear collisions (DED) and has been studied in the range from 10^{16} eV/$\overset{\circ}{A}$ cm^2 to 10^{19} eV/$\overset{\circ}{A}$ cm^2.

Relative values $\Delta T_c/T_c$ as a function of DED show only a relatively small increase in the range from 10^{16} eV/$\overset{\circ}{A}$ cm^2 to 10^{18} eV/$\overset{\circ}{A}$ cm^2 and are similar for vanadium, niobium and tantalum ($0.05 < \Delta T_c/T_c < 0.15$) whereas beyond 10^{18} eV/$\overset{\circ}{A}$ cm^2 (corresponding to about 100 atom displacement per atom) a steeper slope in the dependence on DED has been observed showing slightly higher values for superconductors with a higher T_c. Maximum values for $\Delta T_c/T_c$ were in the range of 0.4 and no saturation so for has been detected.

Preliminary results show that compound superconductors with A-15 structures are very sensitive to radiation damage and a decrease in T_c by factors 3 - 5 depending on fluence have been observed. In superconducting compound layers with NaCl - structure however only a small influence of disorder introduced by heavy ion bombardment on T_c occured.

Annealing experiments and an extension of the bombardment to low tempera-tures will be our next steps to obtain more information on the connection between radiation damage and the superconducting transition temperature.

References

/1/ G. Linker, O. Meyer, M. Gettings, Thin Solids Films 19 (1973), 177

/2/ H. E. Schiott, Mat. Fys. Medd. 35 (1966), Nr. 9

/3/ K. B. Winterbon, Range-Energy Data for KeV Ions in Amorphous Materials,
     November 1968, AECL - 3194

/4/ J. Lindhard, M. Scharff, H. E. Schiott, Mat. Fys. Medd. 33 (1963), Nr. 14

/5/ W. S. Johnson, J. F. Gibbons, Projected Range Statistics in Semiconductors,
     Stanford, Calif. (1970)

3.3   Doping of Superconducting Thin Films by Ion-Implantation

M. Kraatz, O. Meyer and E. Phrilingos

In a previous paper /1/ enhancement of the superconducting transition tem-
perature in transition metal and non transition metal films by ion implantation
as a room-temperature alloying process has been reported. In various diluted
alloys produced by ion implantation such as Fe-Ti, Pd-Zr and Zr-Re the
variation of T_c with concentration has been found to correlate with results
observed by normal alloying.

In addition, T_c-enhancement has been observed by implanting selected ions able
to form intermetallic compounds but which are of low solubility in Mo, W and
Re. The physical reason for this T_c enhancement could not be given in Ref. 1.
Therefore further systematic studies have been performed and it could be shown
that in Mo films the increase in T_c up to 7 K with concentration correlates
with the electronegativity of the implanted ions, whereas the solubility level
as well as the difference in the atomic size between the solvent and the solute
are of minor importance. This is demonstrated in Fig. 45, where the Durken-
Gurry-plot is shown for Mo. Elements in the square around Mo usually show a
high solubility as is described by the Hume-Rothery rules. Thin film x-ray
patterns from implanted and unimplanted areas do not show any remarkable
differences and it is concluded that the observed T_c-enhancement is not due
to grain size effects or to the formation of impurity phases with different

crystal structures. Therefore it is concluded, that the T_c increase is caused by a room-temperature alloying process. In order to equalize the electrochemical potentials between the atomic cells of the starting materials a charge transfer from Mo the solute of higher electronegativity may occur, which will result in a T_c increase as has been discussed by Miedema (1974) for transition metal alloys.

In contrast to these results the electronegativity does not play any role in the T_c-enhancement up to 2.3 K found by implanting selected ions in Al-layers at room-temperature. Here the T_c-enhancement seems to be correlated with atomic size effects presumedly connected with a softening of the average phonon frequency distribution.

24 elements from all groups of the periodic system have been introduced in Al-layers at room-temperature and the main results obtained up to now are summarized as follows.

1. Radiation damage produced by inert gas ions does not show any remarkable influence on T_c

2. Only 4 elements (Cu, Au, Ag, K) out of 24 do not increase T_c above 1.2 K. For all other dopants under consideration a saturation level for T_c in dependance on the dopant concentration c has been found within $1.3 < T_c$ (max) < 2.3 K. The saturation concentration was a function of the different implanted ion species and was found to fall in the region between $0.1 < C_{max} < 10$ at %.

For primary solid solutions Al-Mg, Al-Ge, Al-Ag and Al-Zn the variation of T_c with solute concentration, both the rapid decrease at low concentration as well as the increase of T_c at higher concentration could be described by an analytic expression with two (arbitrary) constants /3/. These constants were found to vary linearily with the square of the difference in valence between solute and solvent and also to correlate with the mean free electron path. Our results for the systems Al-Ge, Al-Mg, Al-Zn and Al-Ag show higher T_c-enhancements than those presented in Ref. 3, and are not limited to systems that have high solubility levels. This indicates, that ion implantation is a versatile technique for room temperature alloying.
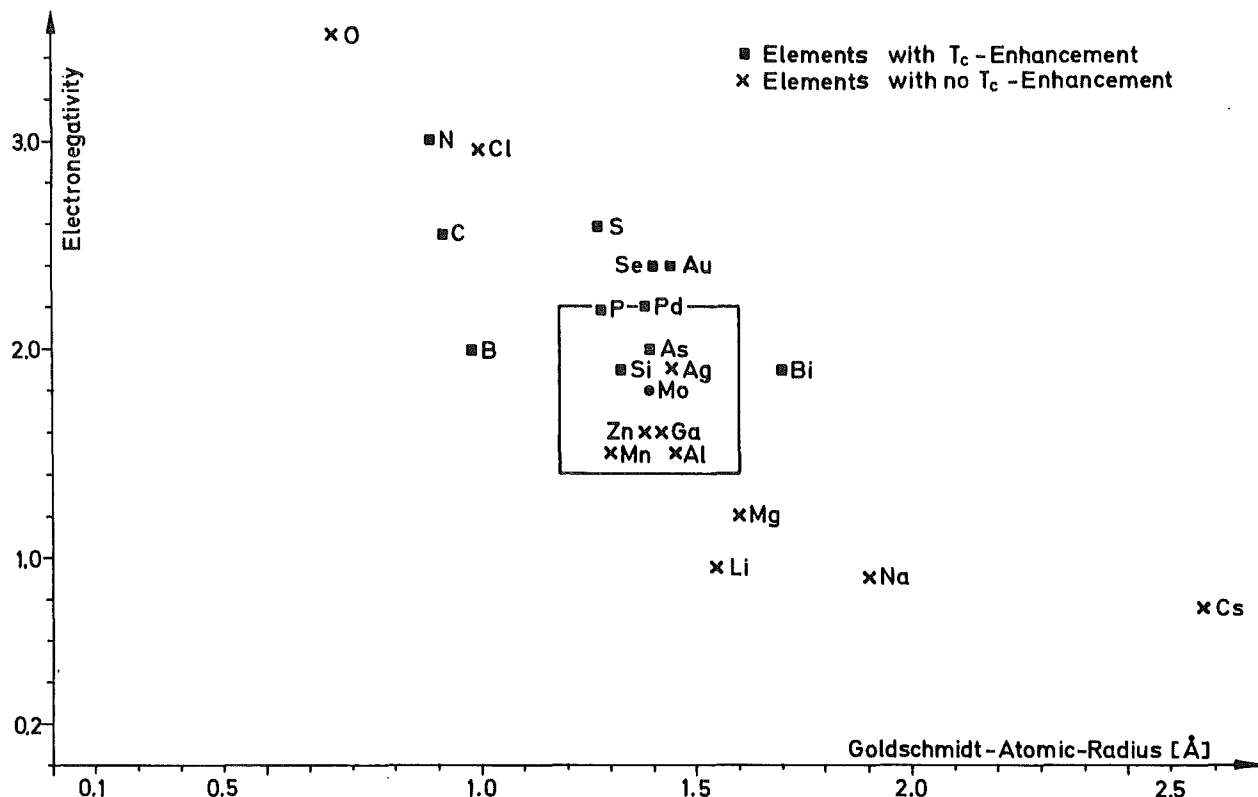
Fig. 45

References

/1/ O. Meyer, H. Mann and E. Phrilingos, International Conference on Application of Ion Beams to Metals Albuquerque, Oct. 1 - 4, 1973

/2/ A. R. Miedema, J. Phys. F Metal Physics 4 (1974), 120

/3/ D. P. Seraphim, C. Chiou and D. J. Quinn, Acta Metalurgica 9 (1961), 861

3.4 Electron Tunneling into Superconducting Niobium Carbide

J. Geerk

In this report, superconducting tunneling studies of the transition metal compound NbC, a superconducting refractory material are described. The starting material used was zone-refined NbC bulk-material with a T_c of 7.6 K. The tunnel junctions were of the type NbC - NbC ox. - Au prepared in the conventional manner. A clean tunneling surface was obtained by electropolishing. The superconducting energy gap Δ_o and the tunneling density of states $N(\omega)$ as a function of energy $(\hbar\omega)$ were determined from

F(ω): —·—·— Weber (calculated)
F(ω): — — — — inel. neutron scatt.(Gompf et.al.)
α²(ω)F(ω): ———— Tunneling

$F(\omega), \alpha^2(\omega)F(\omega)$
(arb. units)

NbC

5   10   15   20   25   30   ENERGY/meV
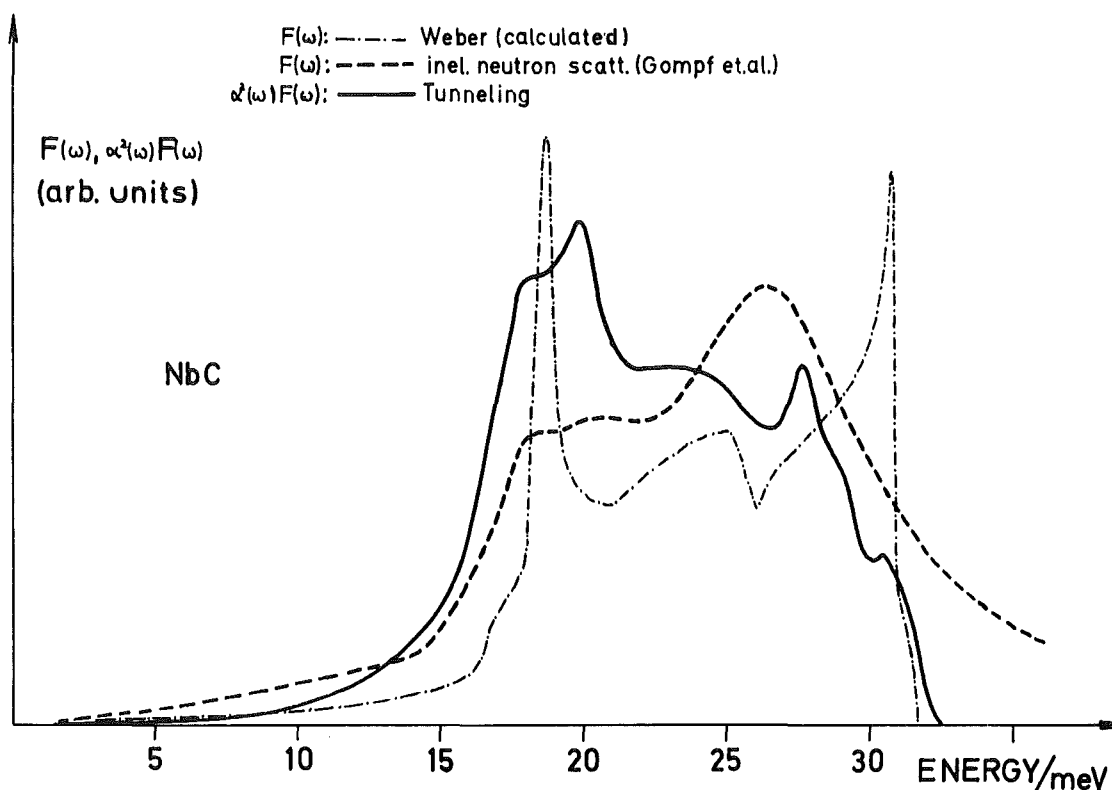
Fig. 46

plots of $dJ/_{dV}$ and $d^2J/_{dV^2}$. With this information one obtains a solution of the Eliashberg gap equations /1/ by the use of MacMillan's program /2/. The most important result of this procedure is $\alpha^2(\omega)$ $F(\omega)$, the product of the electron-phonon interaction function and the phonon density of states. In fig. 46 α^2F (line) is plotted versus energy. The two other curves are acoustic phonon spectra of NbC obtained by different methods. The smeared curve (dashed) is the result of an inelastic coherent neutron scattering measurement performed in our institute by Gompf et al. . The sharp peaked curve (dashed and dotted) is the result of a model calculation of Weber /3/, who fitted his dispersion curves to measured values. In the tunneling experiment no structure in the energy region of the optical phonons of NbC at about 70 meV was found. Analysing the main structures in α^2F one finds, that the pronounced peak at about 20 meV is due to transverse phonons and the peaks at about 28 - 30 meV belong to longitudinal phonons. The obvious weakening of the longitudinal structure is probably caused by the reduced tunneling penetration depth at these energies. The resulting μ^* value of 0.04 also shows, that α^2F was measured to low at least in certain energy regions. A comparison of the tunneling measurement with the two other phonon spectra shows, that the main structures, namely the beginning and

the end of the spectra, are the same. Also the bump in the middle of Weber's spectrum reproduces in the tunneling measurement. A detailed comparison with the more realistic spectrum of Gompf is not possible because of the weakening effect in $\alpha^2 F$ in the longitudinal acoustic energy region and the smearing at those energies in the neutron scattering measurement due to resolution.

References

/1/ G. M. Eliashberg, Zh. Eksperim i Theor. Fiz. 38 (1960), 966 (Sovient Phys. JETP 11 (1969), 696)

/2/ W. L. MacMillan and J. M. Rowell in Superconductivity edited by R. D. Parks (Marcel Dekker, New York, 1969), Vol I

/3/ W. Weber, Dissertation (MPI für Festkörperforschung Stuttgart)

3.5 Influence of Ion Induced Radiation Damage on the Dechannelling Rate of Ni Single Crystals

K. G. Langguth

The channelling - and backscattering technique with light ions like p and He^+ with energies in the MeV-range is an often used method for studying radiation damage induced by heavy ions in single crystals. During these measurements however the analysing beam itself produces defects which are causing dechannelling. Such defects in Ni single crystals were the subject of the present investigation.

The Ni single crystals were irradiated with 2 MeV He^+ ions in a random direction with different fluences. The irradiated samples were analysed with the 2 MeV He^+ beam incident in the <110> direction and the backscattered particles detected under an angle of 168 °. The He^+ fluence used for analysing was small and therefore the damage production during the measurement was negligible in this experiment.

The dechannelling rate increases steadily with increasing fluence up to a fluence of about $2.5 \cdot 10^{17}$ He^+/cm^2 as can be seen in figure 47. Above this fluence the dechannelling rate starts to saturate. Merkle /1, 2/ et al.
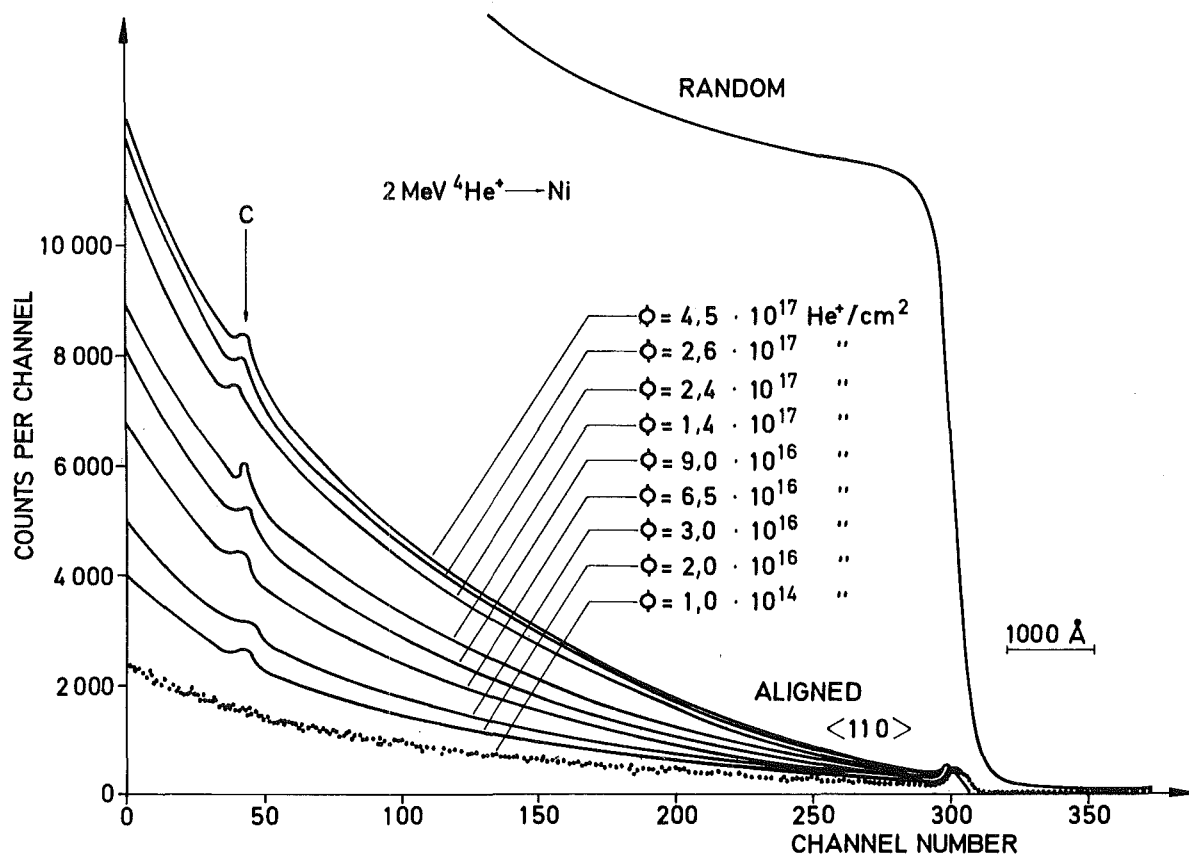
Fig. 47

assume that the dechannelling after He$^+$ bombardment is mainly due to the strain field around vancany clusters (depleted zones) formed during the bombardment. They developed a method to determine the dechannelling cross section σ_d of these clusters and the average radius of the displacement cascades from backscattering data and from measurements with transmission electron microscopy. This method was applied to the radiation damage in Ni single crystals. The dechannelling cross section for defect clusters in Ni was found to be between $4 \cdot 10^{-15}$ cm^2 and $1.7 \cdot 10^{-14}$ cm^2 for 2 MeV He$^+$ ions. These values are within the limits of the dechannelling cross sections determined by Merkle for defect clusters in Au which were between $4 \cdot 10^{-15}$ cm^2 and $2.4 \cdot 10^{-14}$ cm^2 for the same particles and energies.

The average radius of the displacement cascades in Ni after irradiation with 2 MeV He$^+$ ions was found between 50 and 90 Å.

References

/1/ K. L. Merkle, P. P. Pronko, D. S. Gemmel, R. C. Mikkelson, J. R. Wrobel
    Phys. Rev. B Vol. 3 (1973), No. 3

/2/ K. L. Merkle, Phys. Stat. Sol. 18 (1966), 173

3.6   Zucht von NbC-Einkristallen nach dem tiegelfreien Zonen-ziehverfahren

B. Scheerer und W. Reichardt

NbC-Einkristalle wurden mit einer 50 KW HF-Induktionsanlage unter einer Gasatmosphäre von 95 % Ar + 5 % H_2 bei einem Druck von 10 atü nach dem Zonenziehverfahren hergestellt. Ein Graphitnachheizer verminderte den Temperaturgradienten des gezonten Teils. Zur Verringerung der Strahlungsverluste diente ein Mo-Reflektor (Fig. 48).

Das Ausgangsprodukt waren heißgepreßte NbC-Stäbe der Firma Cerac, USA, mit einer Länge von 150 mm und einem Durchmesser von ca. 12,5 mm. Die Schmelzzone wurde mit einer Geschwindigkeit von 11 mm/h von unten nach oben über den NbC-Stab geführt, indem der in Graphithalterungen eingespannte Stab von oben nach unten durch die feststehende HF-Spule geführt wurde. Die beiden Stabenden drehten sich gegenläufig, wodurch eine Durchmischung und somit eine isotrope Temperaturverteilung der Schmelzzone bewirkt wurde. Dieses Verfahren erlaubte es, die Schmelzzone über mehrere Stunden stabil zu halten und den Stab über eine Länge von ca. 70 mm zu zonen.

Aus diesem Schmelzling ließen sich mehrere Einkristalle herausschneiden. Drei Kristalle hatten Größen zwischen 0.5 cm^3 bis 1 cm^3 mit einer Mosaikbreite von ca. 0.4 $^\circ$ (Fig. 49). Die chemische Analyse ergab, daß während des Ziehprozesses Kohlenstoff abgedampft war. Die Zusammensetzung des Endproduktes betrug C/Nb = 0.889, während das Ausgangsprodukt ein C/Nb-Verhältnis von 1.00 und einen Anteil von freiem Kohlenstoff von 0.33 % hatte. Diese Ergebnisse wurden durch Messungen der Gitterkonstanten a = 4.465 $\overset{\circ}{A}$ (Einkristall) bzw. a = 4.469 $\overset{\circ}{A}$ (Pulver) und des supraleitenden Sprungpunktes von 3.7 - 4.5 K (Einkristall) bzw. 9.7 - 10.5 K (Pulver) bestätigt.

Die Ziehversuche an NbC-Einkristallen werden fortgesetzt.
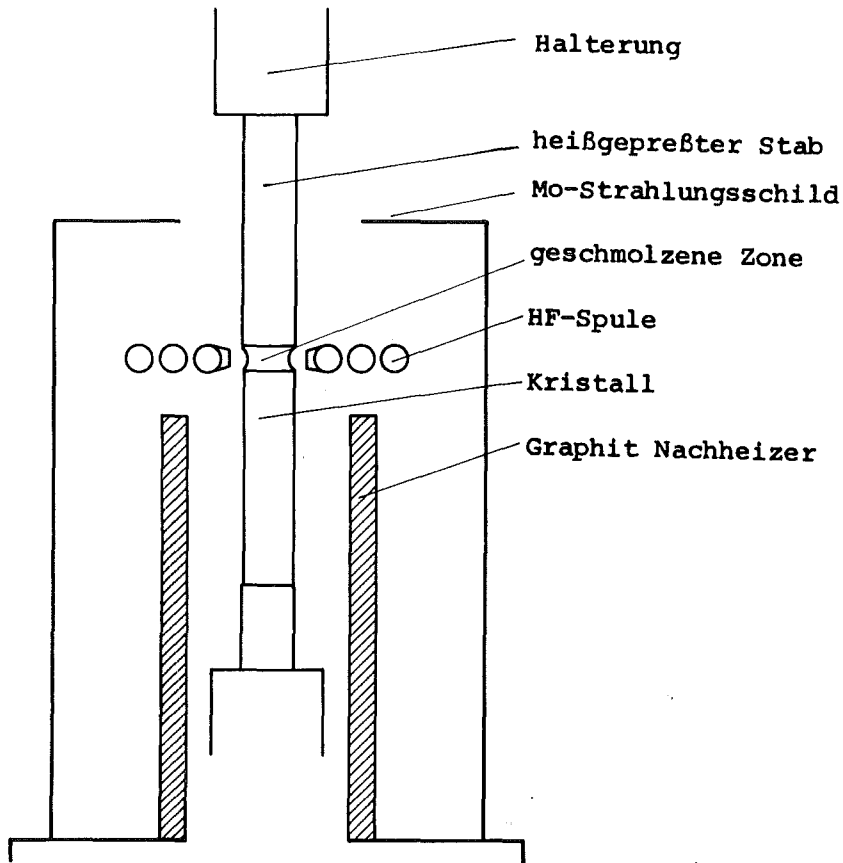
Fig. 48   Anordnung von Spule, NbC-Stab, Graphitnachheizer und Mo-Strahlungs-
schild

Rockingkurve Einkristall $NbC_{0.889}$
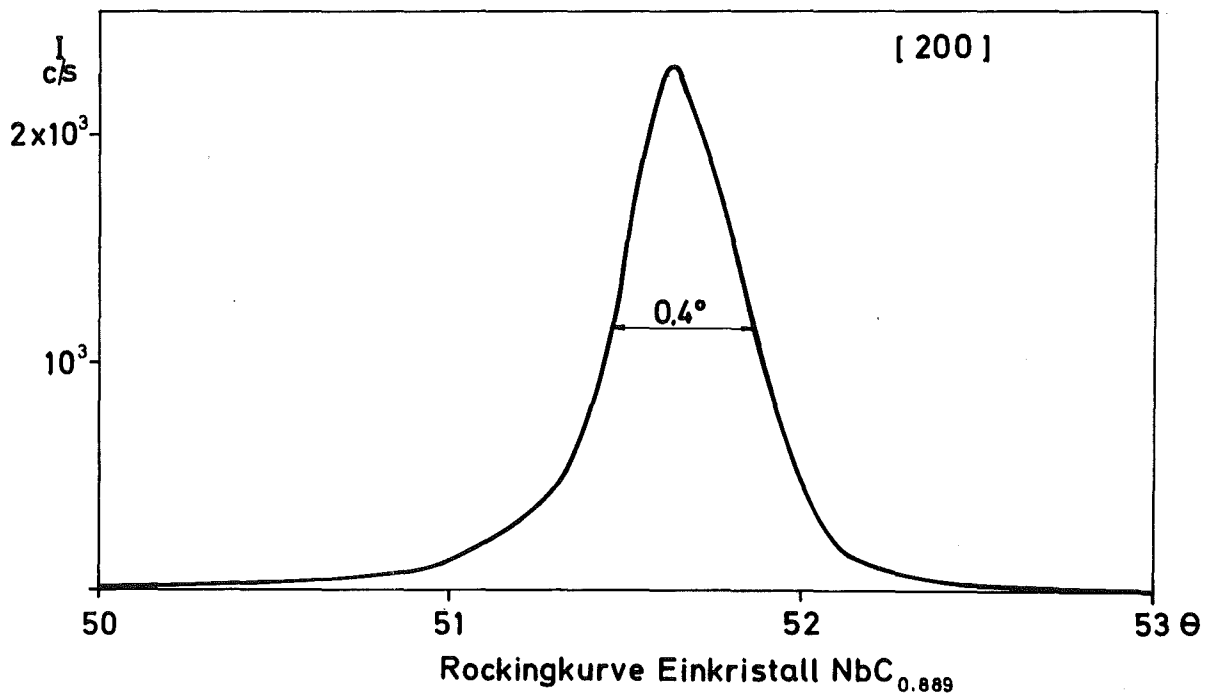
Fig. 49   Rocking Kurve (200 Reflex) für einen aus dem Schmelzling heraus-
geschnittenen Einkristall

3.7   Das Züchten von Be-Einkristallen nach dem tiegelfreien
       Zonenziehverfahren

       B. Scheerer

Be-Einkristalle sind ideale Neutronenmonochromatoren. Leider sind große
Einkristalle nur schwer erhältlich. Wir haben an einer Kristallzuchtan-
lage des MPI für Sondermetalle in Stuttgart, das speziell für die Verarbei-
tung von Be eingerichtet ist, einige Versuche zur Herstellung großer
Einkristalle unternommen.

Als Ausgangsmaterial stand Be-Pulver zur Verfügung, das zuerst gepreßt
und anschließend zur Reinigung unter Argon-Schutzgas-Atmosphäre mehr-
mals aufgeschmolzen werden mußte, wobei sich die Verunreinigungen an
einem Ende ablagerten.
Die zweilagige HF-Spule der Analge war aus 6 mm Kupferrohr gefertigt
und hatte einen Innendurchmesser von 40 mm. Damit war es möglich, Stäbe
bis zu einem Durchmesser von 30 mm zu zonen. Die Schmelzzonenhöhe be-
trug 15 mm bis 20 mm, je nach
Stabdurchmesser und angebotener
Leistung.
Bisher wurden an zwei Be-Stäben
Untersuchungen durchgeführt. Zur
Einkristallzucht wurden sie je
acht mal mit einer Ziehgeschwindig-
keit von 7 cm/h bis 4 cm/h bzw.
ca. 18 cm/h gezont. Bei dem ersten
Stab bildeten sich zwei Einkristalle
etwa gleicher Größe. Fig. 5Oa stellt
eine photographische Aufnahme des
zweiten Be-Kristalls dar, Fig. 5Ob
zeigt, daß hierbei nahezu der ge-
samte Bereich (2,5 - 3 cm Durchmesser,
ca. 10 cm Länge) aus einem Einkristall
besteht.
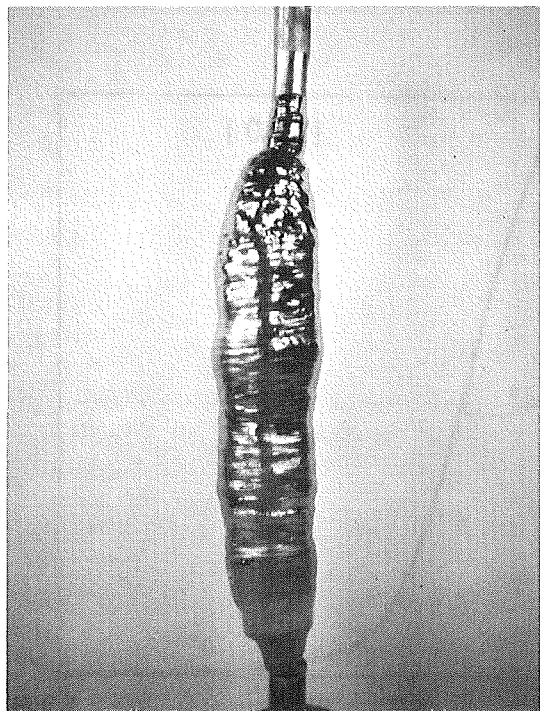
Fig. 5Oa   Zweite Probe   Die Versuche werden fortgesetzt.
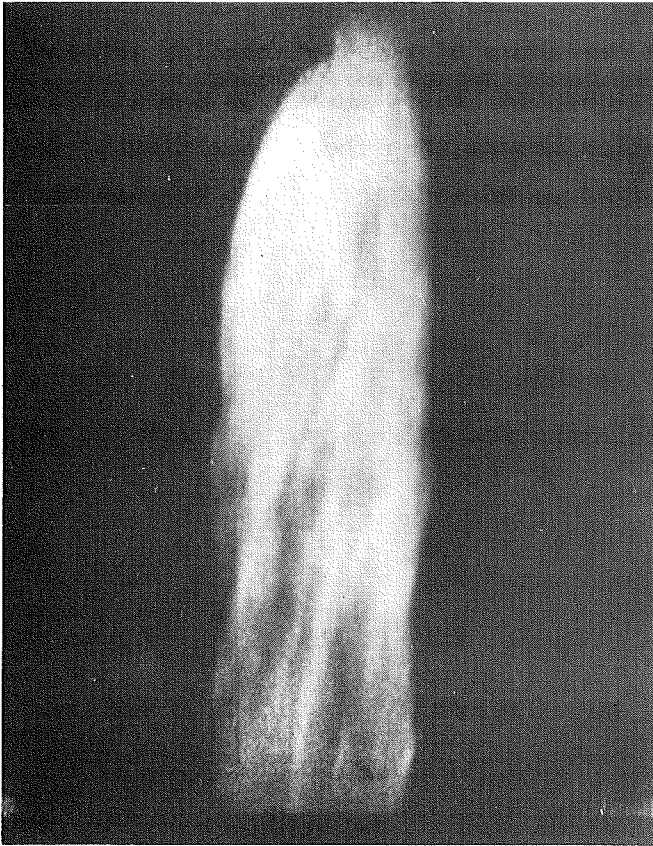
Fig. 50b Photographische
Aufnahme der 002 Ebene
(Wellenlänge des Neutronen-
strahls 1.094 Å)

3.8   Studies to Improve the Performance of Monochromator Crystals

W. Reichardt and K. Weber

Following the work of Brockhouse et al. /1/ we have started investigations
to improve the performance of monochromator crystals by mechanical deforma-
tion. A tool to bend monochromator plates to a curvature of 100 cm was used
for these studies. So far we have investigated three copper crystals with
(311) and (220) major faces. All crystals were repeatedly bent and
straightened until a width of the rocking curve of about 1/2 to 2/3 degrees
was obtained. By this treatment the integrated reflectivity for $\lambda = 1.09$ Å

could be increased by factors between two and three without a decrease
of the peak reflectivity. It turned out that a preferred orientation
of the crystallites following the curvature of the last bending remaind
after the plates were finally straightened. Measurements in a white reactor
beam with moderate angular resolution showed that the intensities of the
reflected beam at the detector varied up to a factor of two between the
focussing and defocussing side.

References

/1/ Brockhouse et al., Neutron Inelastic Scattering, Vol. II (1968), 259,
Vienna

3.9 Pressure Dependence of the Superconducting Transition Temperature of Th_4H_{15}

*M. Dietrich and W. Gey, Institut für Experimentelle Kernphysik,
Kernforschungszentrum Karlsruhe*

H. Rietschel

*C. Satterthwaite, University of Illinois, Solid State Commun.,
in print*

Abstract

Measurements of the superconducting transition temperature of Th_4H_{15}
under hydrostatic pressure up to 28 kbar are reported. The initial
increase is found to be + 42 mK/kbar. Possible explanations of this
result are offered in connection with the band widths of f-metals and
the properties of UH_3 and UD_3.

4. DATA PROCESSING

4.1 Universale Flugzeiteinheit mit integrierter Chopper-steuerung

H. Klann

Für Flugzeitexperimente mit pseudostatistischen Choppern wurde eine neue Flugzeiteinheit entwickelt. Wegen der vielen gemeinsamen Betriebsele-mente wurde die Choppermotorsteuerung in die Einheit integriert. Außerdem wurde für diese Einheit ein neues "non-switched" 5 V/25 A-Netzgerät mit hohem Leistungsvolumen (25 W/l) entwickelt.

Die Motorsteuerung erzeugt für die Leistungsverstärker den 3 ϕ - Sinus, kon-trolliert die Drehzahl, meldet Störungen bei Überlast und Schnellabschal-tung und stellt die Steuer- und Meßsignale für Flugzeitzähler und Detektor-gruppen zusammen. Bei Verwendung eines zweiten Sinusgenerators ist durch den Delay-Trigger und der digitalen PID-Drehzahl- und Phasenregelung der Betrieb eines (pseudostatistischen) Doppelchoppers möglich. Der Flugzeitzähler ist variabel programmierbar mit allen ganzzahligen Vielfachen der kleinsten Ein-heit: Kanalbreite = 0.1 bis 10.0 µsec, Anzahl der Kanäle = 1 bis 2^{12}, Wieder-holungszähler = 1 bis 10. Die Taktzeit der Anlage beträgt 0.1 µsec.

Die Flugzeiteinheit ist vielseitig anwendbar:

a) Pseudostatistische Flugzeit- oder ähnliche Methoden, bei denen die Umlauf-zeit des Choppers gleich oder ein ganzes Vielfaches der Laufzeit des Flug-zeitzählers ist und die Meßzyklen lückenlos aneinandergereiht werden müssen (Synchronlauf $< 10^{-4}$).

b) Konventionelle Flugzeitmessungen, bei denen die Laufzeit des Zählers kürzer ist als die Umlaufzeit. (Wegen Drehzahlkontrolle keine Unsicherheit der Laufzeitmessung). Der Triggerbeginn kann verzögert oder die Meßzeit durch Torzeit eingeschränkt werden.

- 80 -

c) Vielfachzähler, auch in Verbindung mit Timersystemen.

Die Detektoreingänge sind in eine schnelle und eine langsame Gruppe unter-
teilt, die unabhängig voneinander auf zwei getrennte oder einen gemeinsamen
Datenspeicher geschaltet werden können. Gruppe I mit 5 MHz Gesamt-Gleich-
taktimpulsrate hat 2 Eingänge mit je 1 Eingangswortspeicher und nachfolgendem
gemeinsamen 32-Wortspeicher. Gruppe II mit ca. 160 KHz Gesamtgleichtaktimpuls-
rate hat 16 Eingänge mit je 1 Eingangswortspeicher (1.8 µsec Rechenzeit
+ ≈ 4.5 µsec Dialog mit Datenträger).

Das Detektorsingal bewirkt eine Übertragung der aktuellen Flugzeit aus dem
Zähler in den Eingangsspeicher. Alle Eingänge können gleichzeitig ein Signal
übernehmen.

Jeder Eingang besitzt einen Detektorimpulsdehnerdisplay mit Eingangsspeicher-
zustandsanzeige und Speicherüberlaufdisplay so wie einen abschaltbaren Ausgangs-
impuls zur Bildung eines Detektorsummensignals. Es kann auf jeden beliebigen
freien Detektoreingang gegeben werden.

Die Kodierung der Flugzeit erfolgt komprimiert, d. h. die Detektorbereiche
schließen sich unabhängig von der Anzahl der Kanäle lückenlos aneinander an.
Die Sendeadresse wird mit einem Sockel (O bis 2^{12}- 1) versehen und auf Be-
reichsüberschreitung überprüft. Die Übertragung erfolgt 16 Bit parallel nach
Einheitsschnittstelle DVZ/IAK.
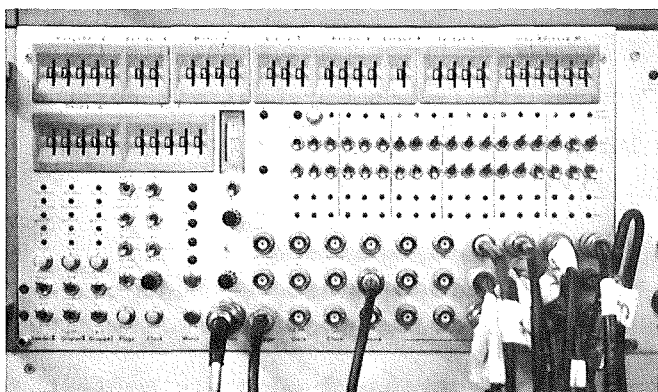
Fig. 51
Flugzeiteinheit in Betrieb

4.2 Design and Implementation of a Multidetector Time-of-Flight Unit

H. Hanak, G. Ehret

The common feature of many neutron time-of-flight experiments is a strongly time-dependent data rate. The high instantaneous data rate during the elastic neutron peak often results in dead-time distorsion of the recorded peakform. The problem is enlarged in a multidetector arrangement.

Solutions have been found by buffering the fully encoded time and detector data between the time-of-flight unit and the following recording unit, e. g. multichannel analyser, magtape or mini-computer (Fig. 52). Thus the influence of the data storage unit on the instantaneous dead time behaviour is eliminated. The binary coder, however, always need some network to prevent address pile up. The consequence is that incoming detector pulses must be handled on a first-come-first-served-basis. Furthermore, two detector pulses which arrive in parallel with respect to given time window must be discarded. These two features are intolerable in a 128 detector environment.

We tried to solve the problem by buffering the incoming detector pulses (Fig. 53). These pulses set the input sync register. The sync register is transferred in parallel to the next register by the overall 2 MHz timing of the unit at this point a decision can be made whether or not any bit is set, indicating, that a least one detector pulse has arrived in the 0.5 μsec time gap. If the test is positive, the whole register is transferred to the buffer.

The output of the buffer register is controlled by a network which:

1. feeds the binary coder sequentially with the bits set by detector pulses,

2. holds the time path of the buffer until one scan is made for all 128 detectors in one line of the buffer matrix, and

3. manages the communication with the succeeding data storage device.

The scan for bits set by detector pulses is done hierarchially in groups of 2 x 8 detectors according to the modular structure of buffer. One scan is so achieved in 0.350 μs. Thus decoding is not a time consuming member in the chain of storing data.
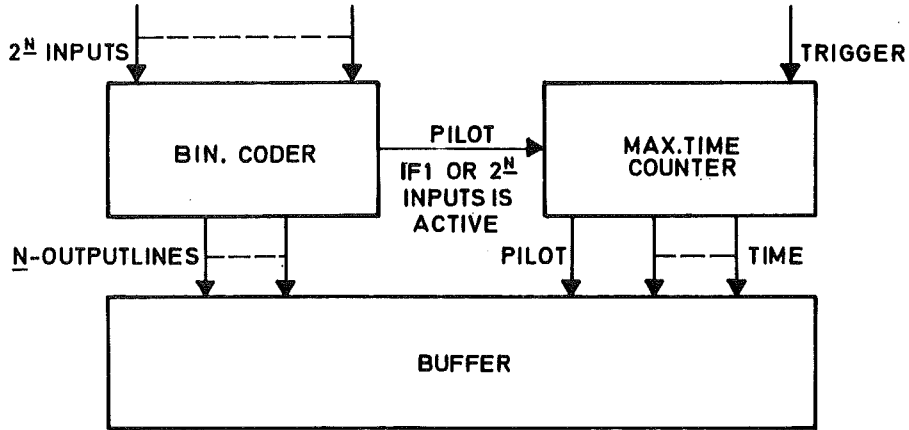
Fig. 52
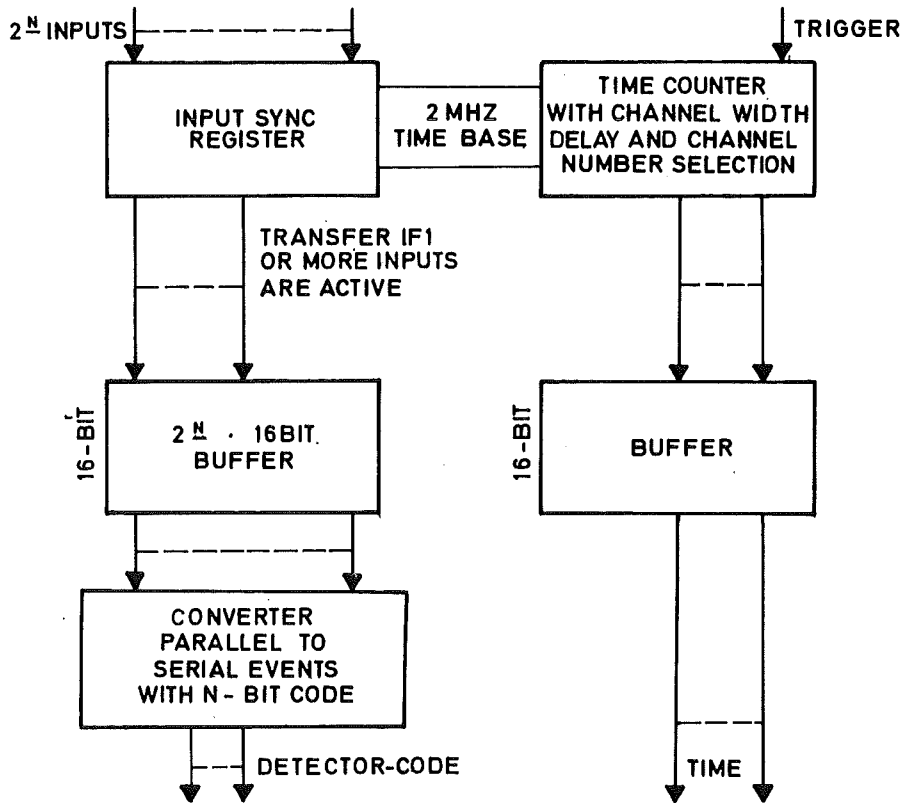
Fig. 53

The buffering of detector pulses, before the coding process, does not lead to loss of pulses arriving in parallel at the same time defined by the 2 MHz clock-time of the sampling register. The advantage of this system is that all pulses are stored only into one line of the buffer. Thus it may be advantageous to accommodate the sampling time either by switch selection or coupling to the channel width of the time-of-flight register.

The prototype multidetector time-of-flight unit is working since the fall of 1970 in the rotating crystal spectrometer at the FR2 reactor. A commercial version in mechanical (but not electrical) CAMAC-standard has been developed on a collaborating basis together with the electronic group at the ILL in Grenoble. They added some features to the system useful for special applications. Informative data (channel width, number of channels, number of detector) are readable by a computer. The computer can initiate a hardware shift of the detector bits tied to the time-of-flight bits (bit compression). Due to the modular conception, units may be assembled in multiples of 16 detectors. For multidetector purposes, without analysing the time parameter, the time-of-flight plug-in may be omitted.

Three systems are now going into operation at the FR2, replacing older units or are in use for a new experimental assembly at the cold source.

4.3   The Use of Minicomputers in an Experimental Environment

G. Ehret, H. Hanak, H. Richelsen, P. Timis

Demands of physical experiments on data acquisition expressed in terms of data storage volume (add-one storage) and counting rate may be divided into four classes

1. few channels but very high (> 0.5 MHz) counting rate
2. up to 20 K channels and less than 0.5 MHz
3. 20 K - 1 M channels and less than 15 kHz
4. more than 1 M channels and less than 1 kHz

The first class can only be handled by scalers external to the computer. Depending on the special application external scalers or prescalers which are read out on the fly may be applied /1/.

The second class requires the use of a minicomputer for such an experiment. Typical applications are experiments for measurements of phonon distribution (conventional and pseudo-random time-of-flight experiments) and for ore prospection (pulse height analysis). The hardware for the add-one logic must be fully integrated into a higher program language. The experimenter is also capable of reducing the measured spectra to a small set of numbers (typical 2 or 3) without being engaged with file handling for programs and data. We are using, e.g. the interactive and completely core resident language BASIC for the NOVA computers.

This 2nd class of experiments also needs a display-unit. We developed a TV-display /2/ with a matrix of 256 x 256 points, which is completely sufficient for most experimental needs. The display system uses 4 K core memory for refreshing the picture and is fully implemented into BASIC to the extent that as graphs, as well as teletype output may be displayed. By bypassing BASIC, the teletype can also be used to letter the graph. Additionally, a concept of a hardcopy unit using a TV-recorder has been developed. To control the experiment a very flexible control unit with a maximum of 2048 output lines and 2048 input lines has been built /3/. All lines are accessible by BASIC as single lines or in groups from 2 to 32 lines. Thus it is only a plug problem if 4 lines are coming from one decade of a decimal counter or if another line is coming from an alarm source generating an interrupt.

Experiments with more than 20 K channels (class 3) are serviced by ASSTRO (Automatisches Summieren von Spektren auf einer Trommel = Automatic Totalizing of Spectra on a Drum) /4/. One million channels are available with 18 or 16 bit channel length at 12 k count/sec (18 kc/sec without write check). Simulation by programs has shown that about 75 - 80 % of the sectors moved can be totalized in the case of a "white" spectrum. Provision has been made that this percentage

is also true in a peaked distribution of spectra. A special controller for
this drum and NOVA computer has been developed allowing chained access for
sectors (with 16 (18) bit length each) on different tracks and chained opera-
tion for succeeding revolutions. Via a computer-computer coupling this ASSTRO
system is connected to the MIDAS at the reactor FR2. Provision has been made to
feed data coming from other experiments to the drum system by bypassing MIDAS,
using a new multiplex-on-line ring to be placed around the reactor FR2.

The structure of the MIDAS communication code has been enlarged. MIDAS has
now access to 512 K channels on the drum. Thus the change to a new more
flexible MIDAS is possible without serious interruptions of the operational
behaviour.

Experiments which need more than 1 M channels (class 4) can only be handled
by recording addresses on magnetic tapes. If it is possible to reduce the
data, point 3 of the classification is applicable. Typical reduction methods
are: digital window, island isolation, hole of reactions etc.. There is at
the moment no experiment at the IAK which cannot be reduced to class three
using these methods. Two ASSTRO-systems, however, must be installed at the
van de Graaff and at the Isocyclotron to overcome bottle necks in data
processing.

References
/1/ C. Weitkamp, KFK 1950, p. 11
/2/ G. Ehret et al. to be published
/3/ H. Hanak et al. to be published
/4/ G. Ehret et al. to be published

4.4   Programm zur automatischen Textaufbereitung

        W. Abel

Der Einsatz des Computers bei der automatischen Textaufbereitung hat sich
als sehr vorteilhaft erwiesen, wenn im Zusammenhang mit Programmdokumenta-

tionen umfangreiche Beschreibungen von Eingabedaten auf den neuesten Stand
gebracht werden müssen. Zur Vermeidung oder zumindest Beschränkung des durch
aufwendiges Korrigieren entstehenden zeitlichen Unterschiedes von der Er-
stellung bis zur Reproduktion eines Manuskriptes wurde ein textverarbeiten-
des Programm in der Programmsprache PL/1 entwickelt.

Mit der Einführung von TSO, der Time Sharing Option des MVT, wurden die
Textsteuerzeichen des Programms den dort gegebenen Möglichkeiten der Text-
verarbeitung hinsichtlich der Struktur der Steuerkodes angeglichen und um
einige Aufbereitungskodes erweitert. Zur Formatierung einer vorliegenden
Textdatei sind u.a. Steuerungen vorgesehen für Zeilenlänge, Zeilen-
abstand, Absatz, Seitennummerierung, Zentrierung von Zeilen, Seitentiefe
und Randausgleich. Bei einer Ausgabe der formatierten Textdateien über
einen Drucker mit der TN-Kette, deren Zeichensatz der INIS-Norm entspricht,
ist im Programm eine Kodierungsvorschrift für die Adressierung der Sonder-
zeichen dieser Druckerkette enthalten. Unterstreichungen in einer Ausgabe-
zeile werden durch das Einfügen von Kontrollzeichen erzeugt. Darüberhinaus
wird dem Benutzer die Möglichkeit gegeben, während eines Programmablaufs
im Teilnehmerbetrieb eine Silbentrennung durchzuführen.

References:

/1/ W. Abel, TEXT352, ein PL/1-Programm zur Textaufbereitung,
(unveröffentlicht)

4.5   Anwendung von interaktiven graphischen Methoden bei der
      Auswertung von Flugzeitspektren thermischer Neutronen

W. Abel

Die Untersuchung der Streuung von thermischen Neutronen an atomaren Systemen,
wie Festkörpern, Flüssigkeiten, u.s.w., ist im allgemeinen ein sehr zeit-
raubender Prozeß von der Durchführung des Streuexperiments und der Bereit-

stellung der akkumulierten Daten bis zur endgültigen Auswertung. Der Einsatz
der on-line-Auswertung mit graphischen Methoden hat gegenüber der sonst
üblichen Auswertung im Batch-Betrieb den Vorteil, daß der Benutzer sehr schnell
einen Einblick in das Verhalten seines physikalischen Systems gewinnen kann,
das mit anderen Methoden nur sehr schwer untersucht werden kann. Andererseits
wird eine bildschirmunterstützte Auswertung von Daten dann notwendig sein,
wenn kein fester Algorithmus für den Rechenprozeß existiert. Die enge Kopplung
von Rechengeschwindigkeit mit der menschlichen Erfahrung und Intuition, die
durch die Einführung interaktiver graphischer Methoden erreicht wird, hat
also im wesentlichen zwei Konsequenzen: erstens, der Zeitaufwand für die
Lösung eines speziellen Problems wird stark reduziert; zweitens, durch die
Flexibilität der graphischen Auswertemethoden kann eine Untersuchung viel de-
taillierter ausgeführt werden, als es normalerweise im Batch-Betrieb möglich
ist. Zur Verarbeitung von graphischer Information wird die Bildschirmeinheit
IBM/2250-1 eingesetzt, die über einen Selektorkanal an die IBM/370-168
angeschlossen ist /1/. Die Bildausgabe erfolgt über einen Bildwiederhol-
speicher von 4 K Bytes mit hoher Geschwindigkeit. Aktive Bildschirmein-
heiten erlauben neben der graphischen Datenausgabe und der Eingabe von
Parametern über die alphanumerische Tastatur eine Steuerung des Programm-
ablaufs über Lichtstift und Funktionstastatur. Zur Unterstützung der Aus-
wertung des Streugesetzes wurden Programme zur Extrapolation der Phononen-
frequenzverteilung $p(\beta)$ und der graphischen Interpolation des Streuge-
setzes $S(\varrho,\omega)$ entwickelt, die insbesondere den Zeitbedarf erheblich er-
niedrigen konnten.

Eine wichtige Größe bei den Studien der Streuung langsamer Neutronen an Fest-
körpern ist die Phononenfrequenzverteilung $p(\beta)$, die im allgemeinen direkt
aus Streuexperimenten bei hinreichend großen Impulsüberträgen oder bei
inkohärenter Streuung gewonnen werden kann. Ausgehend von dem experimentell
bestimmten Streugesetz $S(\alpha,\beta)/\alpha$ wurde ein interaktives Programm nach der
1961 von P. A. Egelstaff vorgeschlagenen Extrapolationsmethode geschrieben /2/.
Der Benutzer kann den Extrapolationsbereich auswählen oder eine Verschiebung
der Extrapolationsgeraden bzw. der aus einer Modellrechnung gewonnenen
$S(\alpha,\beta)/\alpha$-Kurve vornehmen, da bestimmte Voraussetzungen über die Korrelations-
funktion ausschlaggebend sind und nicht zuletzt experimentelle Gesichts-
punkte beachtet werden müssen.

Zur Darstellung des experimentell bestimmten Streugesetzes $S(Q,\omega)$ in einem Übersichtsbild wurde ein Programm entwickelt, mit dem eine interaktive graphische Glättung von $S(Q,\omega)$ durchgeführt werden kann /3/. Das Programm kann darüberhinaus allgemein zur Interpolation von ein- oder zweiparametrischen empirischen Funktionen benutzt werden. Dies ist vor allem bei Simulations- und Entfaltungsproblemen von gemessenen Verteilungen von Vorteil, um das Lösungsverhalten der damit verknüpften Integralgleichungen zu untersuchen.

References

/1/ IBM System/360 Component Description IBM 2250 Display Unit Model 1 Form A27-2701-2

/2/ W. Abel, Interaktives graphisches Programm zur Extrapolation der verallgemeinerten Frequenzverteilung $p(\beta)$ mit der Bildschirmeinheit IBM/2250-1 (unveröffentlicht)

/3/ W. Abel, Interaktives graphisches Programm zur Interpolation des Streugesetzes $S(Q,\omega)$ für $\omega=$ const. mit der Bildschirmeinheit IBM/2250-1, IAK-Arbeitsbericht Nr. 108/74, April 1974 (unveröffentlicht)

4.6   EPHCOPOL

A FORTRAN-4   Routine for the Calculation of the Contributions from One-Phonon-Scattering to Scattering of Thermal Neutrons in Polycrystals

J.-B. Suck, J. Salgado and W. Reichardt

In the first part of the routine phonon density of states $f(\omega)$ and $F(Q,\omega)$ /1/ are calculated by sampling the eigenfrequencies and polarisation-vectors in the range of Brillouin zones reached in the experiment simulated with EPHCOPOL:

$$(1) \quad F(Q,\omega) = \frac{3}{N} \frac{\int_{\theta min}^{\theta max} \int_{\psi min}^{\psi max} \sum_{j=1}^{N} (\vec{Q} \cdot \vec{c}(Q,j))^2 \, \delta(\omega - \omega(Q,j)) \, \sin\theta \, d\theta \, d\psi}{Q^2 \int_{\theta min}^{\theta max} \int_{\psi min}^{\psi max} \sin\theta \, d\theta \, d\psi}$$

with

$$(2) \quad \int_0^\infty F(Q,\omega) \, d\omega = 1 \qquad \text{.and} \qquad \int_0^\infty f(\omega) \, d\omega = 1$$

j: index of dispersion branch
N: 3x the number of atoms in the unit cell

Eigenfrequencies and polarisationvectors are calculated with a simple Born-von Kárman-model for simple cubic, fcc, bcc /2/ and rhombohedric (A7) /3/ structure as desired. In the sampling procedure the Q-vector is varied on spherical shells with constant thickness dQ in the reciprocal space, successively in steps with constant $d\theta$ and $d\psi$.

In the second part of the routine the one phonon contribution to the coherent double differential scattering cross section and to the symmetrized scattering law are calculated for the case of a Bravais lattice.

$$(3) \quad \frac{d^2\sigma}{d\Omega d\omega} = K \, \frac{\sigma_{coh}}{4\pi} \, \frac{k}{k_o} \, \frac{e^{-\alpha\lambda}}{2M} \, \frac{Q^2 F(Q,\omega)}{\omega(e^\beta - 1)} \left[\frac{b}{meV} \right]$$

K   factor for conversion to b/meV
$\beta = \hbar\omega/k_B T$, $\alpha = \hbar^2 Q^2/2Mk_B T$
$\alpha \cdot \lambda$ Debye-Waller-factor

$$(4) \quad S(Q,\omega) = \frac{4\pi}{\sigma_{coh}} \, \frac{k_o}{k} \, e^{\beta/2} \, \frac{d^2\sigma}{d\Omega d\omega} \left[\frac{1}{meV} \right]$$

$$(5) \quad S(\alpha,\beta) = k_B T \, S(Q,\omega)$$

In the third part a measurement of the phonon density of states of a polycrystal (coherent and incoherent) with the detector sampling method is simulated. Given an incoming energy and a range of scattering angles the double differential scattering cross sections for the time-of-flight spectra are calculated from (3). For the incoherent contributions $f(\omega)$ is used, for
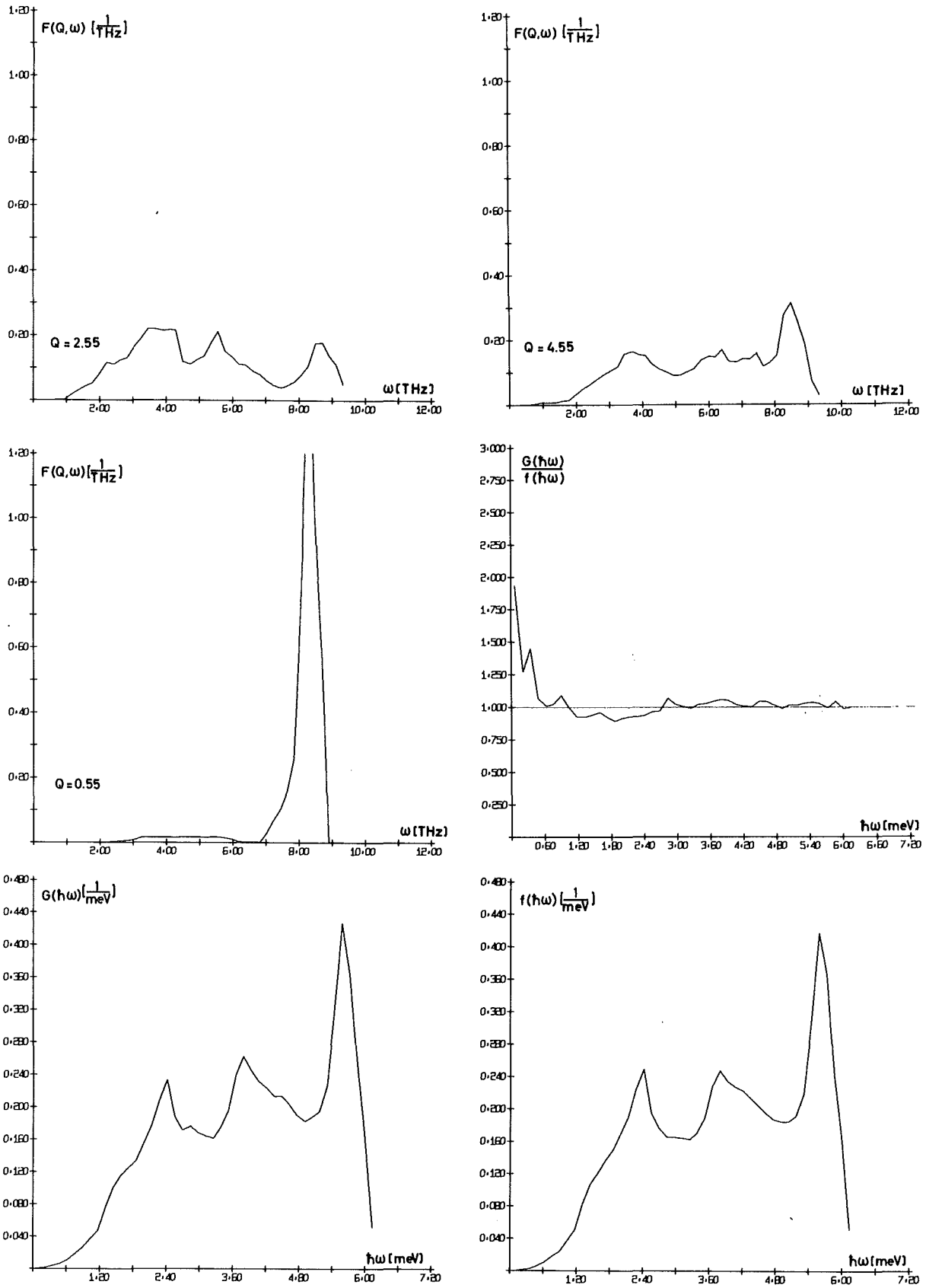
Fig. 54

the coherent contributions $F(Q,\omega)$ is interpolated linearily for the Q-values of the TOF channels. From the sum of all the TOF spectra one obtaines $G(\omega)$ /4/.

$$(6) \quad G(\omega) = \frac{4\pi}{\sigma} \frac{k_o}{k} \frac{d^2\sigma}{d\Omega d\omega} \frac{2M\, e^{\alpha\lambda}\, \omega(e^\beta - 1)\, \sin\theta}{\sin\theta_m\, \sin\theta_h\, (k_o^2 + k^2 - 2k_o k\, \cos\theta_m\, \cos\theta_h)}$$

$$\theta_m = (\theta_{max} + \theta_{min})/2 \quad , \quad \theta_h = (\theta_{max} - \theta_{min})/2$$

Summing up each TOF spectrum yields the one phonon contribution to the differential scattering cross section:

$$(7) \quad \frac{d\sigma}{d\Omega} (\theta = const) = \int_o^{\omega_{max}} (\frac{d^2\sigma_{coh}}{d\Omega d\omega} + \frac{d^2\sigma_{incoh}}{d\Omega d\omega})\, d\omega$$

The double differential cross section can be folded by an energy resolution function.

EPHCOPOL /8/ will be used together with LEAP /5/ (multiphonon contribution in the incoherent app.) and ELASS /6/ as input model for the multiple scattering corrections of our measurements of the scattering law of polycrystalline Rubidium at 123 K and 294 K. Some results of EPHCOPOL are given in fig. 54 for Rb at 123 K. The force constants of Copley and Brockhouse /7/ are used.

References

/1/ F. W. de Wette, A. Rahman, Phys. Rev. 176, 3, 784 (1968)

/2/ G. L. Sgires, Inelastic Scattering of Thermal Neutrons in Solids and Liquids II, IAEA Wien (1963), 71

/3/ Czachor et al., Acta Physika Polonica 1, 37, (1973)

/4/ V. S. Oskotskii, Sov. Phys. Solid State 9, 420, (1967)

/5/ R. Mc Latchie, Routine Description of LEAP, AERE REP (1962)

/6/ U. Löffler, J.-B. Suck, ELASS, FORTRAN 4 Routine for the Calculation of the Elastic Scattering Contribution to Scattering of Thermal Neutrons in Polycrystals (unpublished)

/7/ J. R. D. Copley, B. N. Brockhouse, Can. J. Phys. 51, 657 (1973)

/8/ J.-B. Suck, J. Salgado, W. Reichardt, EPHCOPOL, Routine Description (unpublished)

5. DEVELOPMENT OF DEVICES AND TECHNIQUES

## 5.1 Phasenstarrer Antrieb zweier Drehkristalle

N. Nücker

Das Drehkristallspektrometer am Hochflußreaktor in Grenoble ist mit einem Doppelmonochromator ausgerüstet. Beide Monochromatorkristalle können einzeln oder gemeinsam als Drehkristalle betrieben werden. Drehen sich beide Drehkristalle phasenstarr - im Experiment mit unterschiedlichem Drehsinn - so können infolge der Flugzeit zwischen den Kristallen nur Neutronen einer Wellenlänge an beiden Kristallen reflektiert werden. Die Reflexionen aller anderen Ordnungen werden unterdrückt. Dies ist von Vorteil vor allem bei Graphitkristallen, bei denen viele Ordnungen merkliche Intensitäten liefern (beispielsweise für θ = 30 $^{\circ}$: E = 7.3 meV, 29.3 meV, 66 meV ...).

Die Kristalle werden mit 1/4 PS Synchron-Hysterese-Motoren angetrieben. Die Phasenregelung soll an Hand des Blockschaltbildes erläutert werden (siehe Fig. 55): Ein Quarzoszillator liefert über einen programmierbaren Teiler das Taktsignal für den ersten Drehkristall. Dieses Taktsignal wird gemäß der Laufzeit der Neutronen zwischen den zwei Kristallen digital verzögert und bildet dann das Taktsignal für den zweiten Drehkristall. Zu jedem Drehkristall gibt es einen Magnettonkopf, der je Umlauf ein Triggersignal liefert. Der Antrieb der Drehkristalle wird so nachgeregelt, daß die Triggersignale gleichzeitig mit den entsprechenden Taktsignalen eintreffen.

Tritt ein Phasenfehler auf, so wird der Betrag und das Vorzeichen in der Phasensteuerung digital erfaßt. Für eine dem Phasenfehler proportionale Zeit wird das Untersetzungsverhältnis des Vorteilers entsprechend dem Vorzeichen des Phasenfehler von 1 : 10 auf 1 : 9 bzw. 1 : 11 geändert. Das Steuersignal für den Drehstromgenerator wird somit früher oder später eintreffen. Um ein Aufschaukeln des Phasenfehlers zu vermeiden, darf nur ein Bruchteil des Phasenfehlers in jeder Umdrehung nachgeregelt werden. Ist der Phasenfehler eines Drehkristalls größer als ein vorwählbarer Maximalwert,

so liefert die Phasensteuerung ein Signal, das zum Unterbrechen des Daten-
flußes genutzt werden kann. Der Phasenfehler am Drehkristallspektrometer in
Grenoble beträgt ca. 1 Mikrosekunde.
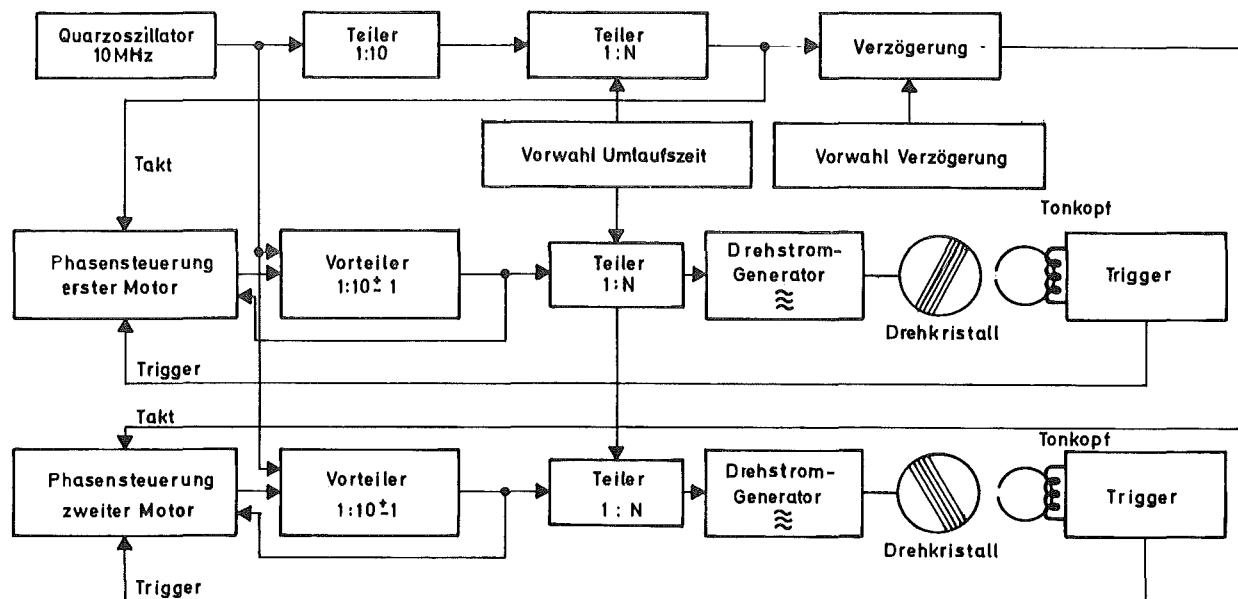
Blockschaltbild Phasenregelung

Fig. 55

5.2 Installation eines Fermi-Choppers am R7 - FR2

K. Weber

Es wird ein Fermi-Chopper beschrieben, welcher zur Erzeugung gepulster
monochromatischer Neutronen in Verbindung mit einem stationären Einkristall
an zwei Experimentiereinrichtungen am FR2 Reaktor eingesetzt ist (Flugzeit-
spektrometer für Phononenmessung und Multidetektor-Flugzeitspektrometer).
Für den Chopper am Flugzeitspektrometer für Phononenmessung (siehe Fig. 56)
wurde ein Mehrfachschlitzsystem mit geraden Schlitzen (2 Pulse/Umdrehung)
gewählt. Die Schlitzbreite beträgt 0.8 mm, die Schlitzlänge 34 mm. Der sich
daraus ergebende durchlässige Winkelbereich beträgt 2.7 $^\circ$. Bei einer zu-
lässigen Drehzahl von 15 000 U/min ergibt sich eine Pulshalbwertsbreite von
15 µsec. Die transparente Fläche ergibt sich aus 8 cm Höhe und 4 cm Breite
zu 32 cm^2. Die Konstruktion sieht eine zylindrische Stahlwalze von 60 mm

MAGN.NULLZEITGEBER

EXT.ANTRIEB

HYSTERESIS-SYNCHRON-
MOTOR

ÖLZULAUF

BORPLASTIK-
FENSTER

ÖLABLAUF

AL-BLECH
MS-BLECH
VERKADMET

KONTIN.
NEUTRONENSTRAHL-
EINGANG

GEP. NEUTRONEN-
STRAHL-
AUSGANG

ROTOR

Fig. 56

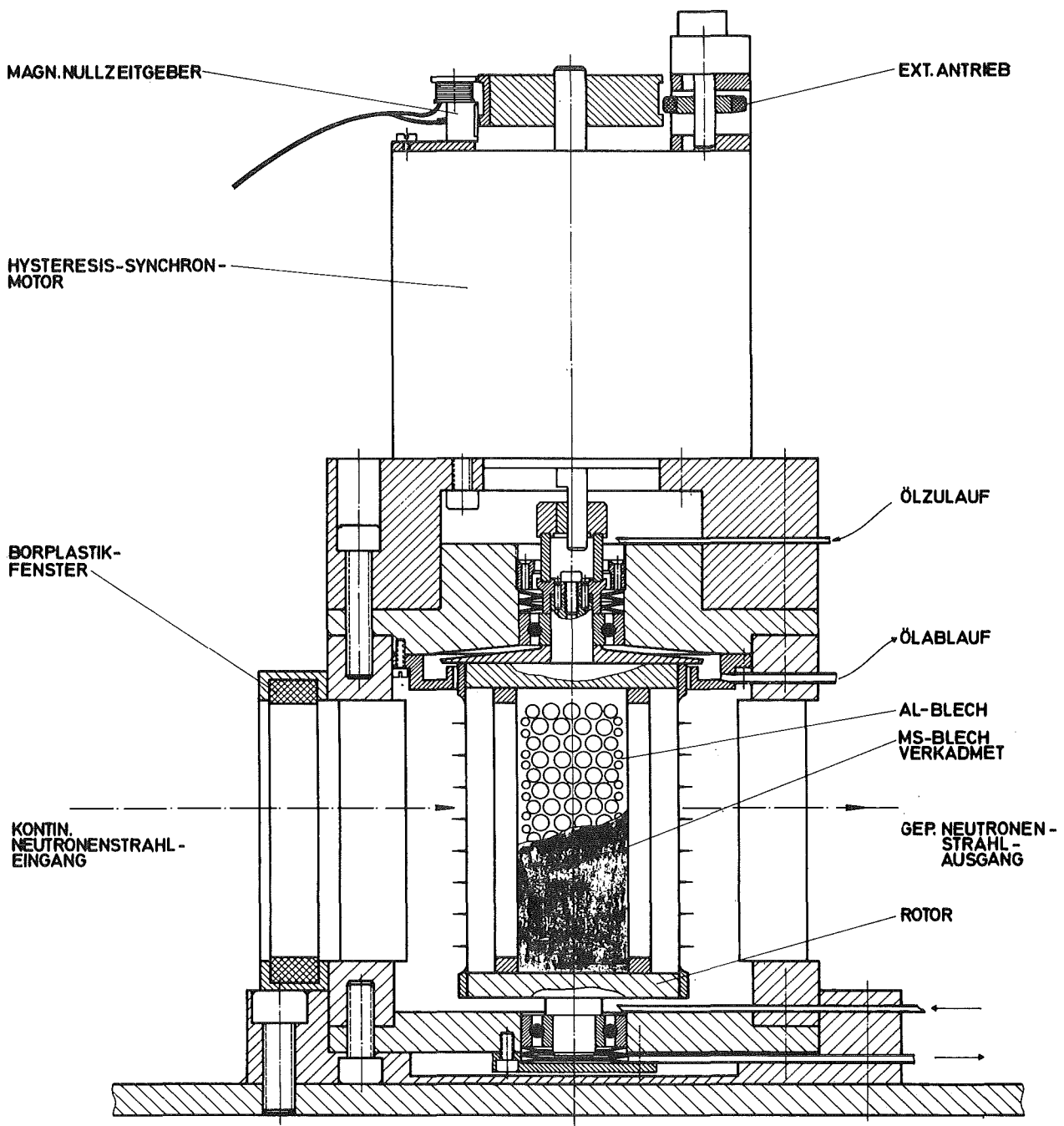Durchmesser vor, in deren rechteckige Aussparung ein Blechpaket mittels
Druckschrauben und Druckplatte eingespannt ist. Dieses Blechpaket, der eigent-
liche Kollimator, wurde wechselweise aus 44 Al-Blechen und 43 Abschirmblechen
hergestellt. Das Al-Blech wurde durch Ausbohren auf 40 % seines Volumens ver-
ringert. Das Abschirmblech aus einer 5/100 dicken Ms-Folie ist beidseitig mit
Gadolinium-Kadmium-Farbe bestrichen.

Ein Stahl-Gehäuse dient der Lagerung des Rotors und zur Aufnahme des Antriebs-
motors. (Hysteresis-Synchron-Motor, 200 W Abgabeleistung). Die Ansteuerung
des Motors erfolgt über 3 Einphasen-Wechselspannungsverstärker mit einstell-
barer Frequenz (50 - 500 Hz).
Die Drehzahl wird mit einem Magnet-Impulsgeber in Verbindung mit einem
Zähler gemessen und registriert (Umlaufkonstanz besser als 0.2 ^{o}/oo). Der
Geberimpuls dient gleichzeitig als Startimpuls für die Flugzeiteinheit.

Der Chopper des Multidetektor-Flugzeitspektrometers ist im wesentlichen ein
Nachbau des eben beschriebenen Gerätes. Er unterscheidet sich hauptsächlich
in den geometrischen Dimensionen. Walzendurchmesser 90 mm, Schlitzbreite
1 mm und Schlitzlänge 44 mm ergeben einen durchlässigen Winkel-
bereich von 2.6 ^{o}. Bei der derzeitigen Drehzahl von 12 000 U/min erhält man
Neutronenimpulse mit einer Halbwertsbreite von 18.1 µsec. Die transparente
Fläche ergibt sich aus der Höhe von 8 cm und der Breite von 6 cm zu 48 cm^2.
Anstelle des Gadolinium-Kadmium Farbauftrags wurde die 5/100 mm starke Ms-
Folie beidseitig galvanisch verkadmet(Schichtdicke ca. 3/100 mm).Auf die auf-
wendige zentrale Ölversorgung konnte durch Einbau von dauergeschmierten
Kugellagern verzichtet werden. Beide Geräte besitzen eine zusätzliche An-
triebsmöglichkeit, um den stehenden Rotor bei Justierarbeiten auf max. Durch-
lässigkeit zu stellen.

5.3   Strahlrohrstopfen am R1-Kanal

K. Weber, W. Benz, RBT/M

Am Strahlrohr R1 des FR2 wurde ein neuer Strahlrohrstopfen eingebaut,
der die Möglichkeit bietet, durch Verwendung verschiedener Einsätze
die für das jeweilige Experiment günstigste Strahlführung zu realisieren.
Die Konstruktion des Stopfens ist aus der Fig. 57 zu ersehen.

Der Stopfen wurde ganz aus V2A gefertigt und ist zum Schutz des Reaktor-
strahlrohres mit Kunststoffgleitkufen aus Resinol V109 versehen. Er ist
evakuierbar. Bei der Abdichtung der coreseitigen Strahlöffnung wurde ein
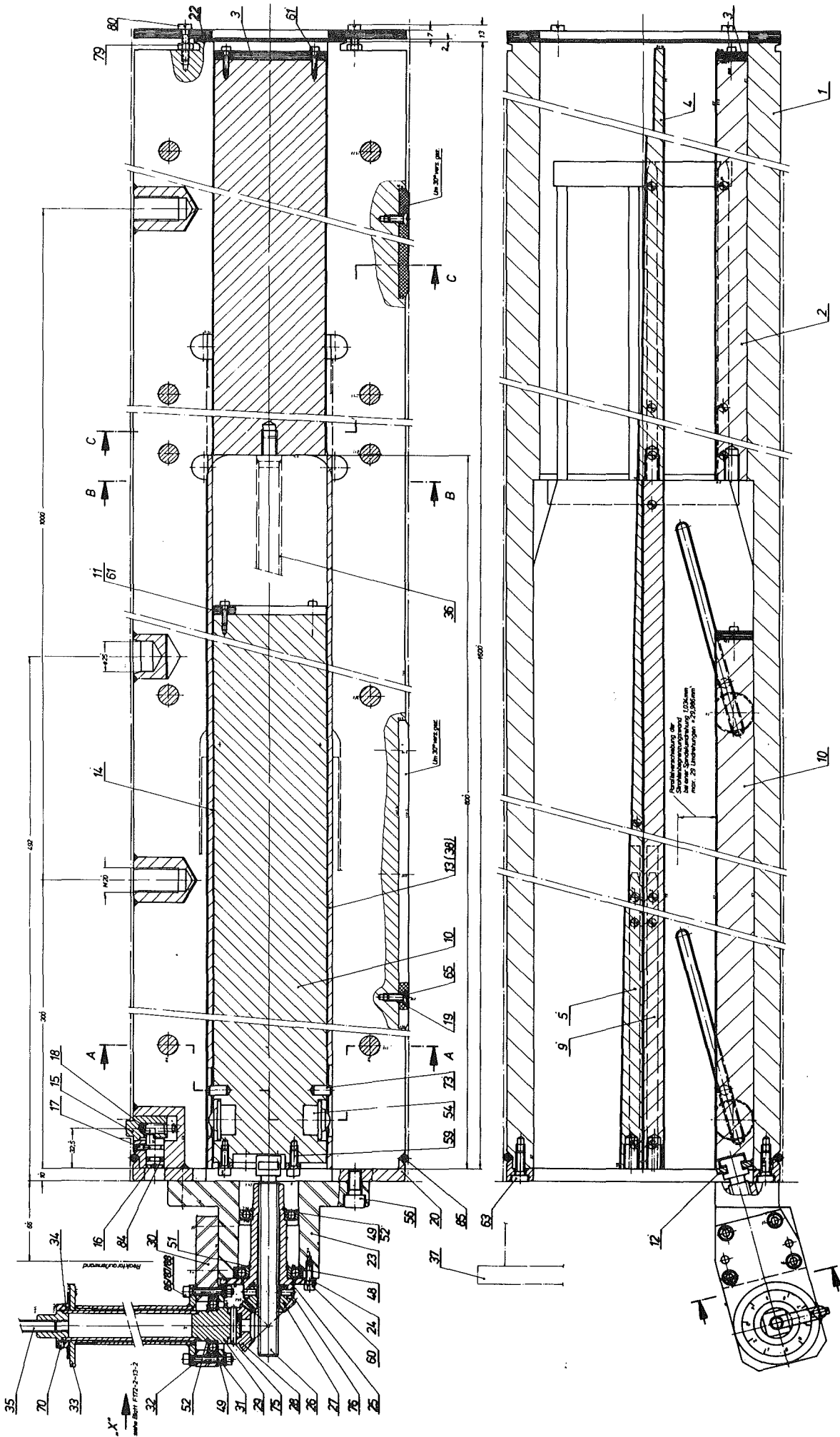
Fig. 57

Spezialblech aus Kupfer-Aluminium (Elektro-Cupal-Blech 70/30) verwendet.
Dabei wurde für die strahldurchlässige Fläche das Kupfer und für die
Schweißverbindung mit dem V2A-Flansch das Aluminium entfernt.

Zur Zeit wird der Kanal R1 für zwei Experimente genutzt, deren Strahlen
bereits im Stopfen vollständig separiert sind und um ca. 1° horizontal diver-
gieren.

Bei einem Strahl wird durch Reflexion an einem Co-Fe-Spiegel ein polari-
sierter Neutronenstrahl erzeugt. Eine im Stopfen angebrachte manuell ver-
stellbare Strahlbegrenzung erlaubt eine optimale Justierung des Strahls.
Am zweiten Strahl soll ein Spektrometer für elastische und unelastische
Streuexperimente hoher Auflösung aufgebaut werden. Der primäre Soller-
Kollimator, der in den Stopfen eingeschoben ist, erlaubt eine variable
Kollimation mit einem minimalen Wert von 6 '.

5.4   Installation of a Triple Axis Spectrometer at the Beam Tube R6

K. Weber, J. Krisch, RBT/M

H. Bialas, H. J. Stolz, Institut für Angewandte Physik
der Universität Heidelberg

A new triple axis spectrometer (TAS 2) has been recently installed
at the thermal beam tube R6. A general lay out of the instrument
is shown in fig. 58. Monochromatisation of the primary beam is achieved
by subsequent Bragg reflections from two identical crystals. The reactor
beam and the monochromatic beam are 80 cm apart. The monochromator take-
off angle can be varied between $40^{\circ} \leq 2\theta_M \leq 140^{\circ}$. The present double
monochromator system is a preliminary set-up which will be replaced in
the near future. It is intended to install a combined double monochromator -
single monochromator system; the single monochromator will be used for
small monochromator take-off angles.

The spectrometer has two detector arms which can be moved independently.
The analyser-detector system is placed in a common shielding drum of 46 cm
internal diameter. At present only one analysing system is installed. The
second spectrometer arm can be provided with the same analysing system
or can be used for diffraction work.

The instrument will be controlled by a NOVA-computer. As a part of the
interface has not yet been completed only a semi-automatic way of
operation is possible at present (scans with constant angular increments).
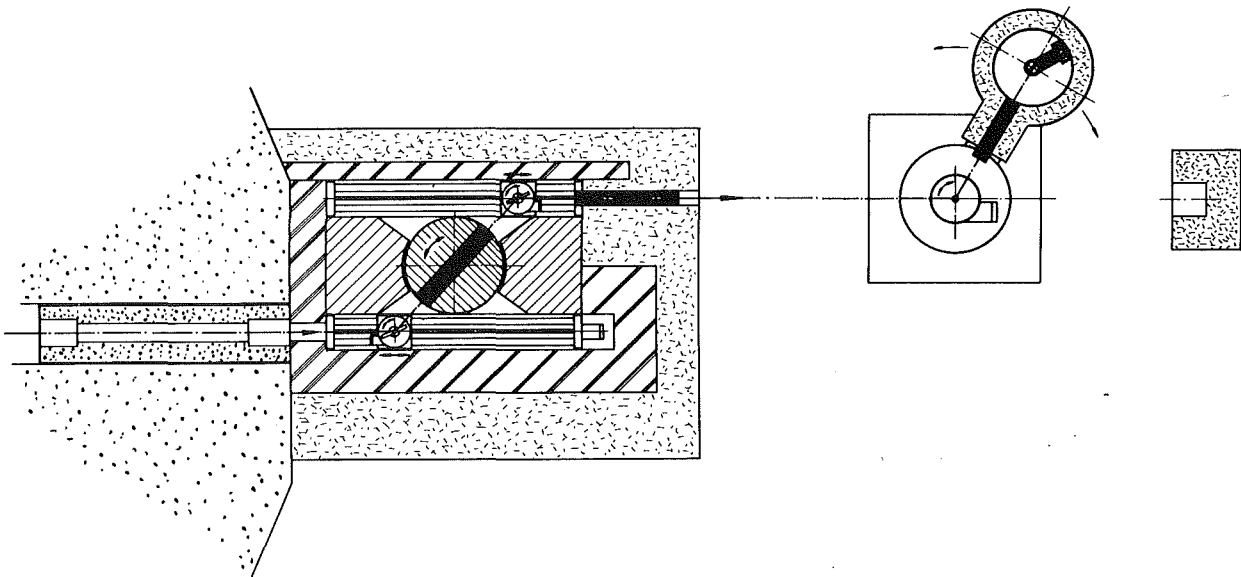

Fig. 58

5.5   A Neutron Time-of-Flight Diffractometer with a
Pseudostatistically Chopped Beam

*H. Kiowski, Institut für Kernphysik der Universität
Frankfurt*

A time-of-flight experiment with a pseudostatistical chopper /1/ has been
built up at the reactor FR2 with a flexible set-up in order to test its
applicability for elastic scattering experiments. Scattering angles between

30 $^\circ$ and 160 $^\circ$ and flight paths between 5 and 7.5 m were realized. Intensity and resolution of the instrument have been measured as a function of these parameters.

Absolute intensity determination requires an accurate knowledge of the reactor spectrum. Therefore its wavelength distribution was determined by several independent methods. Utilizing the specific advantages of the time-of-flight method and especially those of pseudostatistical pulsing the following problems have been investigated:

1. scattering from samples with large absorption or incoherent scattering , e. g. LiH,

2. search for forbidden reflections (222) and (666) in Ge- and Si-single crystals after optimizing the intensity of the Bragg-peaks by appropriate choice of the scattering angle,

3. scattering by liquid Hg to determine the structure factor in a wide range of momentum transfers.

References

/1/ F. Gompf et al., Neutron Inelastic Scattering II, IAEA, Vienna, 1968, p. 417

6. PUBLICATIONS, CONFERENCE CONTRIBUTIONS AND SEMINARS

6.1 PUBLICATIONS

Babel, D.; Wall, F.; Heger, G.;
Die Kristall- und Magnetische Struktur von $CsFeF_4$
Zeitschrift für Naturforschung 29b (1974), 139

Bittermann, K.; Heger, G.;
Growth of Large K_2MnF_4 Single Crystals and Characterization by
X-Ray and Neutron Diffraction Investigations
Journal of Crystals Growth 21 (1971), 82

Gettings, M.; Meyer, O.; Linker, G.;
Radiation Damage in Ion Implanted Vanadium
Radiation Effects 21 (1974), 51

Gläser, W.; Gompf, F.; Reichardt, W.;
Unelastische Streuung langsamer Neutronen an Festkörpern
KFK-Nachrichten, 5 (1973), No. 2, S. 19-26

Gläser, W.;
Streuung thermischer Neutronen an Festkörpern
Genzel, L. (Hrsg.): Die feste Materie, Frankfurt a. Main:
Umschau-Verlag (1973), S. 199-221

Gläser, W.;
Experimental Studies of the Electron-Phonon Interaction
in One-Dimensional Conducting Systems
Festkörperprobleme XIV (1974), p. 205
Friedr. Vieweg+Sohn GmbH, P.O.B.3367, D-3300 Braunschweig,
Germany (West)

Heger, G.;
Magnetic Properties of the Ferrimagnet Na_2NiFeF_7 and the
Linear Antiferromagnet Na_2NiAlF_7
International Journal of Magnetism 5 (1973), 119

Linker, G.; Meyer, O.; Gettings, M.;
Backscattering Energy Loss Parameter Measurements in Thin
Metal Films, Thin Solid Films 19 (1973), 177

Löffler, U.;
Investigations of Collective Atomic Motions in Liquid
Gallium by Inelastic Neutron Scattering
Thesis, Universität Karlsruhe, (1973), KFK 1875

Mertens, J.; Ackermann, H.; Dubbers, D.; Heitjans, P.;
Winnacker, A;, Blanckenhagen, P., von;
Relaxation and Orientation of ^{110}Ag (T$_{1/2}$= 24.4 s)
Nuclei Produced by Capture of Polarized Neutrons in the
Silver Halides
Z. Physik, 262 (1973), 189

Meyer, O.; Linker, G.; Kraeft, B.;
Validity of Bragg's Rule in Sputtered NbN and NbC Films
of Various Compositions
Thin Solid Films 19 (1973), 217

Meyer, O.; Linker, G.;
Ionenimplantation in Metalle und Supraleiter
KFK-Nachrichten, 1 (1974), 1

Nücker, N.; Reichardt, W.;
Der HFR und seine Nutzung
KFK-Nachrichten, 5 (1973), No. 4, S. 1-9

Peterson, S.; Tove, P. A.; Meyer, O.; Sundquist, B.; Johansson, A.;
Comparison of Backscattering Parameters Using High Energy
Oxygen and Helium Ions
Thin Solid Films 19 (1973), 157

Renker, B.; Rietschel, H.; Pintschovius, L.; Gläser, W.;
Bruesch, P.; Kuse, D.; Rice, M. J.;
Observation of Giant Kohn Anomaly in the One-Dimensional
Conductor KCP
Phys. Rev. Lett. 30 (1973), 1144

Renker, B.; Pintschovius, L.; Gläser, W.; Rietschel, H.;
Comés, R.; Liebert, L.; Drexel, W.;
Neutron-Scattering Study of the Structural Phase Transition
in the One-Dimensional Conductor KCP
Phys. Rev. Lett. 32 (1974), 836

Rietschel, H.;
The Giant Kohn Phonon Anomaly in a Peierls Semiconductor
Solid State Commun. 13 (1973), 1859

Rietschel, H.;
Cubic and Quartic Anharmonicities in a One-Dimensional
Metal
Solid State Commun. 14 (1974), 699

Salgado, J.;
Investigations on methods to determine the phonon density
of states with application to the elements of the fifth group
of the periodic Table
Thesis, Universität Karlsruhe, (1974)
KFK 1954 (in print)

6.2 CONFERENCE CONTRIBUTIONS AND SEMINARS

Fink, J.; Czjzek, G.; Schmidt, H.; Breitmeier, U.;
Ruebenbauer, K.; Coey, J. M. D.; Brusetti, R.;
Mößbauerspektroskopie mit ^{61}Ni in hexagonalem NiS
Verhandl. DPG (VI) 9 (1974), 724

Geerk, J.;
Tunneluntersuchungen am Niobkarbid
Verhandl. DPG (VI) p (1974), 796

Gettings, M.; Langguth, K.-G.; Linker, G.;
Radiation Damage and Ion Behaviour in Ion Implanted Vanadium
and Nickel Single Crystals
Int. Conf. Appl. Ion Beams to Metals, Albuquerque, N. M.,
October 1973

Gettings, M.; Meyer, O.;
Herstellung von Nb_3Ge-Schichten mit hohem Sprungpunkt
Verhandl. DPG (VI) 9 (1974), 847

Gläser, W.; Pintschovius, L.; Renker, B.; Rietschel, H.;
Inelastic Neutron Scattering on the One-Dimensional Conductor
$K_2Pt(CN)_4Br_3 \cdot 3H_2O$
Symp. on Superconductivity and Lattice Instabilities,
Gatlingburg, Tenn., September 1973

Gläser, W.;
Gibt es eindimensionale Metalle?
Physikal. Kolloquium, Universität Konstanz, Oktober 1973
Physikal. Kolloquium, Universität Heidelberg, Dezember 1973

Gläser, W.;
Neutron Beam Research at the Karlsruhe Research Reactor FR2
Pakistan Institut of Nuclear Science and Technology,
Nilore-Rawalpindi, Pakistan, November 1973

Gläser, W.;
News on One-Dimensional Systems
Max-Planck-Institut für Festkörperphysik, Stuttgart,
November 1973

Gläser, W.;
Elektron-Phonon-Wechslwirkung in eindimensionalen Festkörper-
systemen, Verhandl. DPG (VI), 9 (1974), 805

Gläser, W.;
Neutron-Scattering Studies of Lattice Dynamics and Structural
Changes in a pseudo-one-dimensional Conductor
Univeritaire Instelling Antwerpen, Mai 1974

Gläser, W.;
Experimental Studies of Lattice Dynamics and Structural
Changes in One-Dimensional Conducting Systems
Meeting of the American Physical Society in
Philadelphia/USA, März 1974
Bull. Am. Phys. Soc. 19 (1974), 242

Heger, G.;
Susceptibility and Neutron Diffraction Studies of Quasi
Two-Dimensional Heisenberg Antiferromagnetis
International Conference on Magnetism, Moskau,
August 1973

Langguth, G.;
Influence of Ion Induced Radiation Damage on the Dechanneling
Rate of Ni Single Crystals
Institut National Des Sciences Et Techniques Nucleaires:
Session an Channeling and Blocking Phenomena, Saclay, May 1974

Linker, G.;
Ion Implantation into Metals
California Institut of Technology, Pasadena, October 1973

Linker, G.;
Ionenimplantation in Metalleinkristalle
Seminar of the BMFT and DFG: "Grundlagen und Anordnungen
der Ionenimplantation in Halbleiter und andere Materialien",
München 1974

Meyer, O.; Mann, H.; Phrilingos, E.;
Ion Implantation in Superconducting Thin Films
Int. Conf. Appl. Ion Beams to Metals, Albuquerque, N. M.
October 1973

Meyer, O.;
Laufende und geplante Arbeiten der Arbeitsgruppe
"Ionenimplantation und Channelingtechnik"
Institut für Angewandte Kernphysik, Kernforschungszentrum,
Karlsruhe

Meyer, O.;
Die Rutherford-Rückstreutechnik als Analysenmethode von
Oberflächen und dünnen Schichten
Fa. Siemens, Erlangen, Juli 1973

Meyer, O.;
Ion Implantation in Metals and Superconducting Thin Films
Hungarian Academy of Sciences, Budapest, August 1973

Reichardt, W.; Schweiß, P.; Salgado, J.; Gompf, F.;
Investigation on the Phonon Density of States of High
Temperatures Superconductors
Symposium on Superconductivity and Lattice Instabilities,
Gatlingburg, Tenn., September 1973
Symposium on Phonons, Leoni/Starnbergersee, September 1973

Renker, B.; Pintschovius, L.;
Temperaturabhängigkeit der Gitterverzerrung in dem eindimen-
sionalen Leiter $K_2Pt(CN)_4Br_3 \cdot 3D_2O$
Verhandl. DPG (VI) 9, (1974), 866

Rietschel, H.;
Wechselwirkung zwischen Elektronen und Phononen in eindimen-
sionalen Metallen
Theoretisch-Physikalisches Kolloquium, Universität Dortmund,
November 1973

Rietschel, H.;
Physik und chemische Verwirklichung eindimensionaler Metalle
Physikalisch-Chemisches Seminar, Universität Karlsruhe,
Januar 1974

Rietschel, H.;
Neutron Scattering Study of KCP
"Conference on Linear Conductors" in Lake Arrowhead, USA,
Mai 1974

Rietschel, H.;
Anharmonizitäten in eindimensionalen Metallen
Verhandl. DPG (VI) 9 (1974), 805

Salgado, J.; Gompf, F.; Reichardt, W.;
Messungen der Phononenzustandsdichten von Arsen, Antimon und
Wismuth
Verhandl. DPG (VI) 9 (1974), 762

Schneider, E.; Reichardt, W.; Rietschel, H.; Tripadus, V.;
Neutronenstreuexperimente an Nb_3Sn
Verhandl. DPG (VI) 9 (1974), 796

Schommers, W.;
Berechnung von Orts- und Zeitkorrelationsfunktionen für
flüssiges Rubidium mit Hilfe der Molekulardynamik
Verhandl. DPG (VI) 9 (1974), 761

Schweiß, P.;
Phononenzustandsdichten von V_3Si bei verschiedenen Temperaturen
Verhandl. DPG (VI) 9 (1974), 792

Schweiß, P.;
Densités d'états des phonons dans des composés A-15
Département de Physique de la Matière Condensée,
Universität Genf, Mai 1974

7. STAFF MEMBERS

Head of Institute: W. Gläser

Professional Staff

P. v. Blanckenhagen	U. Löffler	W. Reichardt	P. Schweiß
G. Czjzek	W. Mehringer	B. Renker	J.-B. Suck
J. Fink	O. Meyer	H. Rietschel	
J. Geerk	N. Nücker	E. Schneider	
F. Gompf	L. Pintschovius	H. Schmidt	
G. Linker	Chr. v. Platen	W. Schommers	

Technical Staff

W. Abel[+]	H. Klann	H. Richelsen[+]	K. Weber
G. Ehret[+]	M. Kraatz	B. Scheerer	
H. Hanak[+]	F. Ratzel	R. Smithy	

Visiting and Attached Scientists

H. Bialas, Universität Heidelberg

J. Daubert, Universität Frankfurt

M. Gettings, Universität Harwell

G. Heger, Universität Marburg

P. Heitjans, Universität Heidelberg

K. Kiowski, Universität Frankfurt

M. Morariu, Guest from Institute of Atomic Physics, Bukarest

K. Ruebenbauer, Guest from Institute of Physics, Kraków

J. Salgado, Guest from Laboratório de Fisika e Engenharia Nucleares, Sacavém,
Portugal

P. N. Timis, Guest from Institute of Atomic Physics, Bukarest

V. Tripadus, Guest from Institute of Atomic Physics, Bukarest

Research Students

R. Block, Universität Karlsruhe	K.-G. Langguth, Universität Karlsruhe
B. Hofmann, Universität Karlsruhe	E. Phrilingos, Universität Karlsruhe
B. Hofmann-Kraeft, Universität Karlsruhe	H. J. Stolz, Universität Heidelberg
H. J. Klein, Universität Karlsruhe	

[+]Member of infrastructure